Engineering Journal

American Institute of Steel Construction

Fourth Quarter 2009 Volume 46, No. 4

www.aisc.org

ENGINEERING JOURNAL

AMERICAN INSTITUTE OF STEEL CONSTRUCTION

Dedicated to the development and improvement of steel construction, through the interchange of ideas, experiences and data.

ENGINEERING JOURNAL (ISSN 0013-8029) is published quarterly. Subscriptions: Members: one subscription, $20 per year, included in dues; Additional Member Subscriptions: $15 per year. Non-Members U.S., Canada, and Mexico: $40 per year, $110 for three years, single copy $15. International Members and Non-Members: $90 per year; $250 for three years; single copy $25. Published by the American Institute of Steel Construction at One East Wacker Drive, Suite 700, Chicago, IL 60601.

Periodicals postage paid at Chicago, IL and additional mailing offices. **Postmaster:** Send address changes to ENGINEERING JOURNAL in care of the American Institute of Steel Construction, One East Wacker Drive, Suite 700, Chicago, IL 60601.

The Best
Engineering Journal
Article of 2009

Visit the AISC website **(www.aisc.org/ejsurvey)** to cast your vote for the best *Engineering Journal* Article of 2009 through March 12, 2010.

The award will be presented to the winning author at the 2010 North American Steel Construction Conference (NASCC: The Steel Conference) to be held in Orlando, Florida, May 12–15. The winning author will receive free registration and travel expenses to attend the 2010 NASCC.

Subscribe to *Engineering Journal* by visiting our web site **www.aisc.org/ej** or by calling 312.670.5444.

Copies of current and past *Engineering Journal* articles are available free to members online at **www.aisc.org/ej.**

Non-members may purchase *Engineering Journal* article downloads at the AISC Bookstore at **www.aisc.org/ej** for $10 each.

Message from the Editor

As I look back on 2009, I'd like to take a moment to thank those who have contributed to the ongoing success of *Engineering Journal* this year.

First, many thanks to our authors, who keep the industry informed with their diligent research and writing endeavors.

Second, a gracious round of applause for our reviewers (see next page), who have generously contributed their time and expertise.

Third, kudos to our readers, for giving AISC and our authors ongoing feedback about the quality and content of our journal. (Congratulations to Thomas McCormick, Scott White, and Donny Cook, the winners of our August 2009 reader survey random drawing.)

Fourth, a big thank you to Cindi Duncan, AISC's Director of Engineering and former editor of *Engineering Journal*, for setting high standards for the journal and for having the patience to get me up to speed.

And finally, I would like to personally thank Janet Cummins, AISC's Engineering and Research Coordinator, for keeping track of the behind-the-scenes correspondence and documentation necessary to produce a quarterly journal.

You will notice a few changes with this issue. We've started including article abstracts and keywords, as well as contact information for all authors. We hope you find these changes useful.

Best wishes for a happy and healthy 2010!

Keith A. Grubb
Editor

P.S. It's time to vote for the Best EJ Paper of 2009. Cast your vote at www.aisc.org/ejsurvey through March 31, 2010. The winning author and one randomly selected voter will receive free registration and travel to the 2010 NASCC: The Steel Conference in Orlando, Florida, May 12–15.

Acknowledgment

All AISC *Engineering Journal* articles are peer reviewed prior to publication for accuracy, content and style. AISC thanks the following engineers for their voluntary review assistance to the *Engineering Journal* Review Board throughout 2009.

Allen Adams
Bentley Systems, Inc.

Farid Alfawakhiri
American Iron and Steel Institute

Allan Baker
Berube Leonard, LLC

Robert E. Bachman
Consultant

William F. Baker
Skidmore Owings & Merrill, LLP

Reidar Bjorhovde
The Bjorhovde Group

Susan B. Burmeister
Cagley & Associates, Inc.

Peter J. Carrato
Bechtel Corporation

Finley A. Charney
Virginia Tech

Michael P. Culmo
CME Associates, Inc.

Richard M. Drake
Fluor Enterprises, Inc.

Jim Davidson
Auburn University

Robert Driver
University of Alberta

Carol J. Drucker
Drucker Zajdel Structural Engineers, Inc.

W. Samuel Easterling
Virginia Tech

Edward Egan
Southern Iron Works, Inc.

Howard I. Epstein
University of Connecticut

Shujin Fang
Sargent & Lundy, LLC

Marshall T. Ferrell
Ferrell Engineering, Inc.

James M. Fisher
Computerized Structural Design, SC

John W. Fisher
Lehigh University

Christopher M. Foley
Marquette University

Timothy P. Fraser
Anvil Corporation

Theodore V. Galambos
University of Minnesota

Louis F. Geschwindner
American Institute of Steel Construction

Rodney D. Gibble
Rodney D. Gibble Consulting Engineers

Michael A. Grubb
BSDI Ltd.

Subhash Goel
University of Michigan

W. Scott Goodrich
Structural Detailing, LLC

Gilbert Grondin
University of Alberta

Jerome F. Hajjar
University of Illinois at
Urbana-Champaign

Ronald O. Hamburger
Simpson Gumpertz & Heger Inc.
Consulting Engineers

Patrick M. Hassett
Hassett Engineering, Inc.

Tony C. Hazel
Ferrell Engineering, Inc.

Richard A. Henige
LeMessurier Consultants, Inc.

Stephen M. Herlache
Computerized Structural Design, SC

Steve Herth
Contech Bridge Solutions, Inc.

Christopher M. Hewitt
Sargent & Lundy, LLC

Keith D. Hjelmstad
Arizona State University

Mark V. Holland
Paxton & Vierling Steel Company

Nestor Iwankiw
Hughes Associates

William P. Jacobs
Stanley D. Lindsey & Associates

Lawrence A. Kloiber
LeJeune Steel

Lawrence F. Kruth
Douglas Steel Fabricating Corporation

Geoffrey L. Kulak
University of Alberta

Keith Landwehr
Schuff Steel Company

Michael E. Lederle
Opus Architects & Engineers, Inc.

Roberto T. Leon
Georgia Institute of Technology

Walterio Lopez
Rutherford & Chekene
Consulting Engineers

LeRoy A. Lutz
Computerized Structural Design, S.C.

Robert A. MacCrimmon
Hatch Canada

William McGuire
Consultant

Sanjeev R. Malushte
Bechtel Corporation

James O. Malley
Degenkolb Engineers

Bonnie E. Manley
American Iron and Steel Institute

Composite Action in CFT Components and Connections

CHARLES W. ROEDER, DAWN E. LEHMAN and RYAN THODY

ABSTRACT

Concrete-filled steel tube (CFT) components provide an attractive alternative to conventional methods of construction. The steel tube serves as formwork and reinforcement to the concrete fill. The fill delays local buckling of the tube and increases the compressive strength, stiffness and ductility of the CFT member if composite action is achieved. As such, the benefits of using CFT components include their efficiency, economy and ability to provide rapid construction. The primary obstacles to using CFT components relate to achieving adequate shear-stress transfer between the two materials needed for composite behavior and to developing robust, constructible connections. There is considerable interaction between this stress transfer and the connections joining CFT members to other structural elements. In many cases, natural bond stress, primarily friction, is adequate to ensure good structural performance of the CFT member, but in other cases mechanical interlock or bearing between the steel and concrete is required. While some mechanical transfer elements may supplement the natural bond transfer, others may destroy this beneficial effect. Additionally, natural bond may be dramatically enhanced by bending of the CFT member and by using appropriate connections to join other members to the CFT element. Therefore, proper quantification and understanding of natural, enhanced and mechanical sources of bond stress are needed to develop robust CFT structural components and their connections.

Keywords: bond stress, columns, composite construction, concrete-filled steel tubes, hollow structural sections, tubes.

INTRODUCTION

Concrete-filled steel tubes (CFT) have been used to support large axial forces induced by gravity or lateral loads. CFT construction is economical because the steel tube serves as a formwork, and it reinforces the concrete fill at the optimal location. The concrete fill stiffens the steel tube and restrains or delays local buckling. The diameter of the tube is sometimes very large, and diameter-to-thickness (d/t) ratios for the tube have sometimes exceeded 100. CFT construction has been used on buildings, such as the Gateway Tower in Seattle shown in Figure 1a, and bridge piers, shown in Figure 1b.

CFT offers great potential as an economical and practical system for providing seismic resistance and rapid construction for a wide range of structural systems. However, there are limitations in the use of CFT because of (1) uncertainty in composite action or interaction between the steel tube and the concrete fill and (2) inherent difficulties in connecting CFT members to other structural elements. The full benefits of CFT construction are achieved only if the steel and concrete work together to develop composite action. Stress transfer between the steel and concrete is necessary to achieve composite behavior, and the alternate methods of achieving this stress transfer and resulting composite action are evaluated. While the issues of composite action and connection of other members to CFT columns appear to be fundamentally different concerns, this paper will show considerable interaction between them and addresses both.

Charles Roeder, Professor, Department of Civil Engineering, University of Washington, 3900 15th Ave. NE, 201 More Hall, Seattle, WA, 98115 (corresponding author). E-mail: croeder@u.washington.edu

Dawn Lehman, Assistant Professor Department of Civil Engineering, University of Washington, 3900 15th Ave. NE, 201 More Hall, Seattle, WA, 98115. E-mail: delehman@u.washington.edu

Ryan Thody, Engineer, Coughlin Porter Lundeen, 413 Pine Street, Suite 300, Seattle, WA, 98101. E-mail: ryant@cplinc.com

NATURAL BOND STRESS

Achieving composite action requires sufficient shear strength at the interface between steel and concrete, which is termed bond strength. There are two general mechanisms used to achieve this strength: (1) natural bond, which includes chemical adhesion and frictional resistance, and (2) mechanical bond, which typically requires supplemental devices or significant irregularities in the steel to permit bearing of steel on concrete. If possible, relying on the natural bond stress between the steel and concrete, rather than mechanical bond-enhancing mechanisms, facilitates construction of CFT elements, since it results in less interference during concrete placement.

A number of research studies have examined the response of CFT sections that rely solely on natural bond stress (Roeder, Cameron and Brown, 1998; Virdi and Dowling, 1975; Furlong, 1967, 1968; Shakir-Kalil, 1991, 1993a, 1993b; Morishita, Tomii, and Yosimura, 1979a, 1979b; Morishita

and Tomii, 1982; Tomii, 1984). These past studies have used push-out tests (typical setup shown in Figure 2) to evaluate bond-stress capacities. These past studies show that the bond stress between the steel tube and the concrete fill exhibits multiple stages, but it is primarily a frictional resistance dependent on the surface roughness of the steel and the contact pressure between the steel and concrete. Secondary benefits are initially provided from adhesion or chemical bonding between the two materials, but these secondary benefits are typically overcome during lower levels of loading.

Most past research expressed push-out test results in terms of an average bond stress over the entire bond area and specimen length. These tests have studied the impact of several variables on the average bond strength, including the strength of the concrete, the shape of the tube (square or circular), diameter and slenderness of the tube, the length of the bonded section, roughness of the interface, and the test setup. Bond stress is inherently variable, and there is great value in understanding why this variability occurs.

The degree of variability in natural bond stress is largely insensitive to the concrete strength, as shown in Figure 3a, since the primary bond stress resistance mechanism is friction, and the coefficient of friction is insensitive to strength. Some variability must be expected with respect to the length of the specimen, because of the nearly exponential bond stress variation over length computed in finite elment analysis prior to slip shown in Figure 4a. After progression of slip, the bond stress distribution approaches a uniform distribution over the slipped length, and the force transfer between steel and concrete approaches linearity as shown in Figure 4b. This behavior is verified by ANSYS finite element computer analysis (Santos, 1997) and experimental results (Roeder et al., 1998). The average stress computed from push-out tests is lower than the peak bond stress prior to slip but is larger than the bond stress over the majority of the specimen length as shown in Figure 4a. As seen in Figure 4a, the peak bond stress is quite large in a local area, and the distribution of bond stress is approximately exponential prior to initiation of slip. At increased load, local slip initiates when the static-friction capacity is exceeded. The extent of slip is limited by the remaining unslipped region. The magnitude of the maximum average bond stress depends on the coefficient of friction, the contact surface length, and the contact stress; however, it must be less than the peak local bond stress value prior to slip.

Natural bond stress is significantly larger for circular CFT than for rectangular or square CFT as shown by comparison of measured results in Figure 3a. As a result, circular CFT more readily develops its full composite resistance than does rectangular CFT. Although the geometry and material properties influence the peak and average bond strength for axially loaded specimens, the most influential parameter is the interface condition of the tube, as illustrated in Figure 3b. In that figure, only data from test series in which the interface condition was intentionally varied are plotted (Virdi and Dowling, 1975, Shakir-Khalil, 1993). The interface conditions were differentiated using a numerical scale from 1 (machined) to 4 (intentionally roughened). Comparing these data and the data on Figure 3a, there are several points of interest:

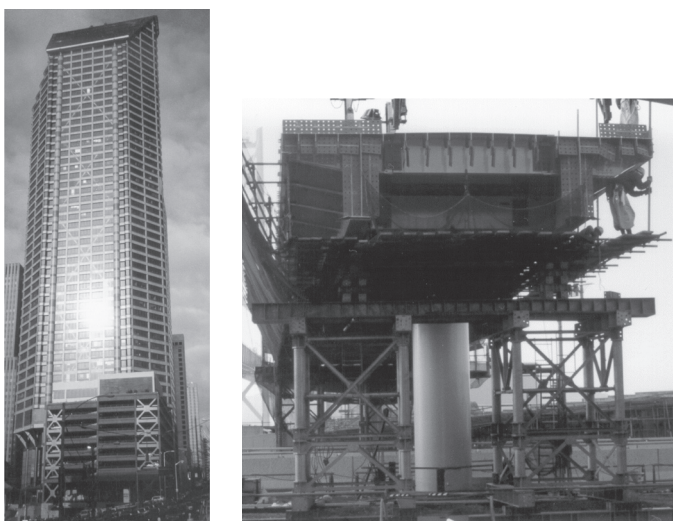

(a) (b)

Fig. 1. Examples of CFT applications; (a) highrise building (Gateway Tower, Seattle), (b) bridge pier.

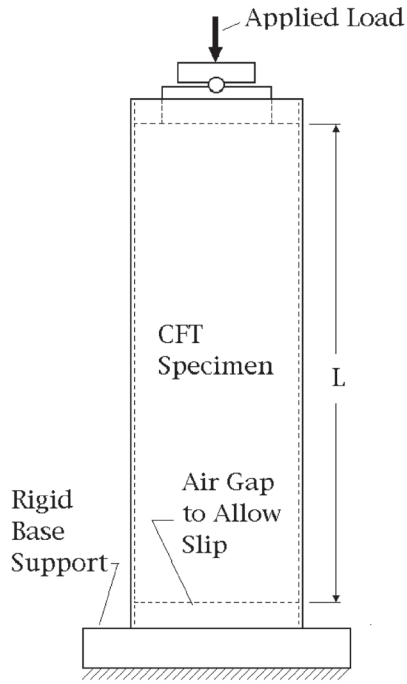

Fig. 2. Push-out test (Roeder et al., 2001).

(1) The range of the average bond stresses is similar in Figures 3a and 3b, although Figure 3b only plots a subset of the data; (2) the data plotted in Figure 3b show that the minimum and maximum average bond stress values are approximately 75 to 350 psi (0.5 to 2.5 MPa) for circular CFT and the variability depends more heavily on the interface condition (i.e., the lowest bond stress is computed for the machined specimens) than the researcher, test setup or specimen length. Rectangular CFT has bond stress values one-half to one-third the values obtained with circular CFT.

Similarly, the average bond stress depends on the degree of the concrete shrinkage and vibration of the concrete (Roeder et al., 1998; Han and Yang, 2001). The bond transfer between the steel tube and the concrete fill depends on the radial displacements due to the pressure of the wet concrete on the shell and the shrinkage of the concrete core, together with the internal surface irregularities of the inside of the tube. CFT columns have axial symmetry, and the pressure of the wet concrete will cause a radial enlargement of the tube, as approximated by Equation 1

$$\Delta_1 = (pd^2)/(4E_s t) \quad (1)$$

where

Δ_1 = radial enlargement
p = internal pressure of wet concrete
d = diameter of the steel tube
t = wall thickness of the steel tube
E_s = modulus of the steel

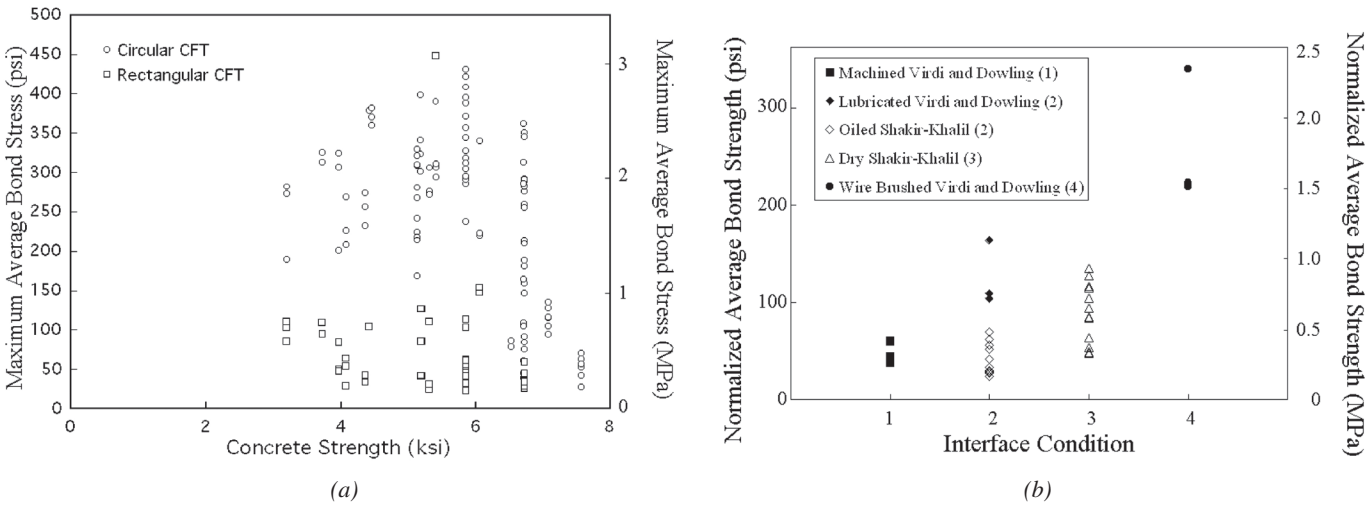

Fig. 3. Measured average bond stress capacity: (a) as function of concrete strength (Roeder et al. 1998); (b) as function of interface condition.

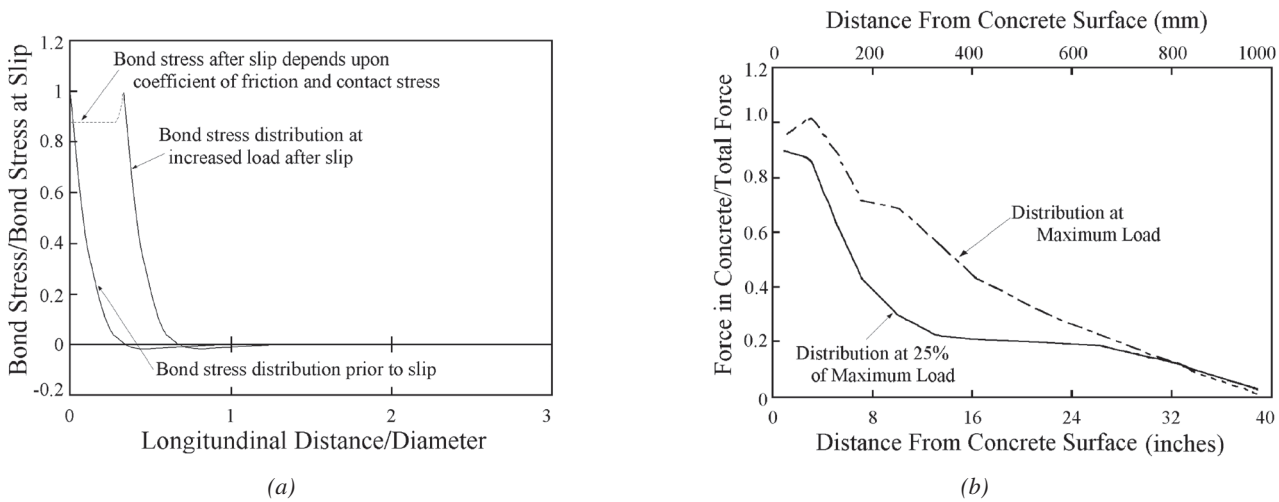

Fig. 4. Measured bond stress distribution at different load levels.

Shrinkage of the concrete during curing produces a radial reduction of the concrete core of

$$\Delta_2 = (-cd)/2 \quad (2)$$

where

Δ_2 = radial reduction of concrete core due to shrinkage
c = shrinkage of a unit volume of concrete

The shrinkage depends on the concrete mix and admixtures, the curing procedures and the diameter. When these deflections are considered, three possible states exist at the interface:

State A: $$\Delta_1 + \Delta_2 > 0 \quad (3)$$

State B: $$\Delta_1 + \Delta_2 < -\Delta_3 \quad (4)$$

State C: $$0 \geq \Delta_1 + \Delta_2 \geq -\Delta_3 \quad (5)$$

where

Δ_3 = amplitude of the rugosity, or roughness, of the interior of the tube

This evaluation is approximate, but it clearly illustrates the issues at hand.

In State A the concrete exerts pressure on the interface after the shrinkage is complete, and the initial bond strength is provided by an adhesion between the steel and the concrete combined with friction due to pressure at the interface. With increasing shear, the initial adhesion (or chemical bond) capacity is exceeded and local slip occurs. This slip deformation may be very small, but friction is the shear transfer mechanism after this occurs. In State B separation between the two materials exists after shrinkage and relative rigid body motion occurs with little bond strength or resistance when one material is pushed relative to the other. In this state, bond stress is developed only when stresses and strains caused by applied loading induce frictional contact at the surface. The effective bond stress in Stage B may be negligible. State C is an intermediate condition. Adhesion is of reducing significance and the mechanical bond or interlock of the surfaces progressively reduces in a relatively unpredictable manner as State B is approached.

The surface roughness or rugosity of steel is typically small, and as a result, the natural bond stress achievable in most practical applications of CFT is small. However, some manufacturing methods such as spiral welding of the tube may increase the roughness or irregularity on the inside of the tube, and thus increase the natural bond stress achieved with the CFT application. This natural bond stress also may be increased if expansive or low shrinkage concrete is employed, and it is significantly larger with circular tubes than square or rectangular tubes (see Figure 3a). This natural bond stress decreases as the diameter or *d*/*t* ratio of the tube increases. Statistic models of bond stress have been developed for straight seam circular tubes, and the (statistically reliable) predicted average bond stress is never greater than approximately 200 psi (1.5 MPa), and it becomes negligible as the *d*/*t* ratio exceeds 50 to 60 or for large diameter tubes (Roeder et al., 1998).

COMBINED BENDING AND AXIAL DEMANDS — AN EXCEPTION TO THE NATURAL BOND STRESS LIMITATION

Recent tests have shown that there is a clear exception to the natural bond limitation for components subjected to large bending demands in addition to axial stresses. Tests by Thody (2006) were conducted to study the impact of the surface condition of the steel on the stiffness, strength and deformability of flexural CFT elements. Figure 5a illustrates a test setup where 20-in.-diameter (508 mm) spiral-weld tubes with large *d*/*t* ratio of 80 and high-strength vanadium-alloy steel ($F_y \approx 525$ MPa or 76 ksi) were subjected to cyclic bending moment demands. In the test program, a series of eight tubes were tested, with four specimens designed specifically to evaluate the influence of the surface and slip condition on bond stress, shear transfer and composite behavior. [The other four specimens studied the effect of variation in the properties of the spirally welds and galvanization on the engineering response of the specimens and are described elsewhere (Thody, 2006)].

The steel tubes were spirally welded with the double submerged arc process from both the outside and inside of the tube. The specimens were filled with a low-shrinkage, self-consolidating concrete with a specified compressive strength of 13 ksi (90 MPa). The steel tubes were approximately 20 ft. (6.1 m) long, and the concrete was placed without vibration. The specimens were subjected to 3-point loading with a span length of 18 ft (5.48 m) and were not subjected to an axial load.

The reference specimen, CFT1, was constructed with no special surface treatment (without capped ends or grease interior) to represent a "normal" bond condition. Past test data suggest that the bond stress under "normal" conditions should be very small because of the large diameter and *d*/*t* ratio of the tube (Roeder et al., 1998). Specimen CFT2 was not filled with concrete but instead was a hollow steel tube (CFT2) to provide a baseline control specimen for demonstrating composite behavior. Specimen CFT3 had capped ends to ensure that slip between the steel and concrete could not occur. Specimen CFT4 was thoroughly greased over the entire interior surface of the tube just prior to concrete placement to minimize the potential friction and natural bond stress at the interface. Table 1 provides a summary of the test specimens and general test results. Shear connections or mechanical devices were not employed in any of these tests, and the concrete fill had no reinforcement other than the steel tube. The specimens were subjected to cyclic inelastic

Table 1. Summary of Flexural Tests									
Specimen	Steel-Concrete Interface or End Condition	Ultimate Failure Mode	Maximum Moment Resistance (kN-m)	Stiffness Ratio $(E_sI_{eff})_{0.9M_y}$ to E_sI_g	Drift Level (%) at Various Benchmarks			At 20% Reduction in Resistance	
					Initial Yield	Local Buckling	Initial Tearing	+ Drift %	– Drift %
CFT1	Normal	Tearing at Buckle	1155	0.52	0.9%	1.7%	2.7%	3.1%	–3.1%
CFT2	Hollow	Tearing at Buckle	816	0.39	0.8%	1.2%	N/A	1.5%	–2.1%
CFT3	Capped Ends	Tearing at Buckle	1182	0.51	1.0%	1.9%	3.1%	3.1%	–3.2%
CFT4	Greased	Tearing at Buckle	1150	0.53	0.7%	1.9%	2.6%	2.9%	–2.9%

deformation histories based upon the ATC-24 test protocol (ATC, 1992).

Table 1 shows that the specimens with concrete fill provided significantly greater ductility, resistance and stiffness than the hollow steel tube. Figure 6 show the measured moment-drift plots for the specimens CFT3 and CFT4, since they represent the extremes expected in composite behavior for these tests. Specimen CFT3 should have ideal bond stress since it has capped ends and full restraint against slip, while Specimen CFT4 should have the least natural bond and composite action with the greased steel-concrete interface. Comparison of these figures and the data of Table 1 indicate that the greased specimen developed nearly the same total composite action in that it had similar maximum resistance, stiffness and inelastic deformation capacity values as the specimen with capped ends. The filled specimens all developed the predicated ultimate capacity of the composite section. This is an important observation because it indicates that the binding action associated with bending is sufficient to prevent relative slip of the concrete and steel thereby ensuring composite action was achieved.

The composite specimens exhibited similar behaviors. Cracking of the concrete was localized to within a narrow region subject to maximum bending moment and occurred at relatively small inelastic deformations (always less than 1% drift). Yielding of the steel tube was typically noted at drift levels in the range 0.7% to 1.0%, and visible local buckling of the tube was observed at drift levels in the range of 1.7% to

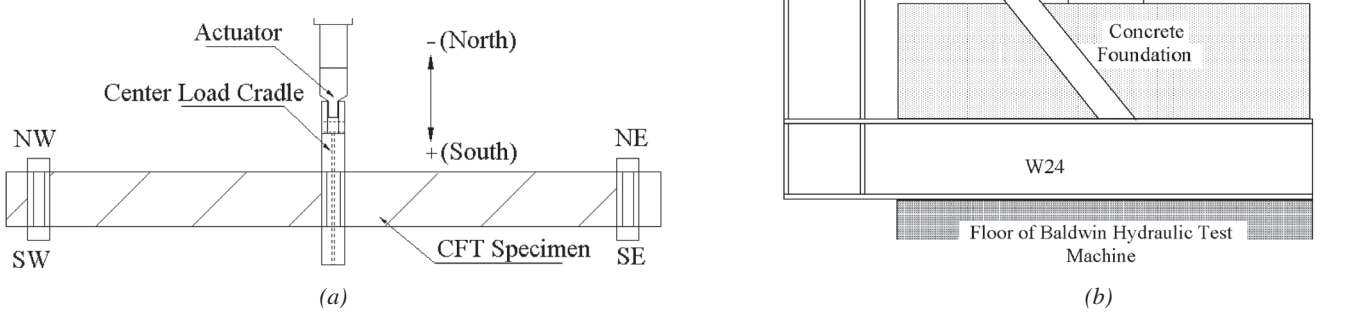

Fig. 5. Schematics of tests setups: (a) cyclic flexural test; (b) cyclic flexure with axial load.

2.0%. The local displacement of the buckled region became increasingly larger with increased inelastic cycles, as shown in Figure 7a. As a larger buckling bulge occurred, large local strains were noted on the peak of the bulge and cracks began to develop in the steel at the peak of the buckling bulge at drifts in the range of 2.6% to 3.1% (Figure 7b). The cracks grew slowly in a ductile manner with increasing deformations, and powdered concrete seeped from the cracks during this time. This indicates that the concrete was completely crushed into a powdered form before severe buckling and steel cracking initiated. The crack length grew with increasing deformation, and ductile tearing progressed around the perimeter of the tube occurred at drift ratios between 3% and 4%. The ductility exhibited in these tests was considerable when it is recognized that the *d/t* ratio greatly exceeds that allowed by current AISC *Seismic Provisions for Structural Steel Buildings* and AISC *Specification for Structural Steel Buildings* (AISC, 2005a, 2005b).

Slip measurements were made between the steel and the concrete fill at the ends of the test specimens. The maximum slip data values measured for CFT1 and CFT4 were 0.07 and 0.11 in. (1.9 and 2.8 mm), respectively. After completion of the test, destructive inspection of the specimen revealed that the primary cracking and concrete crushing occurred within

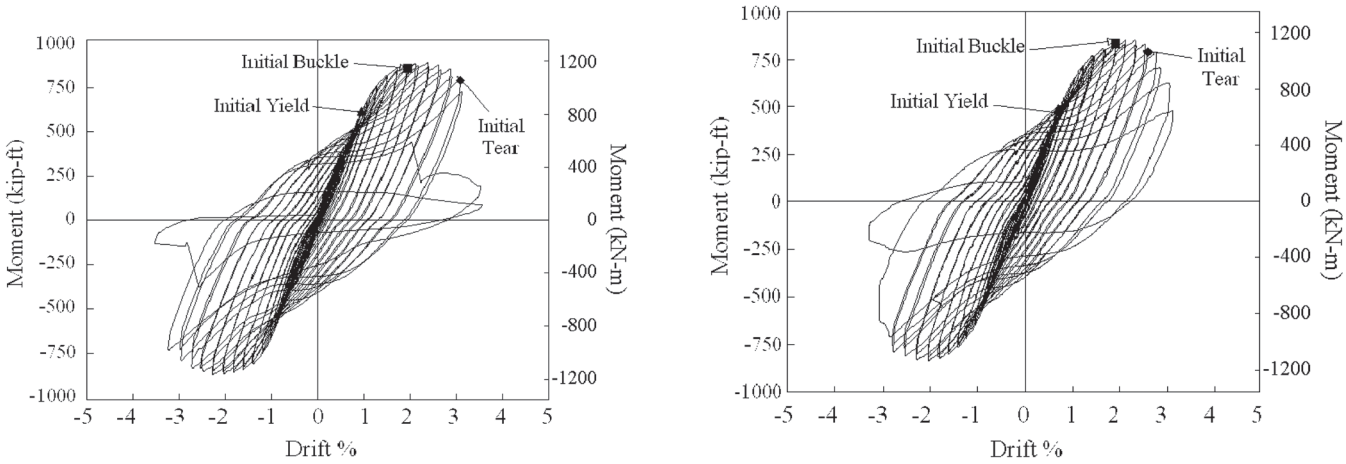

(a) *(b)*

Fig. 6. Moment-drift curves: (a) Specimen CFT3 with capped ends; (b) specimen CFT4 with greased interface.

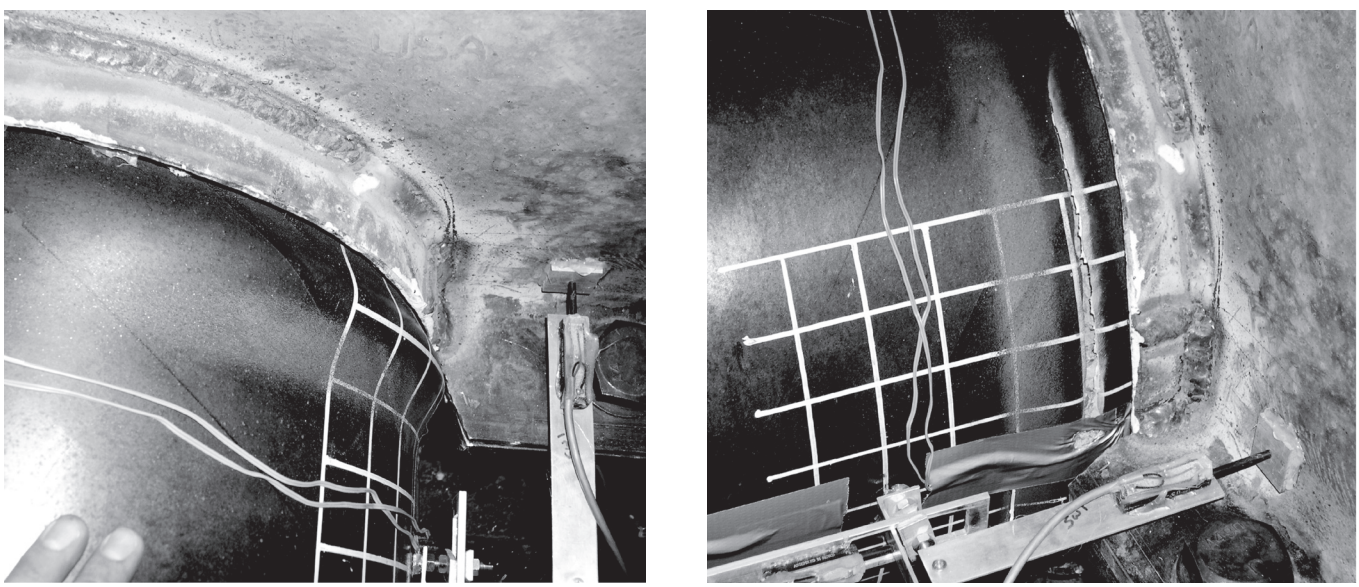

(a) *(b)*

Fig. 7. Photos of behaviors noted in the CFT tests: (a) local buckling; (b) tears developing at the peak of the bulge.

approximately 4 in. (100 mm) of the central load point, as illustrated by the photo in Figure 8. The concrete fill was examined after the test was completed, and no damage or deterioration of the concrete fill at the steel-concrete interface was noted outside this crushed zone. The measured values and observed behavior supports the concept of binding action described later in this paper. The presence of bending in the tube resulted in full composite action even in Specimen CFT3, which was designed to prevent normal bond stress transfer.

The test results show that CFT elements primarily subjected to bending can achieve full composite action without adding supplemental bond stress transfer mechanisms and can meet the flexural performance requirements. Push-out tests that use an eccentrically applied axial load with bending moment show much larger bond stress measurements than concentrically loaded push-out tests, but much of this data is from embedded section bond stress pushout tests (Murrow, 1997). The reason for this effect can be understood in the context of the prior discussion. Members subject to flexure sustain curvature and transverse deflections along their length. If the steel and concrete fill are fully bonded, the transverse deflections and curvature are directly determined through conventional engineering expressions in that full composite action is developed. If the steel and concrete are not fully bonded, the curvature and transverse deflections of the steel and concrete differ, and the different deformations in the steel and concrete will result in binding at multiple locations (minimum of 3) on the inside of the tube. The binding produces a large contact force at these locations and prevents slip of the concrete to permit shear stress transfer between the steel and concrete.

These results and their theoretical arguments suggest that engineers should not consider adding supplemental bond stress transfer mechanisms in cases of combined bending and axial loads but should consider supplemental mechanisms for cases of large axial loads (with or without low bending moment demands). Therefore, it is not necessary to check bond stress with members subject to shear and flexure only. Evaluation of the bond stress for axial loads only should be considered using provisions such as described in the prior section and mechanical force transfer section that follows. This conservative approach is frequently employed in design, and it is rational based upon these test results.

MECHANICAL SHEAR TRANSFER

In view of the limited natural bond capacity in CFT members, many engineers employ mechanical shear transfer elements to achieve full composite action. Some specifications specifically require that the mechanical transfer elements be used for composite columns (ACI 318, 2005). In some structures, shear stud connectors were welded to the inside of the tube, as depicted in Figure 9a. While mechanical devices can provide a calculable slip resistance, shear studs connectors develop their full shear resistance by deformation as shown in Figures 9b and 9c. Deformation of the shear stud also causes slight deformation of the wall of the tube, which may result in local separation of the concrete and steel thereby reducing the natural bond stress at the steel-to-concrete interface. Even very slight deformation of the wall of the tube or damage to the concrete disturbs the contact between the wall of the tube and the concrete fill, resulting in loss of friction in this area.

Tests that have been performed on CFT with and without shear connectors (Roeder et al., 1998; MacRae, Roeder, Gunderson and Kimura, 2004) show that the resistance achieved

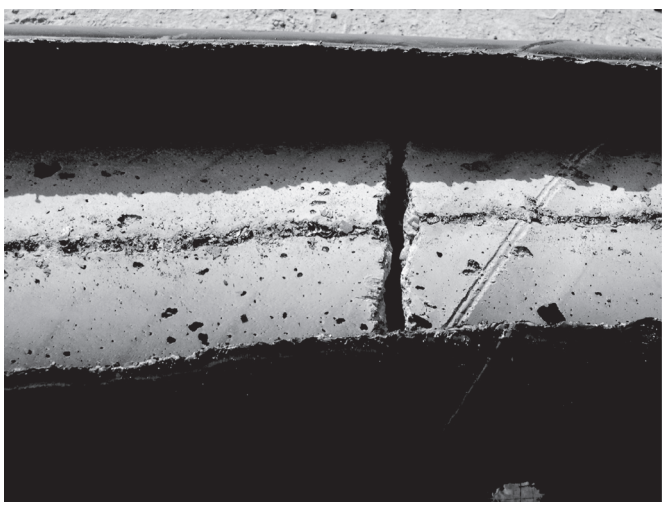

Fig. 8. Photo of the concrete core and damaged concrete region after completion of testing.

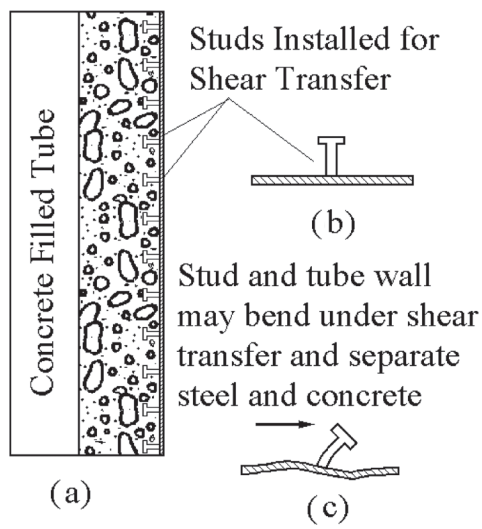

Fig. 9. Force transfer with typical shear stud connectors.

with shear connectors may be smaller than that achieved without any shear studs unless the studs are designed to provide the full stress transfer resistance. If shear studs are employed, the connections should be designed to achieve the full axial stress transfer, and a large number of connectors may be required. It is necessary to note that the shear connectors are not necessarily uniformly loaded when installed in a group (see Figure 4a), and this nonuniform load distribution increases the demand on individual studs. Finally, it must be recognized that installing a large number of shear connectors inside a steel tube can be costly and difficult; as a result, shear studs may not be the optimal choice for providing mechanical stress transfer in CFT applications.

If the slip or connector deformation is large, deterioration of the concrete at the bond interface will occur. Stiff mechanical transfer provides a binding action that prevents relative slip, and the resistance achieved with friction can be very large. The results by Thody (2006) and others suggest that it is desirable to use mechanical elements that have sufficient stiffness to limit slip, because binding action and slip restraint aid in ensuring interface friction and composite action.

Stiff mechanical transfer may be accomplished by several means. Annular rings or stiff bars such as shown in Figure 10 may be very effective if they are placed at regular (but not necessarily close) intervals over the length of the tube. The annular rings must be stiff to transfer force between elements, but not excessively stiff compared to the stiffness of the wall of the tube, because deformation of the wall of the tube is undesirable. The ring thickness need not be overly large to achieve the stiff transfer due to the strength and stiffness of the well-confined concrete. Connectors of this type have been used in some structural applications, but their use has been limited, because the internal rings are difficult to install.

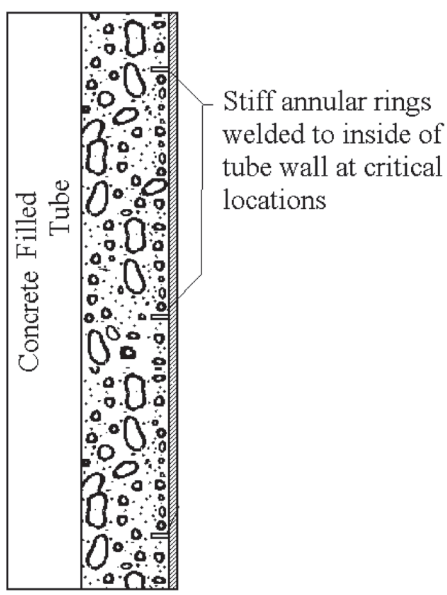

Fig. 10. Annular rings for shear transfer.

CONNECTIONS TO CFT COLUMNS

A more desirable way of accomplishing stiff mechanical transfer is accomplished by using conventional structural connections, to achieve this force or stress transfer. Figure 11 shows three typical structural connections, which accomplish these goals. With respect to composite action, these connections are similar in that (1) they all penetrate the tube with a stiff structural element to provide the binding, and (2) they restrain slip to ensure composite action in the CFT element without any additional transfer elements. In addition, they are designed to transfer the forces between members, as required by the loading and system configuration.

Figure 11a shows an internal diaphragm connection, such as those commonly used in Japan for moment resisting frame connections. These connections join the beam flanges to diaphragms, which penetrate the tube at both the top

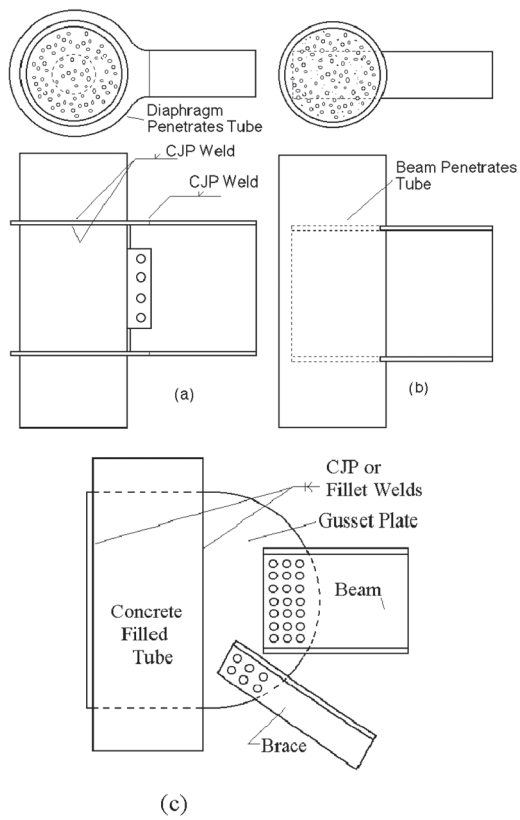

Fig. 11. Penetrating CFT connections: (a) internal diaphragm connection; (b) penetrating beam connection; (c) penetrating braced-frame gusset plate connection.

and bottom flange locations. Research has shown that these connections develop the full plastic moment capacity of the beam, develop the composite behavior of the column, and provide good ductility under seismic loading (Fukumoto, 2005). However, these connections are regarded as very expensive for U.S. practice, because complete joint penetration (CJP) welds are required around the full perimeter of the tube at four locations at each beam-column connection. Figure 11b shows an alternate penetrating connection for seismic resisting moment frames. This connection simply requires an I-shaped slot through the steel tube so that the steel beam can penetrate and engage the concrete fill. The tube must still be welded to the beam, but the weld is quicker and more economical than the four CJP tube welds required for the internal diaphragm connection. This connection was experimentally investigated (Schneider, 1996), and it has been shown to provide excellent ductility and inelastic performance combined with the full plastic resistance of the beam and the full composite resistance of the CFT member. It is a much more economical connection. However, there may be greater difficulty in achieving geometric control during fabrication and erection of this connection, because of less clear and precise fit-up points for the connection.

External connections such as shown in Figure 12 are possible, but in general their performance is inferior to the penetrating connections used with circular CFT. Reasonable performance has been achieved with rectangular CFT and through-bolted connections, such as illustrated in Figure 13. The through bolts in these connections also provide some binding action to limit relative slip between the steel and concrete, and good performance has been achieved (Ricles et al., 2004). However, care must be taken in designing these connections for seismic demands to ensure that the controlling yield mechanism is not the tensile yield capacity of the through bolts, since this yield deformation can lead to early tensile fracture of the bolts (Kanatani et al., 1988).

Concentrically braced frames (CBFs) are commonly used for seismic design, because they economically provide lateral resistance and stiffness needed to ensure good performance during small to moderate seismic loads. CBFs are more commonly used for seismic design in the United States in recent years, because of the problems noted with steel moment resisting frames during the 1994 Northridge earthquake. These problems were resolved through research performed during the SAC Steel Project (FEMA, 350; FEMA, 355), but steel moment resisting frames are today more expensive and complex than prior to the 1994 earthquake. CFT columns are very suitable for CBFs, because there are large axial load demands in the columns of braced frames, and CFT members have large axial stiffness and resistance capacities. However, there is significant difficulty in connecting the CFT column to the other structural members. The penetrating gusset plate connection in Figure 11c has been investigated in a recent research study (MacRae, et al., 2004). This connection has been shown to provide good force transfer and seismic performance of the system without any additional shear connectors or other mechanical stress transfer components inside the tube. This connection is also a penetrating connection and works by direct bearing through edge of the gusset on well-confined concrete. Ribs have been attached to the side of the plate or holes may be cut into the plate to increase bearing resistance where needed, and this connection appears to offer the benefits of direct bearing with an economical connection configuration.

The previous discussion has shown that connections with one or more penetrating elements can provide full composite action negating the need for additional mechanical shear connectors. The stiff penetrating elements block, bind and restrain the concrete fill against significant slip movement. The penetrating elements provide direct bearing force transfer to both the steel and concrete fill, and the resulting restraint provides natural bond stress (both frictional

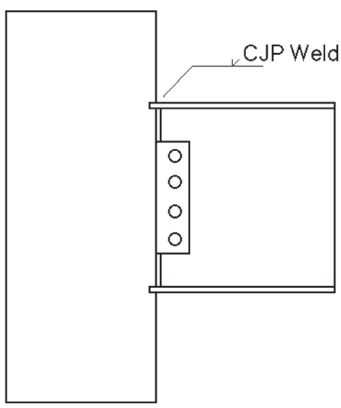

Fig. 12. Typical external steel-to-steel CFT connection.

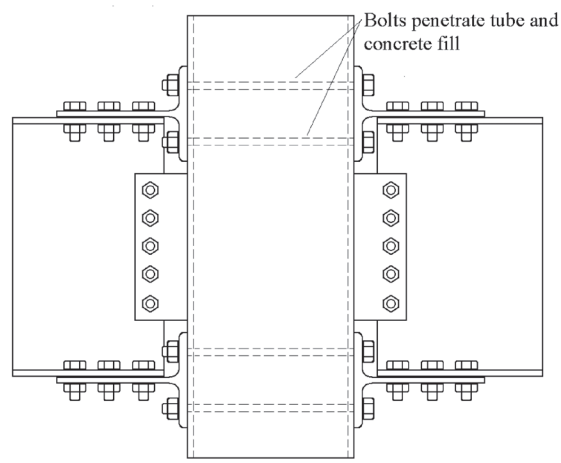

Fig. 13. Through-bolted connection for rectangular CFT.

resistance and adhesion) over a length of the tube. As a result, there is a great deal of interaction between the composite action and bond stress issues and the connections used to join CFT columns to other structural element.

Circular tubes provide significantly better performance as CFT members than rectangular tubes, because of better confinement of the concrete fill, significantly larger natural bond stress, and reduced potential for local buckling and deterioration of the tube. These observations are documented in research results such as Figure 3a, and large body of research performed in Japan and other countries (Morino, 1999). However, the circular geometry is not well adapted to many commonly used structural connections. Research in progress at the University of Washington is aimed at developing improved connections for circular CFT columns in structural applications to take advantage of their promising engineering properties. Several connections are under investigation with this research program, but a primary portion of the study has focused on CFT column-to-footing connections. CFT columns and bridge piers may have large plastic rotation demands at the column-to-foundation and the column-to-pier cap connections. Therefore, robust connections that are capable of transferring the full moment capacity and sustaining cyclic plastic rotation demands are required in high seismic zones.

A new CFT column-to-foundation connection has been proposed (Kingsley, 2005; Kingsley et al., 2005), and is illustrated in Figure 14. The connection is a hybrid of the embedded and base plate connections, and it has been evaluated experimentally using the test setup illustrated in Figure 5b. The proposed connection employs a annular ring or flange, which is welded to the base of the steel tube with a complete joint penetration weld as shown in Figure 15. It is a ring, rather than an end plate, and the ring extends slightly into the tube to provide blocking and binding to the concrete fill, as described earlier in this paper. There are no reinforcement or dowels within or penetrating into the tube. Therefore, the embedded tube and annular ring are solely responsible for the connection force and moment transfer. The connection offers economy, efficiency and continuity of the concrete fill of the CFT pier with the foundation not afforded by full plate connections. The flange serves as a temporary attachment for the tube, while concrete is being placed, and it also serves as a stress transfer rib for the composite connection.

The construction procedure is accomplished in one of two ways. First, the connection can be constructed by placing the footing in two lifts as illustrated in Figure 14a. The lower lift is cast, and the tube is then temporarily attached to the lower lift by anchor bolts. The remainder of the footing and concrete fill are cast in a second lift. The footing is reinforced with shear and flexural reinforcement as required for normal foundation design. This CFT connection was tested and excellent seismic performance resulted, as illustrated in Figure 16.

As an alternative, the footing can be cast in a single operation, and the connection can be constructed as illustrated in Figure 14b. With this alternative, a recess is formed into the concrete footing with light gauge corrugated metal. This recess must be of slightly larger diameter than the outside diameter of the annular ring for the steel tube. The tube is then fit into the recess and temporarily anchored as shown in the top part of Figure 14b. Fiber-reinforced grout is used to fill the recess around the perimeter of the tube, and the concrete fill is placed in the tube, using either traditional or self-consolidating concrete. This connection also has been tested and provides similar or superior performance to that

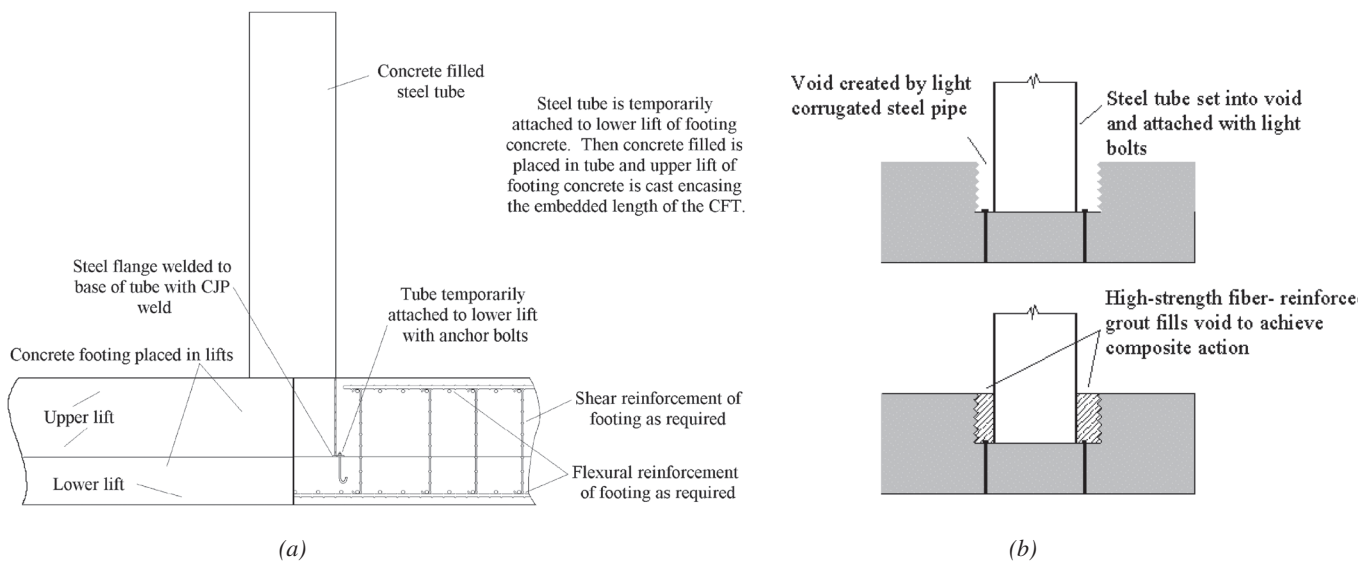

Fig. 14. Proposed CFT foundation connections: (a) embedded type; (b) separated construction type.

illustrated in Figure 16. This alternate connection permits the use of CFT columns or piers with precast caps, although the precast cap options have not been experimentally evaluated.

The experimental research results show that the CFT pier or column member and connection developed good ductility with large energy dissipation and inelastic deformation capacity. The connection developed the full composite resistance and ductility of the CFT column. Yielding occurred within the steel tube, and ultimate failure was buckling of the steel tube and tearing of the steel at the buckled region. This failure did not occur until nearly 8% displacement drift. The photo in Figure 16b shows the CFT column at approximately 6% drift; the tube has buckled but still had minimal deterioration in resistance. The tube retained its integrity through large inelastic deformations, and there were no signs of damage until nearly 4% drift. Thus, the CFT pier is expected to meet serviceability performance limit states at even relatively large drift levels. In comparison, damage to a reinforced concrete pier would be expected at drift ratios of 1.5% to 2%, with significant strength deterioration at 5 to 6% drift (Kingsley et al., 2005). It should be emphasized that the tube is quite slender with relatively thin walls and high strength steel (d/t = 80, and $F_y \approx$ 525 MPa or 76 ksi). Local buckling is well controlled, and excellent cyclic inelastic deformation capacity is achieved. Connections of this type allow CFT members, which may not only improve construction time and costs, but structural performance as well.

Fig. 15. Photo of welded annular flange.

RELEVANCE TO AISC SPECIFICATION

Chapter I of the AISC *Specification* (2005b) is the primary source of design information for CFT columns in the United States. The current provisions recognize that shear transfer is required between the steel tube and the concrete fill. It requires that the transfer be accomplished by "direct bond interaction, shear connection, or direct bearing," but no guidance in assessing the bond interaction is provided. This paper shows that circular CFT with relatively large bending

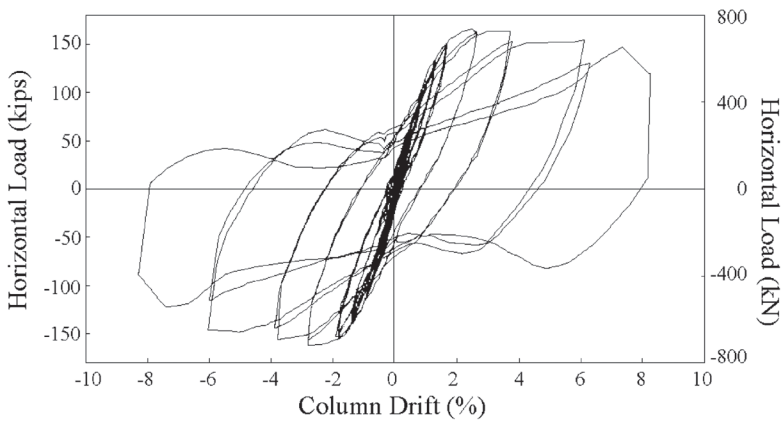

(a)

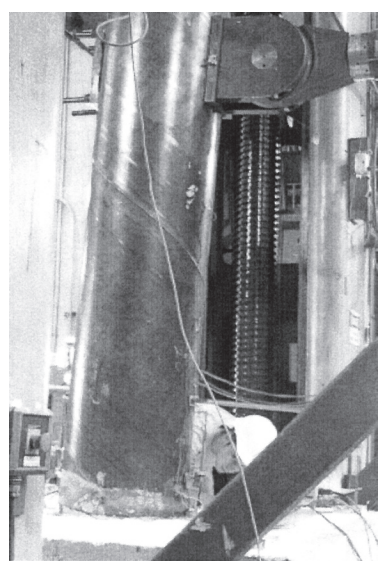

(b)

Fig. 16. Experimental behavior from typical connection test: (a) column shear vs. story drift; (b) photo of specimen at large drift levels.

moments will likely have enough bond stress or "direct bond interaction" to achieve full composite behavior. This paper also suggests that CFT with primarily axial load will require "direct bearing" such as provided by penetrating connections or annular rings unless the diameter and *d*/*t* ratio of the tube are small, because of limitations and variability in bond stress.

The AISC *Specification* makes little distinction between circular and rectangular CFT other than for slenderness limits. Circular tubes also better confine the concrete fill and have greater resistance to local buckling of the tube. Hence, circular CFT offers clear advantages to rectangular CFT, although circular CFT may result in greater difficulty with connections to other structural members. The AISC *Specification* recognizes the greater confinement provided by circular CFT by permitting $0.95f'_c$ for the concrete strength rather than the $0.85f'_c$ permitted for rectangular CFT and other applications. However, Figure 3a clearly shows that circular CFT have much larger bond stress transfer capability and more easily develop full composite action, and no distinction is made for this difference in the provisions.

Finally, the AISC *Specification* limits circular CFT columns to a ratio of $0.15E/F_y$, and with a nominal 70-ksi (480-MPa) yield stress, the slenderness limit is 62. However, this paper has summarized a number of tests with yield stress in excess of 70 ksi (480 MPa) and tube slenderness of 80. The specimens performed well with full composite resistance and good ductility as shown in Figures 6 and 16. Hence, it is reasonable to suggest that relaxation of this slenderness limit may be possible for some applications.

SUMMARY AND CONCLUSIONS

This paper has provided an overview of composite construction with CFT piers and columns. The focus of this work has been on inelastic cyclic deformation capacity and seismic design, but the conclusions apply equally well to other applications. The paper has summarized a range of past articles and reports as well as two recent experimental research efforts. The bond stress and interaction between the steel and concrete are the primary focus of this work. A number of key issues can be noted.

1. Shear transfer between the inside wall of the steel tube and the concrete fill is essential to providing optimal performance and composite behavior of CFT structural components. The natural bond stress achieved between the steel and concrete is contributed by friction, mechanical interlock and adhesion between the two materials. However, in the absence of mechanical shear transfer connectors, friction is by far the dominate effect.

2. Circular CFT offers significant benefits over rectangular CFT, since circular CFT provides better confinement of concrete fill, greater bond stress between the steel and concrete, and greater resistance to local buckling and deterioration of inelastic response during cyclic loading. These facts are documented by experimental comparisons such as Figure 3a and significant body of published research. However, the geometry of circular CFT results in greater difficulty in forming connections between the CFT member and other structural elements.

3. In the absence of mechanical restraint and in the presence of significant axial load, the utility of frictional bond stress is limited to relatively stocky (small *d*/*t* ratios), small-diameter CFT elements, because the benefits of friction are lost due to concrete shrinkage and the smaller radial stiffness of thin wall tubes. Past research (Roeder et al., 1998) shows relatively small bond stress capacity with diameters and *d*/*t* ratios greater than 12 to 16 in. (300 to 400 mm) and 50 or 60, respectively. However, friction is invariably adequate for circular CFT members with large bending moments, because binding action between the concrete fill and the steel tube develops large frictional transfer. Further, the detrimental effect of large diameter and large slender ratio is not apparent with large bending moments. As a result, it is recommended that the bond stress be checked only for axial load transfer.

4. If the natural (frictional) bond stress is inadequate to accomplish the required axial force transfer, mechanical transfer is required. Shear studs are commonly used in composite construction, but they are not a desirable method for transferring shear in CFT members, because shear studs are relatively flexible and they do not work well with natural bond. If shear studs are used, they should be conservatively designed to transfer the entire axial load component. Stiff, annular rings are better shear transfer elements for CFT, but they are difficult to install on the inside of the tube.

5. It is shown that a wide range of penetrating connections offer the benefits of annular rings. These penetrating connections provide direct bearing of the steel on the concrete. The concrete is well confined by the steel tube, and very large bearings stresses can be developed. Several different connections were described and summarized.

6. A brief summary of a new CFT column-to-foundation connection was provided. The connection is economical, simple and rapidly constructed. It provides excellent ductility and inelastic deformation capacity. It also offers promise of the use of precast concrete cap beams with the CFT members. Work continues on this connection.

7. Finally, the experiments described in this paper were all performed on spirally welded high-strength steel tubes ($F_y \approx 525$ MPa or 76 ksi), relatively large diameters (20 in. or 405 mm), thin walls, and relatively large d/t ratios ($d/t = 80$). These tubes are well outside the range currently permitted for seismic design in U.S. design provision. Despite this, the tubes performed well. They achieved considerable ductility and inelastic deformation capacity. Local buckling occurred, but it occurred at relatively large deformations after the concrete had crushed. Ultimate failure occurred as tearing of the steel in the buckled area. The spiral welds did not have a detrimental effect on the inelastic performance of the tube, as long as the spiral welds were of good quality with a matching metal tensile strength, and good CVN toughness characteristics.

ACKNOWLEDGMENTS

The past work summarized in this paper was completed under NSF Grants CMS 9520233 and CMS-9905797, and more recent research was sponsored by the Army Research Laboratory and was accomplished under Cooperative Agreement Number DAAD19-03-2-0036. The views and conclusions contained in this document are those of the authors and should not be interpreted as representing the official policies, either expressed or implied, of the Army Research Laboratory or the U.S. Government.

REFERENCES

ACI 318 (2005), *Building Code Requirements for Structural Concrete (ACI 318-05) and Commentary (ACI 318R-05)*, American Concrete Institute, Farmington Hills, MI.

AISC (2005a), *Seismic Provisions for Structural Steel Buildings*, American Institute of Steel Construction, Chicago, IL.

AISC (2005b), *Steel Construction Manual*, 13th ed., American Institute of Steel Construction, Chicago, IL.

ATC (1992), *ATC-24 Guidelines for Testing Steel Components*, Applied Technology Council, Redwood City, CA.

FEMA 350 (2000), *Recommended Seismic Design Criteria for New Steel Moment-frame Buildings*, Federal Emergency Management Agency, Washington, DC.

FEMA 355D (2000), *State of the Art Report on Connection Performance*, C. Roeder, Team Leader, Federal Emergency Management Agency, Washington, DC.

Fukumoto, T. (2005), "Steel-beam-to-concrete-filled-tube-column Moment Connections in Japan," Korean Society of Steel Construction, *International Journal of Steel Structures,* Vol. 5, No. 4, pp. 357–65.

Furlong, R.W. (1967), "Strength of Steel-Encased Concrete Beam-Columns," ASCE, *Journal of Structural Division*, Vol. 93, No. ST5.

Furlong, R.W. (1986), "Design of Steel-Encased Concrete Beam-Columns," ASCE, *Journal of Structural Division*, Vol. 94, No. ST1.

Han, L-H and Yang, Y-F (2001), "Influence of Concrete Compaction on the Behavior of Concrete Filled Steel Tubes with Rectangular Sections," *Advances in Structural Engineering*, Vol. 4, No. 2, 1 April 2001, pp. 93–100(8).

Kanatani, H., Tabuchi, M., Kamba, T., Hsiaglien, J. and Ishikawa, M. (1988), "A Study on Concrete Filled RHS Column to H-Beam Connections Fabricated with HT Bolts in Rigid Frames," *Composite Construction in Steel and Concrete*, ASCE Special Publication, ASCE, New York, NY.

Kingsley, A.M. (2005), "Experimental and Analytical Investigation of Embedded Column Base Connections for Concrete Filled High Strength Steel Tubes," a thesis submitted in partial fulfillment of the MSCE, University of Washington, Seattle, WA.

MacRae, G.W., Roeder, C.W., Gunderson, C. and Kimura, Y. (2004), "Brace-Beam-Column Connections for Concentrically Braced Frames with CFT Columns," ASCE, *Structural Engineering Journal*, Vol. 130, No. 2, pp. 233–243.

Morino, S. (1999), "Recent Developments on CFT Column Systems—U.S.-Japan Cooperative Earthquake Research Program," *Proceedings 6th ASCCS International Conference on Steel-Concrete Composite Structures*, Vol. 1, pp. 531–538, edited by Y. Xiao and S. A. Mahin, Los Angeles, CA.

Morishita, Y., Tomii, M. and Yoshimura, (1979a), "Experimental Studies on Bond Strength in Concrete Filled Circular Steel Tubular Columns Subjected to Axial Loads," *Transactions of the Japan Concrete Institute*, Vol. 1, pp 351–358.

Morishita, Y., Tomii, M. and Yoshimura, (1979b), "Experimental Studies on Bond Strength in Concrete Filled on Square and Octagonal Steel Tubular Columns Subjected to Axial Loads," *Transactions of the Japan Concrete Institute*, Vol. 1, pp. 359–366.

Morishita, Y., Youichi, and Tomii, M., (1982), "Experimental Studies on Bond Strength Between Square Steel Tube and Encased Concrete Core Under Cyclic Shearing Force and Constant Axial Loads," *Transactions of the Japan Concrete Institute*, Vol. 4, pp. 115-122.

Murrow, D. (1997), "Investigation of Force Transfer in Eccentrically Loaded Composite Columns," unpublished report, Department of Civil Engineering, University of Washington, Seattle, WA.

Ricles, J.M., Peng, S.W. and Lu, L.W. (2004), "Seismic Behavior of Composite Concrete Filled Tubes Column Wide-Flange Beam Moment Connections," ASCE, *Journal of Structural Engineering*, Vol. 130, No. 2, pp. 223–232.

Roeder, C.W., Cameron, B. and Brown, C.B., (1998), "Composite Action in Concrete Filled Tubes," ASCE, *Journal of Structural Engineering*, Vol. 125, No. 5, pp. 747–756.

Santos, P. (1997), "Analysis of Bond Stress Using ANSYS," a thesis submitted in partial fulfillment of MSCE degree, University of Washington, Seattle, WA.

Shakir-Khalil, H. (1991), "Bond Strength in Concrete-Filled Steel Hollow Section," *International Conference on Steel and Aluminum Structures*, ICSAS 91, 22–24, pp. 157–168.

Shakir-Khalil, H. (1993a), "Pushout Strength of Concrete-Filled Steel Hollow Sections," *The Structural Engineer*, Vol. 71, No. 13, pp. 230–233.

Shakir-Khalil, H. (1993b), "Resistance of Concrete-Filled Steel Hollow Tubes to Pushout Forces," *The Structural Engineer*, Vol. 71, No. 13, pp. 234–243.

Schneider, S.P. (1996), "Connections to Concrete-Filled Steel Tubes," *Report UILU-ENG-96-2011*, Department of Civil Engineering, University of Illinois, Urbana.

Thody, R. (2006), "Experimental Investigation of the Flexural Properties of High-Strength Concrete Filled Steel Tubes," a thesis submitted in partial fulfillment of the MSCE, University of Washington, Seattle, WA.

Tomii, M. (1984), "Bond Check for Concrete-Filled Steel Tubular Columns," *Composite and Mixed Construction*, ASCE Special Publication, New York, NY, pp. 195–214.

Virdi, K.S. and Dowling, P.J. (1975), "Bond Strength in Concrete Filled Circular Steel Tubes," *CESLIC Rep. CC11*, Engineering Structural Laboratory, Civil Engineering Department, Imperial College, England.

Williams, T. (2006), "Experimental Investigation of High Strength Concrete Filled Steel Tubes in Embedded Column Base Foundation Connections," a thesis submitted in partial fulfillment of the MSCE, University of Washington, Seattle, WA.

Response of Concrete-Filled HSS Columns in Real Fires

VENKATESH K.R. KODUR and RUSTIN FIKE

ABSTRACT

The use of concrete filling offers a practical alternative for achieving the required fire resistance in steel hollow structural section (HSS) columns. However, the current prescriptive-based approach has a number of constraints that in many applications restrict the utilization of concrete filling for achieving the required fire resistance. To overcome such constraints, a performance-based methodology for fire resistance design is presented in this paper. A set of numerical simulations were carried out to investigate the effect of realistic fire scenarios, loading and stability-based failure criterion on the fire resistance of concrete-filled HSS columns with lengths ranging from 3.8 m (12.5 ft) to 10 m (32.8 ft). It is demonstrated that by adopting a performance-based approach, it is possible to achieve the required fire resistance in CFHSS columns in most practical situations.

Keywords: column stability, hollow structural sections, standard fire, design fire, concrete-filled steel tubes, fire resistance, fire and temperature effects, performance-based design.

BACKGROUND

Steel hollow structural sections (HSS) are very efficient in resisting compression, torsional and seismic loads and are widely used as compressions members in the construction of framed structures. Fire safety is one of the primary considerations in the design of high-rise buildings, and hence, building codes specify fire protection requirements for HSS columns to maintain overall structural stability in the event of fire. Providing such external fire protection to HSS columns involves additional cost, reduces aesthetics, increases weight of the structure, and decreases usable space. Also, durability of fire proofing (adhesion to steel) is often a questionable issue, and hence, requires periodic inspection and regular maintenance, which in turn, incurs additional costs during the lifetime of the structure (FEMA, 2002; NIST, 2005).

Often these HSS sections are filled with concrete to enhance their stiffness, torsional rigidity and load-bearing capacity. The two components of the composite column complement each other ideally. The steel casing confines the concrete laterally, allowing it to act as in tri-axial compression and develop its optimum compressive strength, while the concrete, in turn, enhances resistance to elastic local buckling of the steel wall, and global buckling of the column. In addition, a higher fire resistance is obtained without using external fire protection for the steel, thus increasing the usable space in the building and removing the need for application and maintenance of the external fire protection. Properly designed concrete-filled columns can lead economically to the realization of architectural and structural design with visible steel, without any restrictions on fire safety (Kodur and Lie, 1995a; Klingsch and Wuerker, 1985; Twilt et. al., 1996).

Design guidelines for achieving fire resistance through concrete filling have been incorporated into codes and standards (ASCE, 1999; AISC, 2005; NBC, 2005). However, the current fire guidelines are limited in scope and restrictive in application since they were developed based on the standard fire test from ASTM E-119, *Standard Methods for Fire Tests of Building Construction and Materials* (ASTM, 2007). Hence, they are valid only for the standard fire exposure conditions and for column lengths dictated by the capacity of available testing furnaces. In many applications, such as atriums, schools and airports, where long spans of exposed steel are highly desired, the current prescriptive provisions cannot be applied due to limitations on column size. Thus, designers cannot take advantage of the intrinsic fire resistance present in concrete-filled steel columns.

This paper presents a performance-based methodology for fire safety design of concrete-filled HSS (CFHSS) columns. A review of the fire performance of CFHSS columns is presented, and the drawbacks and limitations of the current fire resistance evaluation approaches are discussed. Results from a numerical study on a set of CFHSS columns exposed to various fire and loading scenarios are presented. The analysis was carried out using finite element–based computational

Venkatesh K.R. Kodur, Professor, Department of Civil and Environmental Engineering, 3546 Engineering Building, Michi-gan State University, East Lansing, MI, 48824 (corresponding author). E-mail: kodur@egr.msu.edu

Rustin Fike, Graduate Student, Department of Civil and Environmental Engineering, 3546 Engineering Building, Michigan State University, East Lansing, MI, 48824. E-mail: fikerust@msu.edu

model SAFIR, wherein the material and geometric nonlinearity, and stability-based failure criterion are considered. Results from the analysis are used to present a framework for a performance-based fire engineering methodology. It is demonstrated that fire resistance in HSS columns in the full practical range can be achieved through concrete filling.

PERFORMANCE-BASED DESIGN

Recently there has been an impetus to move toward a performance-based approach for fire safety design (Meacham and Custer, 1992; Kodur, 1999). This is mainly due to the fact that the current prescriptive-based approach has serious limitations and does not provide alternate, cost-effective and innovative solutions. There are two basic methods by which performance-based fire safety design can be accomplished: tests can be performed wherein the structural performance of the system to be built is evaluated, or numerical/computational simulations can be used to evaluate the system to be built. Due to the cost, time and effort associated with full-scale fire testing, the first option is mostly used to validate numerical models. The validated models can then be used to undertake performance-based fire safety design. The most important factors to be considered in any performance-based fire safety design are fire scenario, load level, failure criterion and geometric conditions (Parkinson and Kodur, 2007). These main components are discussed in the following sections.

Fire Scenario

The current practice of evaluating fire resistance of CFHSS columns is based on standard fire tests or models, in which the column is exposed to a standard fire as specified in standards such as ASTM E-119 or ISO 834 (ISO, 1975). While standard fire resistance tests are useful benchmarks to establish the relative performance of different CFHSS columns, they should not be relied upon to determine the survival time of CFHSS columns under realistic fire scenarios. Additionally, the standard heating condition has little resemblance to the often less severe heating environments encountered in real fires.

Unlike standard fires, design fires are derived based on different combinations of fuel load and ventilation scenarios in compartments. In the standard fires (ASTM E-119 fire and hydrocarbon fire) (ASTM, 2007; ASTM, 2001), the fire severity is the same (irrespective of compartment characteristics), and temperature increases with time throughout the fire duration with no decay phase. However, in real fires, the fire severity is a function of compartment characteristics, such as ventilation, fuel load and lining materials, and there is a decay phase following the initial growth phase as shown in Figure 1 (Magnusson and Thelandersson, 1970). Often, in the decay phase, the cross section of the column enters the cooling phase, in which the steel recovers part of its strength and stiffness, leading to an enhanced fire resistance that allows the column to withstand compartment burnout.

Figure 1 shows time-temperature curves for two standard fire exposures (ASTM E-119 and ASTM E-1529) (ASTM, 2007; ASTM, 2001) and three levels of design fires: severe, medium and mild. To simulate a "mild" fire, a ventilation factor of 0.04 and a fuel load of 200 MJ/m^2 were chosen (FV04-200), while for a "medium" fire, a ventilation factor of 0.12 was chosen with a fuel load of 900 MJ/m^2 (FV12-900). A "severe" fire was simulated using a ventilation factor of 0.08, and a fuel load of 800 MJ/m^2 (FV08-800). Specific time-temperature relationships for a given compartment can be developed through simple spreadsheet calculations or retrieved from published tables (Magnusson and Thelandersson, 1970) as was done in this study.

Load Ratio

The current provisions in codes of practice for evaluating fire resistance are generally based on a load ratio of about 50%. Load ratio is defined as the ratio of the applied load on the column under fire conditions to the strength capacity of the column at room temperature. Load ratio depends on many factors including the type of occupancy, the dead load to live load ratio, and the safety factors (load and capacity factors) used for design under both room temperature and fire conditions. The loads on the column under fire exposure scenarios can be estimated based on the guidance given in ASCE 7 standard (ASCE, 2005) (1.2 dead load + 0.5 live load or through actual calculations based on different load combinations). Based on specifications in ASCE 7 (ASCE, 2005) and the AISC *Manual* (AISC, 2005), for typical dead to live load ratios (in the range of two to three), the loads on a CFHSS column under fire scenario can range between 30% and 50% of its ultimate capacity. The low load ratio effective

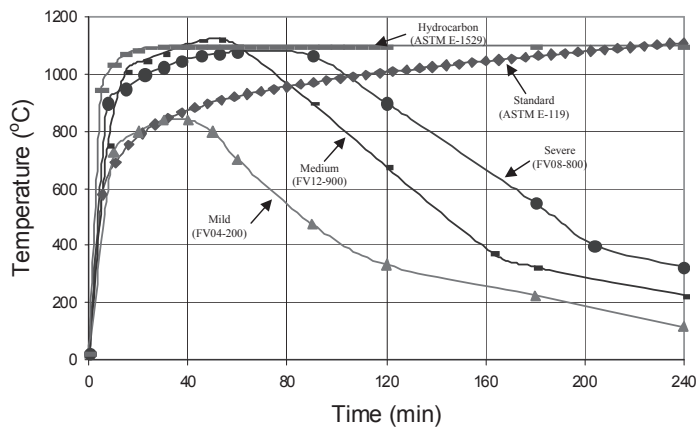

Fig. 1. Time-temperature relationships for various fire scenarios.

under fire conditions is mainly due to the fact that fire is a rare event so only service loads (with reduced live loads) are considered in the analysis.

Load ratio could presumably influence the fire resistance of CFHSS columns calculated based on realistic failure criteria. Thus, for innovative, realistic and cost-effective performance-based fire safety design, it is important to evaluate the fire resistance of CFHSS columns based on actual load levels.

Failure Criterion

For evaluating fire resistance of steel structures, a limiting temperature criterion is often used to define failure. It is commonly assumed that once the steel section reaches a critical temperature of 538 °C (1000 °F), approximately 50% of the room temperature strength is lost (Eurocode, 2005a) and failure is eminent. While sufficient for traditionally protected steel sections, the effect of the concrete core is not properly captured by the limiting temperature criterion. To overcome this drawback, strength and stability limit states of the column under fire conditions need to be considered. Depending on factors such as the support conditions and overall column length, buckling or crushing could occur well after the limiting (critical) temperature of 538 °C (1000 °F) is reached. In addition, CFHSS columns can fail locally (without collapse) due to local crushing of the concrete on the inside, or local buckling of the steel wall (Kodur, 2005; Kodur and Lie, 1996; Kodur and Lie, 1997). Thus, local stability should also be accounted for in the analysis.

STATE OF THE ART

Alternate approaches for achieving fire resistance in HSS columns have been studied in the past three decades. Methods such as filling the HSS columns with liquid (water) and concrete are among the most popular approaches studied by researchers (Kodur and Lie, 1995a; Bond, 1975; Klingsch and Wittnecker, 1988). However, the use of concrete filling is the most attractive and feasible proposition developed thus far.

Experimental and Numerical Studies

Fire resistance tests on CFHSS columns were predominantly carried out at the National Research Council of Canada (NRCC), a few organizations in Europe, and more recently in China. The experimental program at NRCC consisted of fire tests on about 80 full-scale CFHSS columns (Kodur and Lie, 1995a, 1995b; Lie and Chabot, 1992; Lie and Caron, 1988; Lie and Irwin, 1991). Both square and circular HSS columns were tested, and the influence of various factors including type of concrete filling, concrete strength, intensity of loading, and column size were investigated under the ASTM E-119 standard fire exposure. The tests reported by European and Chinese studies (Klingsch and Wittbecker, 1998; Grandjean et. al., 1981; FCSA, 1989; Han and Lin, 2004) are similar to NRCC tests, but the fire exposure was that of the ISO 834 (ISO, 1975) standard fire; which has a time-temperature curve similar to that of ASTM E-119.

The numerical studies, primarily carried out at NRCC, consisted of developing mathematical models for predicting the fire behavior of circular and square CFHSS columns (Kodur, 1997; Lie and Chabot, 1991; Lie and Kodur, 1996). In these models, the fire resistance is evaluated in various time steps, consisting of the calculation of the fire temperature, the temperatures in the cross-section of the column, its deformations, its strength during exposure to fire, and finally, its fire resistance. Full details on the development and validation of these models are given in Kodur and Lie (1997), Lie and Chabot (1992) and Kodur (1997).

Data reported from NRCC tests and numerical studies can be used to illustrate the behaviour of concrete-filled HSS columns under standard fire conditions. Figure 2 shows the axial deformation as a function of time for three typical HSS columns, each filled with a different type of concrete filling, namely, plain concrete, steel-fiber-reinforced concrete, or bar reinforced concrete (Kodur and Lie, 1995b). The three columns were of similar size and were subjected to similar load levels, hence the results can be used to illustrate the comparative behavior of the three types of concrete filling.

In CFHSS columns prior to fire exposure, the applied load on the composite column is carried by both the concrete and the steel. When the column is exposed to fire, steel carries most of the load during the early stages because the steel section expands more rapidly than the concrete core. As time progresses and temperatures increase, the steel section gradually yields due to loss of strength in steel at elevated temperatures, and the expansion phase gives way to a contraction

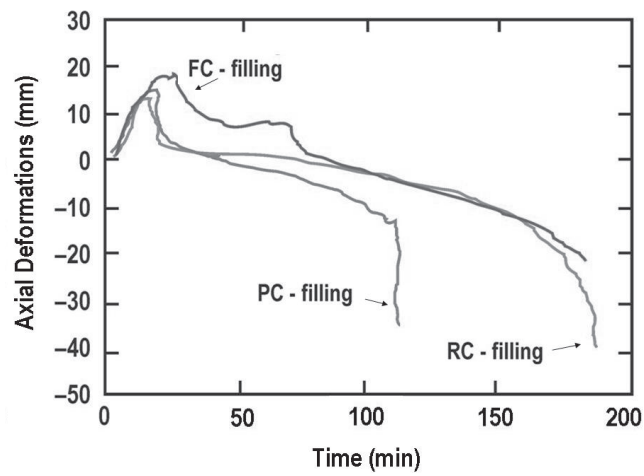

Fig. 2. Axial deformation in CFHSS columns as a function of time.

phase after about 20 minutes of fire exposure. At this stage, the concrete starts to carry an increased portion of the load. As fire progresses, the strength of concrete also deteriorates to a level where the column strength is less than the applied load, and failure occurs in the column. The elapsed time from ignition to failure is the fire resistance of the column.

It can be seen in Figure 2 that the deformation behavior of HSS columns filled with bar and steel-fiber-reinforced concrete is similar in the expansion zone to that of columns filled with plain concrete. The initial slightly higher deformation in the steel-fiber-reinforced concrete-filled HSS column could be attributed to higher thermal expansion of steel-fiber-reinforced concrete. In the contraction phase, the behavior of HSS columns filled with bar- and steel-fiber-reinforced concrete is significantly different than columns filled with plain concrete due to the contraction in these columns being slower. This can be attributed to slower loss of strength and stiffness in the concrete due to the presence of steel reinforcement. Consequently, this results in higher fire resistance in HSS columns filled with steel-fiber- and bar-reinforced concrete as compared to that of columns filled with plain concrete.

Design Equation and Method for Evaluating Fire Resistance

Based on the experimental and numerical studies reported in literature (Kodur and Lie, 1996; Kodur, 1997; Lie and Stringer, 1994), it was found that the parameters with the most influence on fire resistance of CFHSS columns are type of concrete filling (plain, bar-reinforced, and fiber-reinforced), outside diameter or width of the column, load on the column, effective length of the column, concrete strength, and type of aggregate. Using this as the basis, the following unified design equation has been developed to calculate the fire resistance of circular and square HSS columns filled with any of the three types of concrete (Lie and Stringer, 1994; Kodur, 1999; Kodur and McKinnon, 2000):

$$R = f\frac{(f_c' + 20)}{(KL - 1000)}D^2\sqrt{\frac{D}{C}} \quad (1)$$

where R = fire resistance in minutes; f_c' = specified 28-day concrete strength in MPa; D = outside diameter or width of the column in mm; C = applied load in kN; K = effective length factor; L = unsupported length of the column in mm; f = a parameter to account for the type of concrete filling (plain, steel-fiber-reinforced, or bar-reinforced concrete), the type of aggregate used (carbonate or siliceous) in concrete, the percentage of reinforcement, the thickness of concrete cover, and the cross-sectional shape of the HSS column (circular or square), values of which can be found in Lie and Kodur (1996).

Equation 1 has been validated by comparing the predictions from the equation with data from fire tests conducted at various laboratories (Twilt et. al., 1996; Kodur, 1997; Lie and Kodur, 1996). The fire resistances obtained using the equation are conservative (about 10–15%) compared to those obtained from the tests, particularly for fire resistances over three hours.

Eurocode 4 (Eurocode, 2005b) also presents a method by which the fire resistance of CFHSS columns exposed to standard fire can be determined. The analysis is composed of two steps: determination of the temperature distribution and calculation of the field buckling load at the temperature previously determined. For further details on the calculation method presented in Eurocode 4, the reader is directed to that reference (Eurocode, 2005b).

Limitations

Both the design equation and the Eurocode method just presented, though providing a convenient way of evaluating fire resistance of CFHSS columns, have a number of limitations—the greatest of which is that they are only applicable for the prescriptive-based standard fire scenario, in which no consideration is given to a decay phase. This is a serious limitation since the high fire performance that can be achieved using CFHSS columns under most design fire scenarios cannot be realized. As an illustration, plain concrete-filled HSS columns can only provide fire resistance of an hour or less in some situations. While recognizing that columns filled with steel- and bar-reinforced concrete perform better than columns filled with plain concrete, the fire rating assigned to these columns is still markedly less than the fire resistance which can be obtained in design fire scenarios. In addition, the application of Equation 1 is limited to CFHSS columns up to only 4.5 m (14.75 ft) in length, since the equation was derived based on test data which ranged in length from 2.5 to 4.5 m (8.2 to 14.75 ft) (restricted by furnace construction). In applications such as airports, schools, atriums and

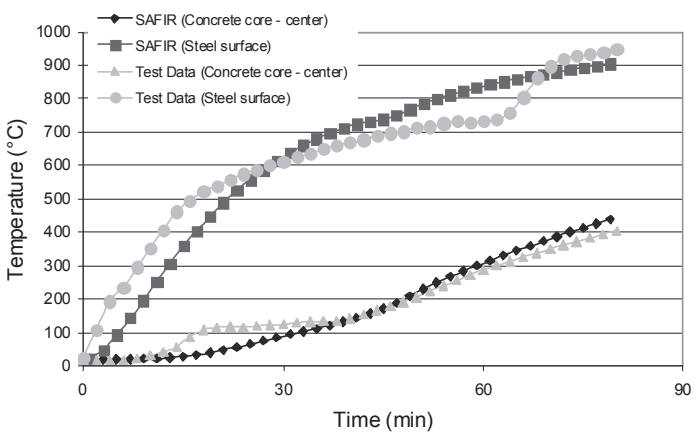

Fig. 3. Comparison of temperatures from SAFIR with test data for column SP-178.

Table 1. Current Design Limitations and Range of Parameters Encountered in Practical Applications		
Parameter	**Current Limitation**	**Practical Applications**
Column shape	square and circular	square, circular and rectangular
Column size	400 mm	600 mm and beyond
Column length	4.5 m	6–10 m
Concrete strength	55 MPa	100 MPa
Fire scenarios	ASTM E-119	design fires and hydrocarbon fires
Load level	strength of concrete core	service loads
Eccentric loads	not allowed	always present

hotels, columns are generally longer than 4.5 m (14.75 ft), and hence designers cannot capitalize on the intrinsic fire resistance present in CFHSS columns.

The various limitations on the applicability of design Equation 1 are presented in Table 1, along with the range of variables encountered in most practical applications. It can be seen that the current design equation, in addition to the limitations on length and fire exposure, is valid only over a narrow range of column parameters such as diameters up to 400 mm (15.75 in.), concrete strengths up to 55 MPa (8.0 ksi), and concentric loads. Therefore, design Equation 1, and relevant solutions, cannot practically be used under the recently introduced performance-based codes, which provide rational, cost-effective and innovative fire safety solutions. Only in rare circumstances (such as the Orange County Performing Arts Center in California) has performance-based fire design incorporating design fires been undertaken for utilizing CFHSS columns (Chen and Gemeny, 2004).

The previously stated limitations restrict architects and designers from taking advantage of high fire resistance ratings (and other advantages) that can be achieved through CFHSS columns. Also, the limitations of the preceeding research for only ASTM E-119 fire exposure hinders the use of HSS columns in offshore structures and oil platform applications. Thus, the full potential for the use of CFHSS columns has not been realized.

NUMERICAL STUDIES

To overcome some of the previously stated limitations, a numerical study was carried out to develop an approach for performance-based fire resistant design of CFHSS columns. The analysis was carried out using finite element-based computer program SAFIR, and the fire response of CFHSS columns was simulated under various fire and loading scenarios. Some of the details associated with the analysis are presented here.

Computer Program

The computer program SAFIR, developed at the University of Liege in Belgium, is capable of accounting for multiple materials in a cross section, both heating and cooling phase of fire exposure, large displacements, different strain components, nonlinear material properties according to Eurocode 3 (Eurocode, 2005), and residual stresses. Additionally, SAFIR allows the user to input any time-temperature relationship to facilitate the use of design fire scenarios. SAFIR has undergone extensive validation and predictions from SAFIR have been shown to closely match test data and predictions from other numerical models (Franssen, 2005; Gilvary, 1997; Talamona, 2005).

In SAFIR, the thermal and structural analyses are performed independently. For thermal analysis, 2D solid elements are used where the fire exposed sides and the exposure types are specified by the user. The thermal model in SAFIR neglects heat transfer in the longitudinal direction and assumes that every cross-section has the same temperature profile unless otherwise specified. The energy consumed for evaporation of water present in the concrete is included, but that associated with hydraulic migration within the cross-section is neglected. Additionally, due to the lack of a material model for steel-fiber-reinforced concrete within SAFIR, the thermal properties of steel-fiber-reinforced concrete were assumed to be the same as those for normal concrete (Lie and Kodur, 1996).

For structural analysis, SAFIR uses a fiber-based approach wherein each of the solid elements in the thermal model is considered as a fiber in the structural model. These fibers can have different material properties, allowing the modeling of the steel shell and steel bars in bar-reinforced concrete-filled CFHSS columns. A stress and temperature dependent stiffness matrix is established that incorporates all of the fibers. Due to the increasing temperature in the

Table 2. Summary of Test Parameters and Fire Resistance Values for CFHSS Columns						
Column Designation	Diameter or Width (mm)	Length (mm)	AISC Factored Load (kN)	Load Ratio	Fire Resistance (min.)	
					Test	SAFIR
RP-168	168.3	3810	1197	0.13	81	82
RP-273	273.1	3810	3508	0.15	143	128
RP-355	355.6	3810	5120	0.18	170	164
SP-152	152.4	3810	1409	0.20	86	74
SP-178	177.8	3810	1976	0.28	80	71
RF-324	323.9	3810	4573	0.35	199	200
RF-356	355.6	3810	6616	0.23	227	238
SF-203	203.2	3810	3506	0.26	128	121
SF-219	219.1	3810	3793	0.16	174	185
RB-273a	273.1	3810	3323	0.32	188	158
RB-273b	273.1	3810	3333	0.57	96	98
SB-203	203.2	3810	2345	0.21	150	130
SB-254a	254	3810	3405	0.42	113	110
SB-254b	254	3810	3405	0.65	70	69

column, the stiffness decreases to a point where the column can no longer support the applied load, and failure occurs. Through the use of beam elements to simulate columns, both crushing and buckling failure of the columns can be captured. The main limitation of the structural model is the assumption that there is no slip between the steel and the concrete. While the assumption of no slip will initially place higher tension on the concrete core due to the differential thermal expansion of the steel and concrete, the steel rapidly looses strength (within 20 minutes) such that during the critical portion of fire exposure this assumption does not place unrealistic loads on the concrete core. As was the case in the thermal model, SAFIR does not include a mechanical model for steel-fiber-reinforced concrete. As such, the same constitutive model was used for steel-fiber-reinforced concrete as normal concrete, with the exception that the tensile strength of the concrete was increased to account for the steel fibers. This is believed to be a conservative assumption due to the superior stiffness retention demonstrated in steel-fiber-reinforced concrete (Kodur and Harmathy, 2002; Lie and Kodur, 1996).

Test Columns

Fourteen CFHSS columns tested at NRCC under the standard fire scenario were selected for numerical studies (Kodur and Lie, 1996; Lie and Kodur, 1996; Lie and Chabot, 1992; Lie and Irwin, 1995; Chabot and Lie, 1992). All pertinent information for the CFHSS columns is provided in Table 2. In the designation of columns (for example, RP-355), the first letter (R) represents section shape (round or square), the second letter (P, F, B) denotes filling type (plain, steel-fiber-reinforced concrete, and bar-reinforced concrete, respectively), and the number (355) denotes the diameter (for circular) or width (for square) of the HSS column section in mm.

Model Validation

For the validation of SAFIR, fourteen columns were analyzed under ASTM E-119 fire exposure. The thermal and structural response and ultimate failure times generated by SAFIR were compared with the measured test data for all of the columns. All of the columns for which test data were available underwent the same level of scrutiny as the single column used to illustrate the following validation. However, results from the validation of all columns could not be presented due to space constraints.

A comparison of the temperatures predicted by SAFIR and those measured in a fire test at the steel surface (HSS section) and at the center of the concrete core is shown for column SP-178. Good agreement between predicted and measured temperatures is observed for the concrete core after 100 °C (212 °F), at which point free water is driven off. The steel temperatures initially deviate such that temperatures observed in tests are hotter than those predicted by SAFIR. This can be attributed to the assumption in SAFIR that there is perfect thermal contact between the steel and the concrete. However, when the steel approaches the critical phase transformation temperature of 700 to 750 °C (1300 to 1400 °F), at which point the bonded water in the concrete is also driven off, SAFIR begins to overpredict the temperature in the steel. This is mainly due to the

assumption in SAFIR that hydraulic migration in concrete can be neglected. Toward the end of the test, the temperatures compare reasonably well such that there is only a 30 °C (90 °F) temperature difference between the test data and the SAFIR simulation. Overall, the temperature predictions from SAFIR are in reasonable agreement with data measured from tests.

The structural response predicted by SAFIR was validated by comparing the axial deformations for column SP-178 with those measured during tests (Figure 4). The column initially expands as a result of the quick rise in steel temperatures. This increased temperature leads to eventual loss of strength and yielding of steel, at which point concrete starts to take over most of the load bearing function, causing the column to contract slightly. A peak deflection (expansion) of 18.3 mm (0.72 in.) was observed in the tests, while the corresponding peak deflection from SAFIR was 17.9 mm (0.705 in.). These two maximum deflections show good agreement occurring at 20 and 23 minutes, respectively. The differences in deflection between SAFIR data and test data are a result of the temperature discrepancies seen in Figure 3. The initially higher temperatures in the steel shell produces higher expansion of the column in the fire test than in SAFIR, as seen in Figure 4. After peak deflections are reached, the temperatures in the steel shell as predicted by SAFIR are hotter than those observed in tests. This results in the steel retaining slightly higher strength in tests than in the SAFIR simulation. Thus, there is a slightly larger contraction of the column in the SAFIR simulation than observed in the test. Overall, the predicted deformations compare well with those measured during the fire test.

The predicted and measured values of fire resistance for the 14 CFHSS columns are tabulated in Table 2. All of the columns were simulated with the loads applied centrally, with a fixed connection at the base and a connection only allowing vertical translation (under loading) at the top. The failure times in fire tests shown in Table 2 correspond to the point at which the column could not sustain the applied load. In SAFIR, failure is likewise taken as the point where the column can no longer support the applied load. The time to reach that point is defined as the fire resistance of the column. A comparison of the fire resistance values indicates that the SAFIR predictions are in good agreement with measured fire resistance values. Due to the inherent variability of laboratory testing, and assumptions made within a computational model, the results presented here are in reasonable agreement, and the models, (both the thermal and structural) constructed here are deemed acceptably conservative to continue with the parametric studies.

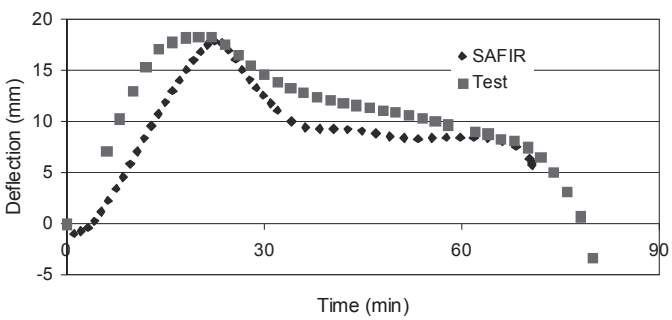

Fig. 4. Comparison of axial deformations from SAFIR with test data for column SP-178.

PARAMETRIC STUDIES

The validated computer program SAFIR was used to carry out a set of parametric studies to quantify the effect of critical parameters on the fire resistance of CFHSS columns. For the parametric studies, 20 CFHSS columns were selected. Fourteen of these columns were used in previous fire tests (listed in Table 2), while the remaining six are columns specifically selected to cover a wider range of column variables. In order to fully investigate the effect of length on fire resistance, columns 3.81, 5, 6, 7, 8, 9 and 10 m (12.5, 16.4, 19.7, 23.0, 26.3, 29.5 and 32.8 ft) long were modeled for each cross-section. Fire exposure was assumed on all four sides with the bottom and top 5% of the column unexposed to fire. Fire loading other than four-side exposure should be considered as a topic of future research. Loads were modified to maintain a constant load ratio for all of the lengths modeled for a specific cross-section according to the AISC analysis procedure (AISC, 2005). The applied loads on the columns take into account the effect that the type of concrete filling has on fire resistance: steel-fiber- and bar-reinforced concrete-filled HSS columns can take higher loads. Each of these cross section-length combinations were modeled under seven fire scenarios, five of which are shown in Figure 1. The remaining two fire scenarios were also design fires. This parametric study generated a total of 980 numerical simulations covering a wide range of loads, geometry, concrete types and fire scenarios. The trends (results) discussed later were observed for all of the filling types (plain, bar-reinforced, and steel-fiber-reinforced) considered unless otherwise noted. However, the results and discussion are mainly illustrated using plain-concrete-filled HSS columns. Another point to be noted is that the analysis was continued until the column attained failure or 240 minutes of exposure to fire. As such, if a fire resistance of 240 minutes is reached, it is indicative of the column withstanding compartment burnout, not that the column failed at 240 minutes unless otherwise noted.

Effect of Fire Exposure

The effect of fire severity on fire resistance is illustrated in Figure 5 by plotting the fire resistance as a function of length for column RP-273 under different fire scenarios.

Intuitively, as the fire severity decreases, the fire resistance of the column increases. It can be seen in Figure 5 that a fire resistance of four hours or more can be obtained for columns up to 10 m (32.8 ft) long under mild fire conditions. However, for other fire exposures fire resistance decreases with an increase in length. A closer look at Figure 5 indicates that fire resistance of a 5 m (16.4 ft) long CFHSS column ranges from 240 minutes for medium and mild fire exposure to 68 minutes under severe exposure, with ASTM exposure yielding 100 minutes. The reason for this decreased fire resistance with increased fire severity can be attributed to the higher internal temperatures attained under severe fire exposure. Consequently, the column loses its strength and stiffness at a faster rate leading to early failure. Figures 6 and 7 show the difference in internal temperatures observed in the steel shell and at the center of the concrete core for the fire exposures shown in Figure 1.

It can be seen in Figure 6 that two of the three design fires produce higher initial temperatures in steel than the ASTM E-119 fire. This effect is seen in concrete temperatures also (see Figure 7), though to a lesser extent. The presence of the decay phase in the design fires causes the temperatures in all locations of the column to be less than those for the ASTM E-119 fire at the end of the simulation period. Column stability is maintained under design fires, despite the more severe initial temperatures, due to the decay phase of the fire allowing cooling of the steel before significant loss of strength in the concrete core occurs.

To illustrate the effect of fire scenario on the structural response, Figure 8 displays the axial deformation of column RP-273 resulting from ASTM E-119, severe, medium and mild fire exposure. In all simulations, the column initially expanded due to the increasing steel temperature. After this initial expansion, the response of the column is significantly influenced by the type of fire exposure. In the case of severe and medium fire scenarios, significant contraction occurs before failure of the column. This could be attributed to the

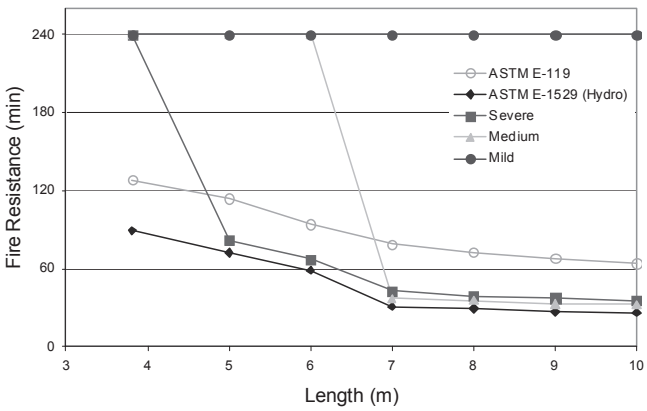

Fig. 5. Fire resistance as a function of length for column RP-273 under different fire scenarios.

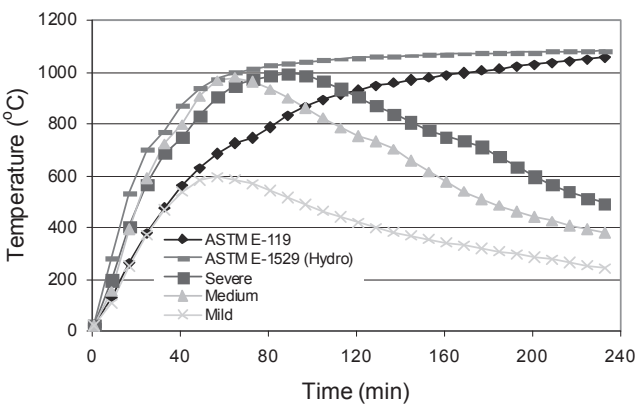

Fig. 6. Temperatures on the steel surface for column RP-273 exposed to different fire scenarios.

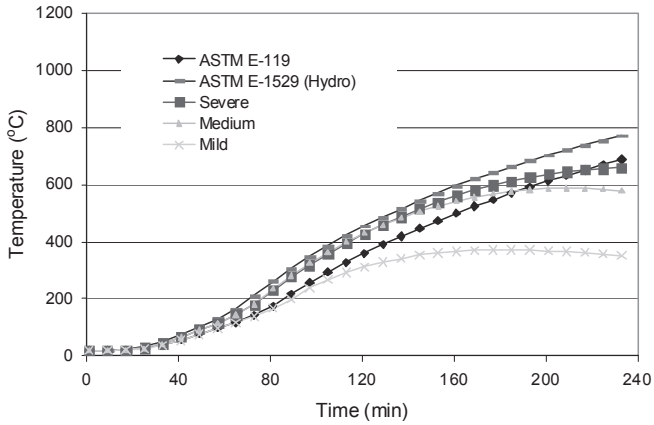

Fig. 7. Temperatures at the center of concrete core for column RP-273 exposed to different fire scenarios.

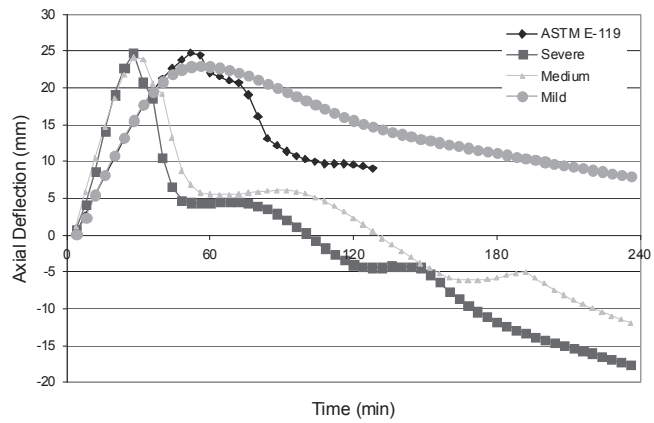

Fig. 8. Axial deformation as a function of time for column RP-273 under different fire scenarios.

presence of a cooling phase in design fire scenarios. However, under ASTM E-119 fire exposure, the column failed in 32 minutes without too much contraction.

Effect of Length

The results presented in Figure 5 can be used to demonstrate the effect of length on the fire resistance of CFHSS columns. In the analysis, the load on the column was reduced as the length was increased such that the load ratio on a single column was kept constant through all of the simulations. As would be expected, fire resistance for a given fire exposure decreases with an increase in length of the column. This is due to the increase in slenderness that accompanies the increase in length. Fire resistance is drastically reduced when the failure mode switches from crushing to buckling with increased length. This is most pronounced for the "medium" and "severe" fire exposure as can be seen in Figure 5. Fire resistance under the medium fire drops from 240 to 45 minutes when length is increased from 5 to 7 m (16.4 to 23 ft). Under severe fire exposure, the fire resistance decreases from 240 to 75 minutes for an increase in length from 3.81 to 5 m (12.5 to 16.4 ft). However, under mild fire exposure, fire resistance remains high for all cases, and the length does not have any influence. This study clearly illustrates the fact that length has a significant influence on the resulting fire resistance, specifically under severe fire exposures.

Effect of Concrete Filling

The effect of the type of concrete filling on fire resistance is illustrated by analyzing HSS columns with different concrete filling types under ASTM E-119 fire exposure. As was the case with the effect of length, the applied load was modified according to AISC analysis procedures (AISC, 2005) to account for the different types of concrete filling for this analysis. The fire resistance is plotted as a function of length for three similar CFHSS columns (Figure 9), each with a different type (plain, steel-fiber-reinforced, bar-reinforced) of concrete filling, columns selected for this comparison are RP-355, RF-356 and RB-406, respectively. The fire resistance decreases with an increase in length for all of the filling types. However, columns filled with bar or steel-fiber-reinforced concrete demonstrate higher fire resistance than plain concrete-filled columns at all lengths. This can be attributed to the increased load carrying capacity of the concrete core provided by the inclusion of reinforcement, and is also due to the slower loss of strength in columns filled with bar- and steel-fiber-reinforced concrete. These results indicate that it is possible to significantly enhance the fire resistance of CFHSS columns by changing the type of concrete filling. The required fire resistance in most situations can be obtained for columns up to 10 m (32.8 ft) in length by simply altering the type of concrete filling.

Effect of Load Ratio

The effect of load ratio on fire resistance was investigated by analyzing three columns under ASTM E-119 fire with load ratios ranging from 10% to 100% (0.1 to 1.0). The analysis was carried out for three types of concrete filling, namely, plain (RP-273), steel-fiber-reinforced (SF-219), and bar-reinforced (RB-273) filling. It can be seen in Figure 10 that only the bar-reinforced concrete-filled HSS column withstood the ASTM E-119 fire for 240 minutes (actual failure time) with a load ratio of 10% (0.1). Columns SF-219 and RP-273 lasted for 234 and 170 minutes, respectively. The fire resistance decreases rapidly with an increase in load ratio up to 0.4, after which the rate of decrease in resistance is slower. This can be attributed to the fact that concrete filling generally provides a load bearing contribution of about 30% to 40% of the overall composite column capacity. In a fire scenario, the steel shell looses its strength very quickly, and concrete carries most of the load. Thus, for load ratios higher

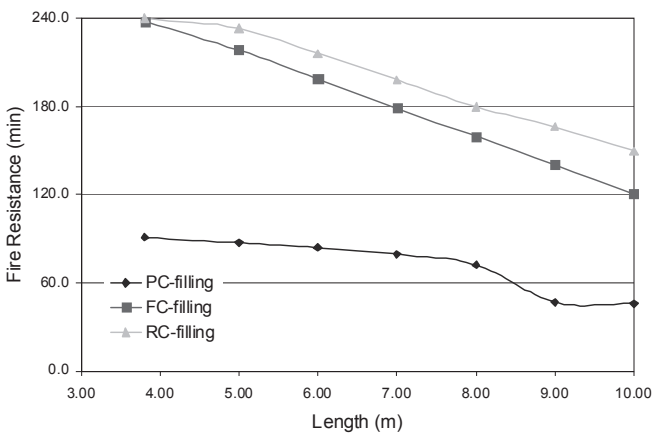

Fig. 9. Effect of concrete filling on fire resistance of CFHSS columns.

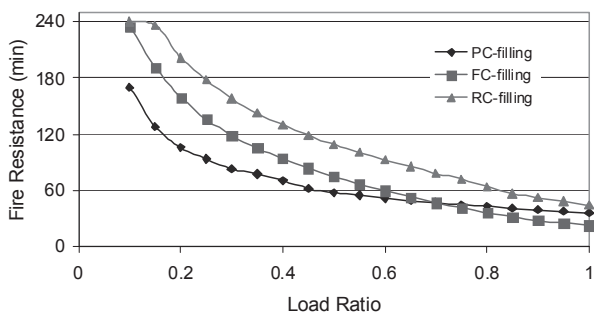

Fig. 10. Effect of load ratio on fire resistance of CFHSS columns.

than 40%, the concrete filling has to be strengthened either through the use of bar reinforcement, or through the use of steel fibers to achieve higher fire resistance as can be seen in Figure 5. In design fires, the same trend is observed as in the ASTM E-119 fire, with the exception that the times to reach failure are increased depending on the type of design fire considered. Design fires allow the use of load ratios in the range of 40% to 50% while still achieving the required fire resistance. It should be noted that only concentric loads were considered in the analysis presented here. Other loading types such as eccentric or combined axial and bending loads can influence the fire resistance of CFHSS columns and require further research.

Effect of Cross-Section Size

Results from the analysis indicate that the fire resistance of CFHSS columns increases with an increase in cross-sectional size. This is due to the increased contribution of the concrete core to the column strength. When cross-section size is increased, the concrete core comprises a larger percentage of the load-bearing capacity of the section. When a CFHSS column is exposed to fire, the steel section loses its strength quickly and transfers the load to the concrete core. The larger core is capable of providing longer fire resistance times. The strength loss in the concrete core is slower than in the HSS section, allowing the column to achieve enhanced fire resistance. The increased cross-sectional size also enhances stiffness, and thus resistance to buckling of the column, allowing higher fire resistances to be achieved in longer columns. Columns filled with plain concrete, however, realize no additional advantage from cross-section increases beyond 400 mm (15.75 in.). This is due to high-temperature instability of the concrete core causing premature failure for larger cross-sectional sizes.

Effect of Aggregate Type

Results from the analysis indicate that the type of aggregate has a moderate influence on the fire resistance of CFHSS columns. The two common types of aggregate used in CFHSS columns are carbonate aggregate (primarily consisting of limestone) and siliceous aggregate (primarily consisting of quartz). Carbonate aggregate concrete typically demonstrate higher fire resistance than siliceous aggregate concrete (Kodur and Lie, 1996; Kodur and Lie, 1997). This is due to an endothermic reaction occurring in carbonate aggregate at 600 to 800 °C (1100 to 1500 °F), in which the dolomite within the aggregate dissociates. Consequently, the heat capacity of carbonate aggregate increases significantly and is approximately 10 times higher than siliceous aggregate in the same temperature range. As a result, there is a slower increase in temperature in the carbonate aggregate concrete, and thus a slower loss of strength. Therefore, the fire resistance of CFHSS columns filled with carbonate aggregate concrete is about 10% higher than siliceous aggregate concrete-filled HSS columns.

Effect of Failure Criterion

The two limit states considered for defining failure of steel columns under fire conditions are limiting temperature and stability retention. ASTM E 119 defines fire resistance as the time it takes to reach a maximum average section temperature of 538 °C (1000 °F), or a maximum point temperature of 649 °C (1200 °F). On the contrary, stability-based failure criteria are based on the duration of time during which a column maintains structural stability (strength) during fire exposure. In the case of CFHSS columns, using the limiting temperature criterion does not reflect realistic fire resistance ratings. As an illustration, column RP-273 achieved fire resistance of 143 minutes in testing and 128 minutes in the SAFIR simulation. Thermal failure criterion, however, would only yield a resistance of 38 minutes for this column. Clearly, thermal failure criteria do not reflect the contribution of the concrete filling to the fire resistance of CFHSS columns. As such, it is necessary to employ stability-based failure criterion in the evaluation of the fire resistance of CFHSS columns.

PERFORMANCE-BASED DESIGN METHODOLOGY

In recent years, the performance-based approach to fire safety design is becoming popular since cost-effective and rational fire safety solutions can be developed using this approach (Kodur, 1999). One of the key aspects in any performance-based design is the fire-resistant design of structural members. Through the application of a performance-based approach, the full benefits of CFHSS columns under fire condition can be realized. For evaluating fire resistance, numerical models that can simulate the response of CFHSS columns under realistic fire, loading and restraint scenarios can be used. The main steps involved in undertaking a rational approach for performance-based design are:

1. Identifying proper design (realistic) fire scenarios and realistic loading levels on the CFHSS columns under consideration.

2. Carrying out detailed thermal and structural analysis by exposing the CFHSS column to fire conditions.

3. Developing relevant practical solutions, such as the use of different types of concrete filling, to achieve required fire resistance.

Development of Fire Scenario and Loading

The design fire scenarios for any given situation can be established either through the use of parametric fires (time-temperature curves) specified in Eurocode 1 (Eurocode, 2002) or through design tables (Magnusson and Thelandersson,

1970) based on ventilation, fuel load and surface lining characteristics. To use the design tables, the ventilation factor, F_v, has to be established using the relationship:

$$F_v = \frac{A_v}{A_t}\sqrt{H_v} \quad (2)$$

where A_v is the area of the window opening (m^2), A_t is the total internal area of the bounding surface (m^2), and H_v is the height of the window opening (m) (Buchanan, 2005). The fuel load in the compartment is determined by considering the total bounding surface (not just the floor surface area). Typical fuel loads for common compartment types are available (Parkinson and Kodur, 2007; Buchanan, 2005). Figure 1 shows typical design fire curves that can be generated using performance-based fire safety design. The presence of sprinklers can also be accounted for in the development of design fire scenarios.

The loads that are to be considered on concrete-filled HSS columns under fire conditions should be estimated based on the guidance given in ASCE 7 (1.2 dead load + 0.5 live load) (ASCE, 2005) or through actual calculations based on different load combinations.

Structural Analysis Under Fire Exposure

Once the fire scenarios and load level are established, the next step is to select a computer program for the analysis of CFHSS columns exposed to fire. The computer program should be able to trace the response of the CFHSS column in the entire range of loading up to collapse under fire. Computer programs such as SAFIR (as demonstrated in this paper), ANSYS, or ABAQUS can be adopted for the analysis. Using the computer program, a coupled thermal-structural analysis shall be carried out at various time steps. In each time step, the fire behavior of a CFHSS column is estimated using a complex, coupled heat transfer/strain equilibrium analysis, based on theoretical heat transfer and mechanics principles. The analysis should be performed in three steps: calculation of fire temperatures to which the column is exposed; calculation of temperatures in the column; and calculation of resulting deflections and strength, including an analysis of the stress and strain distribution.

The computer program used in the analysis should be capable of accounting for nonlinear high-temperature material properties, complete structural (column) behavior, various fire scenarios, high-temperature creep, different concrete types (concrete with and without steel fibers), and failure criteria. In the analysis, geometric nonlinearity, an important factor for the slender columns that are used in many practical applications, should be taken into consideration. Thus, the fire response of the column may be traced in the entire range of behavior, from a linear elastic stage to the collapse stage under any given fire and loading scenario. Through this coupled thermal-structural analysis, various critical output parameters such as temperatures, stresses, strains, deflections and strengths have to be generated at each time step.

The temperatures in the concrete and reinforcement, strength capacities and computed deflections of the column shall be used to evaluate failure of the column at each time step. At every time step, the failure of the column shall be checked against a predetermined set of failure criteria. The time increments continue until a certain point at which the strength failure criterion has been reached, or the axial deformations reach their limiting state. At this point, the column becomes unstable and will be assumed to have failed. The time to reach this failure point is the fire resistance of the column.

Development of Practical Alternatives

Results from the analysis can be utilized to develop practical solutions for achieving the required fire resistance in CFHSS columns. The most feasible solution is through changing the type of concrete filling (plain, bar-reinforced, or steel-fiber-reinforced concrete). Other factors, such as the type of aggregate in the concrete, reinforcement in the column or load level can be varied to achieve the required fire resistance in HSS columns. As an example, while plain concrete filling can provide one-hour fire resistance in HSS columns, by switching to steel-fiber-reinforced concrete filling, up to three hours of fire resistance can be obtained even under severe design fire scenarios. As is currently the case with CFHSS columns, it is required that steam vent holes be provided at the top and the bottom of compartment elevations for any fire resistance to be achieved.

DESIGN IMPLICATIONS

The approach presented here is capable of tracing the behavior of CFHSS columns from the initial pre-fire stage to the failure of the column under realistic fire, loading and failure criterion. The proposed approach can be used to overcome many of the current limitations in achieving unprotected steel in HSS columns in most practical applications. Thus, the use of this approach will lead to designs that are not only economical, but that are based on rational design principles. Further, the approach can be applied to conduct parametric studies, which can then be used to develop rational fire safety design guidelines for incorporation into codes and standards.

Through implementation of the design process outlined here, structural safety and integrity will be improved, construction time and cost will be reduced, and exposed structural steel can be achieved. Applications for these CFHSS columns could include airports, schools, detention facilities and high-rise buildings, where structural stability in fire is paramount and relatively high fire resistance is required.

CONCLUSIONS

Based on the results of this study, the following conclusions can be drawn:

- The current fire resistance provisions, developed based on limited standard fire tests under "standard fire scenarios," are prescriptive and simplistic in application and, thus, cannot be applied for rational fire safety design of CFHSS columns under performance-based codes.

- Type of fire exposure has a significant influence on the fire resistance of CFHSS columns. The fire resistance of CFHSS columns under most design fire scenarios is higher than that under ASTM E-119 standard fire exposure.

- Apart from fire exposure, the other significant factors that affect the fire resistance of CFHSS columns are length, type of concrete filling, load ratio and failure criteria.

- It is possible to obtain unprotected CFHSS columns up to 10 m (32.8 ft) in length capable of withstanding complete compartment burnout through the use of different types of concrete filling.

- Through the use of a performance-based design approach, it is possible to significantly enhance the fire resistance of CFHSS columns by varying parameters such as the type of concrete filling, type of aggregate in the concrete, and the fire scenario.

- The limiting criterion, used for determining failure, has a significant influence on the fire resistance of CFHSS columns. The conventional failure criteria—for example, limiting steel temperature—cannot be applied to CFHSS columns. Strength and deformation failure criteria should be considered for evaluating fire resistance of CFHSS columns.

- Further research is needed to develop simplified design equations to evaluate the fire resistance of CFHSS columns under design fire exposure without the need for advanced numerical models.

ACKNOWLEDGMENT

The research presented in this paper was primarily supported by the American Institute of Steel Construction through an AISC Faculty Fellowship Award to Venkatesh Kodur.

REFERENCES

AISC (2005), *Steel Construction Manual*, 13th ed., American Institute of Steel Construction, Chicago, IL.

ASCE 7-05 (2005), *Minimum Design Loads for Buildings and Other Structures*, American Society of Civil Engineers, Reston, VA.

ASCE/SFPE 29 (1999), *Standard Calculation Method for Structural Fire Protection*, American Society of Civil Engineers, Reston, VA.

ASTM (2001), *Standard Methods for Fire Test of Building Construction and Materials*, Test Method E1529-93, American Society for Testing and Materials, West Conshohocken, PA.

ASTM (2007), *Standard Methods of Fire Test of Building Construction and Materials*, Test Method E119-00, American Society for Testing and Materials, West Conshohocken, PA.

Bond, G.V.L. (1975), *Fire and Steel Construction, Water cooled Hollow Columns*, Constrado, Croydon.

Buchanan, A.H. (2005), *Structural Design for Fire Safety*, John Wiley and Sons Ltd., New York.

Chabot, M. and Lie, T.T., (1992), "Experimental Studies on the Fire Resistance of Hollow Steel Columns Filled with Bar-Reinforced Concrete," IRC Internal Report No. 628, National Research Council of Canada.

Chen, F.F. and Gemeny, D.F. (2004), "Case Study Using SAFIR to Predict Fire Resistance of a Column in a Performance-Based Environment," *SFPE Fire Protection Magazine,* No. 23, Summer 2004, pp. 30–35.

Eurocode 1 (2002), ENV 1991 1-2: "General Actions—Actions on Structures Exposed to Fire," European Committee for Standardization.

Eurocode 3 (2005a), ENV 1993 1-2: "General Rules—Structural Fire Design," European Committee for Standardization.

Eurocode 4 (2005b), ENV 1994 1-2: "Design of Composite Steel and Concrete Structures," European Committee for Standardization.

FCSA (1989), *Fire Technical Design Manual for Composite Columns with Concrete Filled Hollow Steel Sections*, Finnish Constructional Steelwork Association, Helsinki, Finland, pp. 66.

FEMA (2002), "World Trade Center Building Performance Study: Data Collection, Preliminary Observations, and Recommendations," Federal Emergency Management Agency, Washington, DC.

Franssen, J.M. (2005), "SAFIR: A Thermal/Structural Program for Modeling Structures Under Fire," *Engineering Journal,* Vol. 42, No. 3, pp. 143–155.

Gilvary, K. and Dexter, R. (1997), "Evaluation of Alternative Methods for Fire Rating Structural Elements," NIST Building and Fire Research Laboratory, Gaithersburg, MD.

Grandjean, G., Grimault, J.P. and Petit, L. (1981), "Determination de la durée au feu des profils creux remplis de béton," Rapport final, Commission des Communautés Européennes, Recherche Technique Acier, Luxembourg.

Han, L. and Lin, X. (2004), "Test on Cyclic Behavior of Concrete Filled Hollow Structural Steel Columns after Exposure to the ISO-834 Standard Fire," *Journal of Structural Engineering,* Vol. 130, No. 11, pp. 1807–1819.

ISO 834 (1975), "Fire Resistance Tests—Elements of Building Construction," International Organization for Standardization, Geneva, Switzerland.

Klingsch, W. and Wittbecker, F.W. (1988), "Fire Resistance of Hollow Section Composite Columns of Small Cross Sections," Bergische Universität, Wuppertal, Germany, pp. 103.

Klingsch, W. and Wuerker, K. (1985), "New Developments in Fire Resistance of Hollow Section Structures," *Proceedings of the Symposium on Hollow Structural Sections in Building Construction,* Chicago, IL.

Kodur, V.K.R. (2005), "Achieving Fire Resistance Through Steel Concrete Composite Construction," *Proceedings of the 2005 ASCE Structures Congress*, New York.

Kodur, V.K.R. (1999), "Performance-based Fire Resistance Design of Concrete-filled Steel Columns," *Journal of Constructional Steel Research*, Vol. 51, pp. 21–36.

Kodur, V.K.R. (1997), "Design Equations for Evaluating Fire Resistance of SFRC-filled Steel Columns," *Journal of Structural Engineering*, Vol. 124, No. 6, pp. 671–678.

Kodur, V.K.R. and Harmathy, T.Z. (2002), "Properties of Building Materials," *SFPE Handbook of Fire Protection Engineering*, National Fire Protection Association, Quincy, MA.

Kodur, V.K.R. and Lie, T.T. (1995a), "Experimental Studies on the Fire Resistance of Circular Hollow Steel Columns Filled With Steel Fibre Reinforced Concrete," IRC Internal Report No. 691, National Research Council of Canada.

Kodur, V.K.R. and Lie, T.T. (1995b), "Fire Performance of Concrete-filled Hollow Steel Columns," *Journal of Fire Protection Engineering*, Vol. 7, No. 3, pp. 89–98.

Kodur, V.K.R. and Lie, T.T. (1996), "Fire Resistance of Circular Steel Columns Filled With Fiber-reinforced Concrete," *Journal of Structural Engineering*, Vol. 122, No. 7, pp. 776–782.

Kodur, V.K.R. and Lie, T.T. (1997), "Evaluation of Fire Resistance of Rectangular Steel Columns Filled With Fiber-Reinforce Concrete," *Canadian Journal of Civil Engineering*, Vol. 24, pp. 339–349.

Kodur, V.K.R. and MacKinnon, D.H. (2000), "Fire Endurance of Concrete-filled Hollow Structural Steel Columns," *Engineering Journal*, Vol. 37, No. 1, pp. 13–24.

Lie, T.T. and Caron, S.E. (1988), "Fire Resistance of Circular Hollow Steel Columns Filled with Carbonate Aggregate Concrete: Test Results," IRC Internal Report No. 573, National Research Council of Canada.

Lie, T.T. and Chabot, M. (1990), "A Method to Predict the Fire Resistance of Circular Concrete Filled Hollow Steel Columns," *Journal of Fire Protection Engineering*, Vol. 2, No. 4, 111–126.

Lie, T.T. and Chabot, M. (1992), "Experimental Studies on the Fire Resistance of Hollow Steel Columns Filled With Plain Concrete," IRC Internal Report No. 611, National Research Council of Canada.

Lie, T.T. and Irwin, R.J. (1995), "Fire Resistance of Rectangular Columns Filled with Bar-Reinforced Concrete," *Journal of Structural Engineering*, Vol. 121, No. 5, pp. 797–805.

Lie, T.T., Irwin, R.J., and Chabot, M (1991), "Factors Affecting the Fire Resistance of Circular Hollow Steel Columns Filled With Plain Concrete," IRC Internal Report No. 612, National Research Council of Canada.

Lie, T.T. and Kodur, V.K.R. (1996), "Fire Resistance of Steel Columns Filled With Bar-reinforced Concrete," *Journal Structural Engineering*, Vol. 122, No. 1, pp. 30–36.

Lie, T.T. and Kodur, V.K.R. (1996), "Thermal and Mechanical Properties of Steel Fiber Reinforced Concrete at Elevated Temperatures," *Canadian Journal of Civil Engineering*, Vol. 23, No. 2, pp. 511–517.

Lie, T.T. and Stringer, D.C. (1994), "Calculation of Fire Resistance of Steel Hollow Structural Steel Columns Filled With Plain Concrete," *Canadian Journal of Civil Engineering*, Vol. 21, No. 3, pp. 382–385.

Magnusson, S.E. and Thelandersson, S. (1970), "Temperature-Time Curves of Complete Process of Fire Development; Theoretical Study of Wood Fuel Fires in Enclosed Spaces," *Civil Engineering and Building* Series 65, Acta, Polytechnica, Scandinavia.

Meacham, B.J. and Custer, R.P.L. (1992), "Performance-based Fire Safety Engineering: An Introduction of Basic Concepts," *Journal of Constructional Steel Research*, Vol. 7, pp. 35–54.

NBC (2005), *National Building Code of Canada,* National Research Council of Canada, Canada.

NIST (2005), "Final Report of the National Construction Safety Team on the Collapse of World Trade Center Towers," NCSTAR1, National Institute of Standards and Technology, Gaithersburg, MD.

Parkinson, D.L. and Kodur, V.K.R. (2007), "Performance-Based Design of Structural Steel for Fire Conditions—A Calculation Methodology," *International Journal of Steel Structures,* Vol. 7, No. 3, pp. 219–226.

Talamona, D. (2005), "A Quadralateral Shell Finite Element for Concrete and Steel Structures Subject to Fire," *Journal of Fire Protection Engineering,* Vol. 15, No. 4, pp. 237–264.

Twilt, L. Hass, R. Klingsch, W. Edwards, M. and Dutta, D. (1996), *Design Guide 4 for Structural Hollow Section Columns Exposed to Fire*, first edition, CIDECT.

Design and Behavior of Multi-Orientation Fillet Weld Connections

LOGAN J. CALLELE, ROBERT G. DRIVER and GILBERT Y. GRONDIN

Abstract

Several independent research projects have demonstrated that the strength and ductility of fillet welds are a function of the angle between the weld axis and the line of action of the applied load. It has been demonstrated that transverse welds are about 50% stronger than longitudinal welds, but have considerably lower ductility. This difference in behavior can have a significant impact on the design of welded connections with multiple weld orientations within the same joint. Tests on concentrically loaded welded double lapped joints have recently been conducted to investigate the strength of connections with multiple weld segments of different orientations. The tests indicate that these joints possess capacities significantly lower than the sum of the individual weld segment strengths. The tested connections' capacities are a function of the interaction of the load versus deformation characteristics of the individual weld segments. A general approach for the design of welded joints that combine welds in various directions that reflects the individual segments' load versus deformation interaction is recommended.

Keywords: multi-orientation fillet welds, transverse welds, longitudinal welds, connections, steel construction.

INTRODUCTION

Recent research conducted at the University of Alberta by Deng et al. (2006) and Ng et al. (2004) have verified the suitability of the current North American design equations for evaluating fillet weld strength: clause 13.13.2.2(b) of S16–01 (CSA, 2001) and equations J2-4 and J2-5 of the AISC *Specification* (AISC, 2005). That research examined concentrically loaded fillet-welded connections fabricated such that all the welds had the same loading orientation—these types of connections are referred to as single-orientation fillet weld (SOFW) connections in this paper. However, fillet-welded connections commonly include welds at different orientations to the applied load—these types of connections are referred to as multi-orientation fillet weld (MOFW) connections.

It is well-known that fillet welds oriented transverse to the applied load exhibit higher unit strengths but generally lower deformation capacity than longitudinal fillet welds (Butler, Pal and Kulak, 1972; Lesik and Kennedy, 1990). This paper examines how the strength and behavior of MOFW connections with equal weld sizes in the various weld segments are affected by the variation in strength and deformation capacity of fillet welds with respect to loading orientation. A method of designing concentrically loaded MOFW connections for any given critical segments (weld segments with an orientation closest to 90°) and noncritical weld segments (the remaining weld segments in the connection) is presented. This design procedure is compared with the results of 19 MOFW connection tests conducted as part of this research program.

Logan Callele, Structural Engineer, Waiward Steel Fabricators Ltd., 10030-34 St., Edmonton, AB, T6B 2V5, Canada (corresponding author). E-mail: logan.callele@waiward.com

Robert G. Driver, Professor, Department of Civil and Environmental Engineering, 3-133 Natural Resources Engineering Facility, University of Alberta, Edmonton, AB, T6G 2W2, Canada. E-mail: rdriver@ualberta.ca

Gilbert Y. Grondin, Professor, Department of Civil and Environmental Engineering, 3-025 Natural Resources Engineering Facility, University of Alberta, Edmonton, AB, T6G 2W2, Canada. E-mail: ggrondin@ualberta.ca

BACKGROUND

Previous research on eccentrically loaded fillet weld connections provides information on fillet weld deformation capacity and load–response behavior (e.g., Butler et al., 1972; Lesik and Kennedy, 1990). These two research programs investigated the behavior of eccentrically loaded connections using the method of the instantaneous center of rotation. This method of analysis requires a way of predicting the strength, deformation capacity, and load–deformation behavior of fillet welds of any loading orientation.

The fillet weld deformation capacity and load–deformation behavior used by Butler et al. (1972) and Lesik and Kennedy (1990) for transverse and longitudinal fillet welds are shown in Figure 1, where Δ is the deformation of the weld and d is the leg size. These curves reveal that if both longitudinal and transverse welds are used in a single connection such that all of the welds undergo the same deformation, the longitudinal welds would not reach their ultimate strength by the time the transverse welds have reached theirs. Thus,

the lower deformation capacity of the transverse fillet welds limits the connection capacity.

The effect of fillet weld deformation capacity on connection capacity has also been examined by Manuel and Kulak (2000) for transverse and longitudinal welds. This work investigated the behavior of connections combining high-strength structural bolts and fillet welds. These researchers observed that in connections where both transverse and longitudinal welds are present, the longitudinal welds reach only 85% of their predicted ultimate strength at the ultimate capacity of the connection. They stated that the capacity of the longitudinal fillet welds at the connection capacity is directly related to fracture deformation of the transverse fillet welds.

The work of Butler et al. (1972), Lesik and Kennedy (1990), and Manuel and Kulak (2000) indicates that the deformation capacity and load–deformation characteristics of fillet welds affect the capacity of MOFW connections and that this behavioral aspect should be taken into account in design. One common connection that is composed of fillet welds with more than one loading orientation is one with both transverse and longitudinal welds. An examination of Figure 1 shows that the capacity of a connection composed of both transverse and longitudinal fillet welds would be affected primarily by the deformation capacity of the transverse fillet weld and, to a lesser degree, the load–deformation characteristics of the longitudinal fillet weld. The load–deformation response proposed by Butler et al. (1972) indicates that the longitudinal weld will contribute 94% of its capacity to the connection capacity, whereas that of Lesik and Kennedy (1990) indicates that the longitudinal weld will contribute 80% of its capacity. This discrepancy is primarily a result of the greater transverse fillet weld deformation capacity predicted by Butler et al. (1972). The larger deformation capacity of the transverse weld allows for more deformation to be available to develop the longitudinal fillet weld capacity.

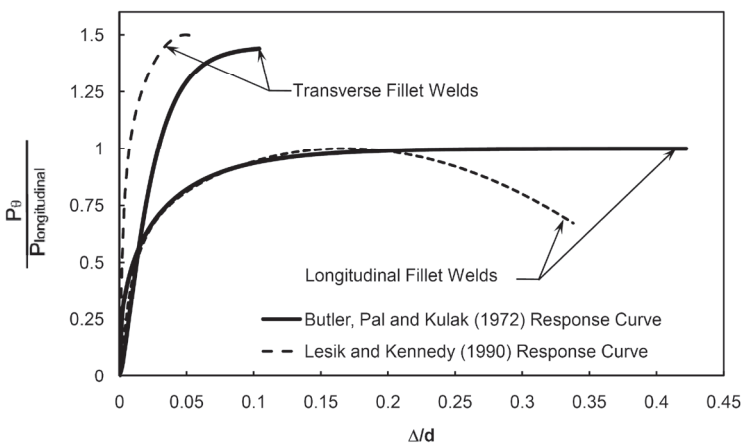

Fig. 1. Previous research into fillet weld behavior.

The significance of the effect of fillet weld deformation capacity and load–deformation response on the capacity of MOFW connections requires that an accurate estimate of these two fillet weld characteristics be obtained. The research programs by Butler et al. (1972), Lesik and Kennedy (1990), and Manuel and Kulak (2000) were all based upon fillet-welded connections fabricated using the shielded metal arc welding (SMAW) process. However, the flux cored arc welding (FCAW) process is much more prevalent in current structural steel fabrication practice. The SMAW process can produce fillet welds that have higher toughness than the FCAW process (Deng et al., 2006). This difference in toughness raises the question as to whether or not the fillet weld load–deformation responses developed for SMAW fillet welds are adequate to analyze connections fabricated with FCAW fillet welds at multiple loading orientations.

Two recent research projects at the University of Alberta investigated the accuracy of the current fillet weld strength predictions by North American design specifications (Ng et al., 2004; Deng et al., 2006). The primary focus was to investigate whether or not the strength of concentrically loaded SOFW connections fabricated using the FCAW process could be estimated adequately and safely by current North American design provisions. The fillet weld deformation capacity and load–deformation characteristics from the work of Deng et al. (2006) are used to analyze the tested connections from the current research on FCAW fillet weld connections with more than one fillet weld loading orientation.

EXPERIMENTAL INVESTIGATIONS

Two connection arrangements were tested to investigate welded connections containing more than one fillet weld loading orientation. The first connection type combined transverse and longitudinal fillet welds ("TL" specimens), while the second combined transverse and 45° fillet welds ("TF" specimens). Both connections types were fabricated by welding a lap plate on both sides of two main plates. The connection geometries and weld information are given in Table 1 and Figures 2 and 3.

Of the 19 MOFW connection specimens tested, 11 were TL specimens and 8 were TF specimens. The default nominal weld leg size is 12.7 mm (½ in.), and the suffix "a" is used to denote where 7.9 mm (5⁄16 in.) fillets were used instead. Four TF specimens and four TFa specimens were tested. The TL specimens are also distinguished in their designation by the longitudinal weld length: four TL50 specimens, four TL50a specimens and three TL100 specimens.

In order to analyze the MOFW connection specimens, it was necessary to conduct a complementary testing program

Table 1. Test Specimen Geometry and Weld Information					
Nominal Dimensions (See Figures 2 and 4)	**Specimen Designation**				
	TL50	**TL50a**	**TL100**	**L100**	**L150**
Length of test region, L_T (mm)	51	51	102	102	152
Length of reinforced region, L_R (mm)	102	102	152	203	254
Plate thickness, t (mm)	44	44	70	41	70
Main plate length, X (mm)	457	457	610	610	610
Fillet weld leg size (mm)	12.7	7.9	12.7	12.7	12.7
Number of passes	3	1	3	3	3

to supplement the information from Deng et al. (2006). The test specimens were double lap plate connections with only longitudinal fillet welds ("L" specimens) or transverse fillet welds ("T" specimens); Figures 4 and 5, along with Table 1, provide the geometric and welding information. Three L100, L150, and T specimens were fabricated for a total of nine extra specimens that make up the complementary tests. The complementary tests were chosen to be SOFW connections that were fabricated with identical weld filler metal, load orientation and nominal size as an individual segment from the MOFW connections. The observed behavior of the complementary tests thus formed the basis of the assumed behavior of the individual segments of the MOFW connections that were tested.

The nine complementary tests are of a similar arrangement to those presented in Deng et al. (2006) with the following exceptions: the L100 and L150 tests have longer longitudinal welds than the L1, L2 and L3 tests of Deng et al. (2006), and the transverse weld specimens' connection plates remained elastic, whereas those tested by Deng et al. (2006) yielded at, or prior to, reaching the connection capacity.

All 28 specimens (i.e., both the complementary and MOFW connection specimens) were fabricated with E70T-7 filler metal and with plates that were thick enough to ensure that plate yielding did not take place during testing. E70T-7 wire is a self-shielding wire used for FCAW. No start/stops were permitted within the tested welds during fabrication of all specimens. Test specimens TL50, TL50a,

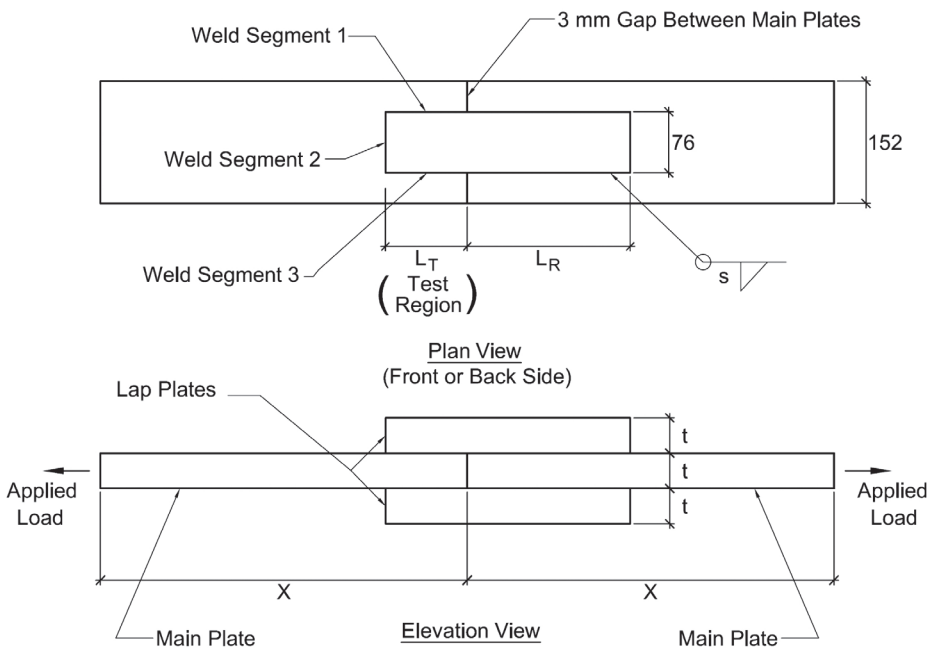

Fig. 2. Typical lap plate connection combining transverse and longitudinal welds (TL specimens).

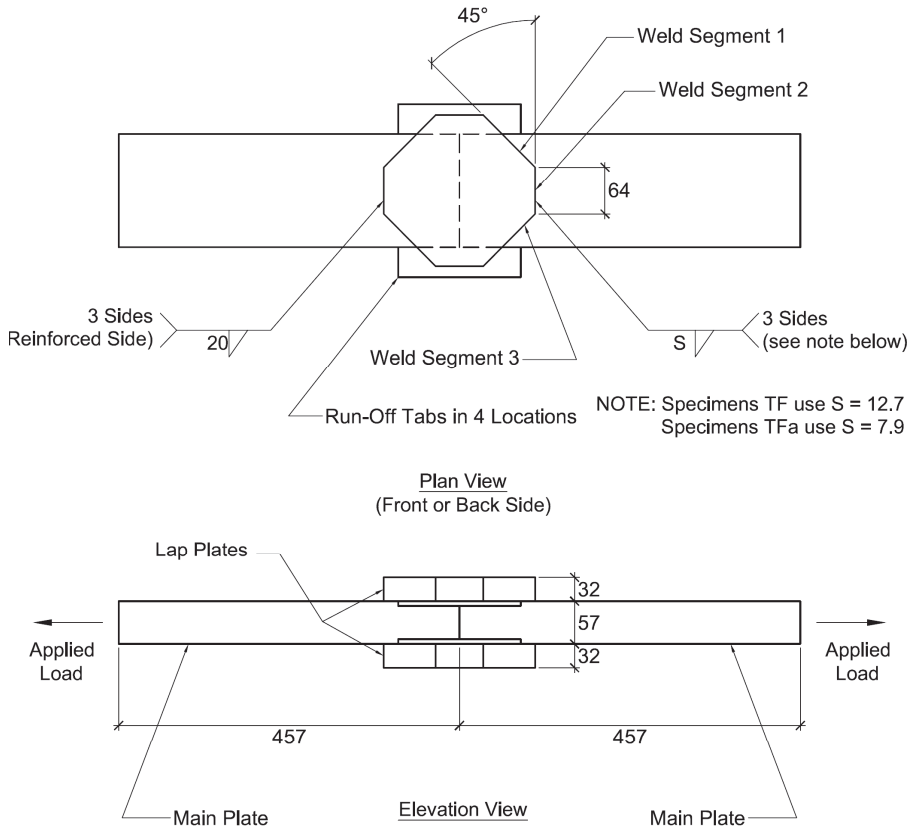

Fig. 3. TF and TFa specimens.

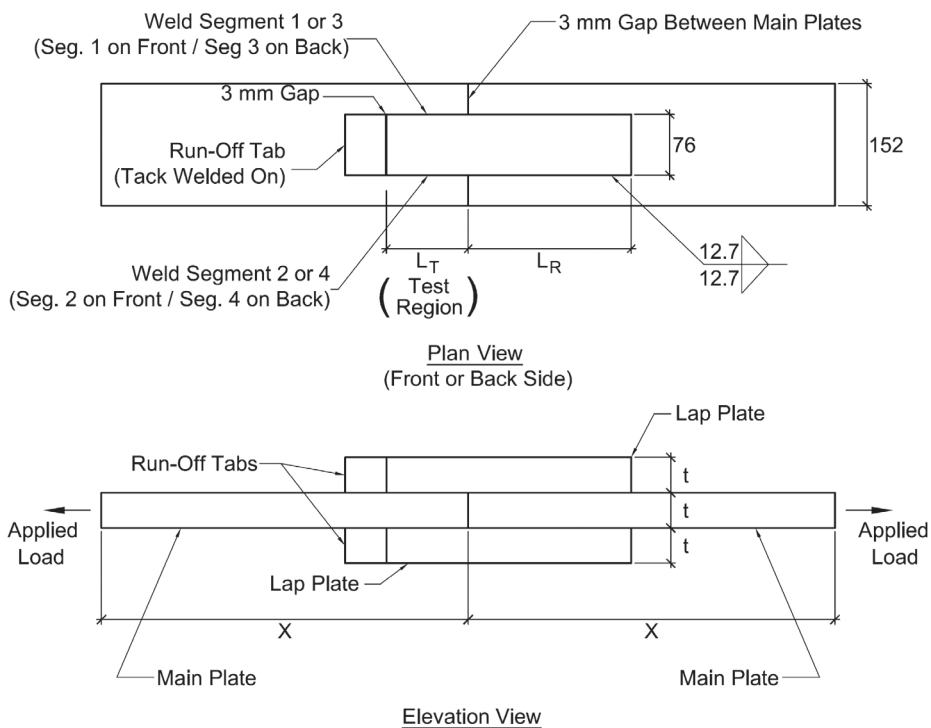

Fig. 4. Complementary test longitudinal fillet weld (L) specimen.

TF and TFa were fabricated from one heat of E70T-7 wire, while the remaining specimens were fabricated from a different heat. To establish the ultimate strength of the E70T-7 weld metal from both heats, six all-weld-metal tension coupons were fabricated and tested. These coupons had a 50-mm (2-in.) gage length and were fabricated in accordance with Clause 9 of ANSI/AWS A5.20/A5.20M:2005 (AWS, 2005). The plates used in the fabrication of all specimens met the requirements of ASTM A572 grade 50 and CAN/CSA-G40.21 350W steel.

Prior to testing, all test fillet welds were measured. Values for the measured fillet weld main plate leg (MPL) and lap plate leg (LPL) sizes, as well as the measured weld segment lengths, are given in Tables 2 through 5 for all of the specimens tested. Figure 6 provides a description of MPL and LPL and their relationship to the minimum throat dimension (MTD). The MTD neglects both the root penetration and the weld reinforcement, as is typically done in design. It should be noted, however, that fillet welds generally do not fail on the minimum throat plane (Miazga and Kennedy, 1989) and that the MTD values are used to normalize the test data as shown in the subsequent section. For further information on the fillet weld measurements, including post-fracture measurements, refer to Callele et al. (2005).

The testing of each specimen took place by loading the connection in concentric tension until rupture of one or all of the fillet welds occurred. The tests were carried out quasi-statically in a universal testing machine under displacement control. At several points during testing the displacement was held constant until the load stabilized. Linear variable differential transformers (LVDTs) were used to measure the fillet weld deformations in the direction of the applied load. Typical specimen test setup is shown in Figure 7. For further information on the test setup refer to Callele et al. (2005).

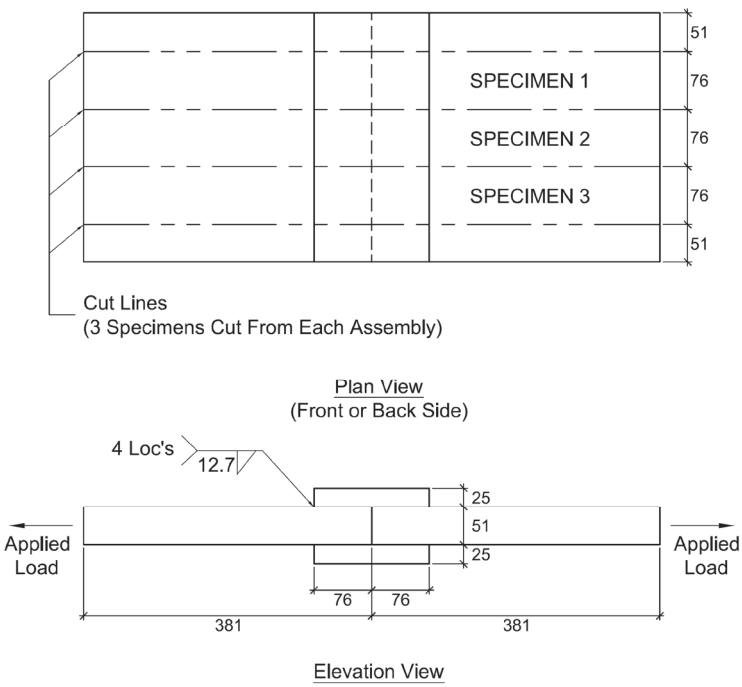

Fig. 5. Complementary test transverse weld (T) specimen.

The fillet weld deformations measured in the complementary tests were used to establish fillet weld load–deformation response curves. Since the complementary tests are used to model the assumed behavior of the individual segments of the tested MOFW connections, these response curves are used to predict the capacities of the MOFW connections.

After each test was complete, the fracture surface of the test fillet welds from each specimen was measured. In this way the degree of root penetration, the fracture angle, and the fracture throat area were assessed.

EXPERIMENTAL RESULTS

As previously stated, although all the test specimens were fabricated with E70T-7 wire, specimens TL50, TL50a, TF and TFa were fabricated with one heat (Heat 1) and the remainder were fabricated with another (Heat 2). The results of three all-weld-metal tensile tests for each of the two heats showed that the Heat 1 wire had an average tensile strength (UTS) of 575 MPa and the Heat 2 wire had an average tensile strength of 569 MPa.

The results of the tests carried out on the longitudinal fillet weld ("L100" and "L150" specimens) and transverse fillet weld specimens ("T" specimens) are given in Table 6. Test results reported by Deng et al. (2006) are also provided in Table 6 since these data are also used to analyze the MOFW connection test results.

The test capacities given in Table 6 have been normalized at two levels in order to facilitate direct comparisons and to allow for the analysis of the MOFW test specimens. The first normalization is to account for the fillet weld throat area, represented by P/A_{throat} in Table 6. The values of P/A_{throat} are calculated by dividing the ultimate capacity of the specimen by the minimum throat area of the test welds. The minimum throat area is the length of the fillet weld segment multiplied by the segment's minimum throat dimension (MTD) determined from the measured leg sizes. The second normalization takes into account the tensile strength of the weld metal used to fabricate the specimen and is termed the normalized P/A_{throat} in Table 6. The normalized P/A_{throat} value is calculated by dividing the P/A_{throat} value by the weld metal's tensile strength.

The normalized values of the fillet weld deformation are given in the last column of Table 6, represented by Δ/d^*, where Δ is the weld deformation measured in the direction of the applied load and d^* is defined as follows:

Table 2. TL Specimen Weld Sizes and Calculated Throat Size									
Specimen	Segment	Front				Back			
		Fillet Weld Leg Size		Segment Length (mm)	MTD* (mm)	Fillet Weld Leg Size		Segment Length (mm)	MTD* (mm)
		MPL* (mm)	LPL* (mm)			MPL* (mm)	LPL* (mm)		
TL50-1	1	15.7	11.5	51.4	9.3	14.1	10.0	51.3	8.2
	2	16.4	12.3	76.2	9.8	16.0	11.0	76.1	9.0
	3	12.9	12.9	51.2	9.1	12.8	11.6	51.2	8.6
TL50-2	1	13.7	12.2	51.4	9.1	13.5	10.3	50.2	8.2
	2	15.2	11.9	76.4	9.4	13.5	11.9	77.0	8.9
	3	14.9	12.2	51.2	9.4	13.1	11.9	52.5	8.8
TL50-3	1	14.2	10.7	52.1	8.5	14.0	11.1	50.6	8.7
	2	15.3	12.8	76.3	9.8	15.3	11.8	76.7	9.3
	3	11.9	12.9	51.7	8.8	12.8	9.8	50.8	7.8
TL50-4	1	17.1	10.2	53.0	8.8	13.1	11.3	52.4	8.5
	2	18.3	11.0	78.4	9.4	15.8	11.2	76.6	9.1
	3	13.7	11.8	51.5	8.9	14.6	11.8	51.6	9.1
TL50a-1	1	9.6	7.8	51.0	6.1	8.4	7.4	50.9	5.5
	2	10.7	8.3	75.8	6.6	10.7	8.2	76.2	6.5
	3	9.2	8.4	51.2	6.2	8.6	8.5	52.1	6.0
TL50a-2	1	9.6	7.8	51.2	6.0	9.2	8.5	50.8	6.3
	2	10.6	8.3	76.2	6.6	11.3	8.2	76.8	6.6
	3	9.8	8.2	51.0	6.3	10.0	8.4	51.4	6.4
TL50a-3	1	8.4	7.5	50.1	5.6	9.0	9.2	50.2	6.4
	2	10.7	8.2	76.5	6.5	10.1	9.0	75.6	6.7
	3	9.7	8.0	51.8	6.2	9.7	8.3	50.3	6.3
TL50a-4	1	10.0	8.5	52.7	6.4	10.8	8.7	50.3	6.8
	2	11.8	9.1	78.3	7.2	12.3	7.9	78.2	6.7
	3	9.1	9.6	51.7	6.6	10.0	9.4	51.4	6.9
TL100-1	1	13.9	12.9	97.9	9.5	14.5	12.9	96.9	9.7
	2	17.1	12.4	76.6	10.0	17.5	13.0	77.0	10.4
	3	15.1	13.9	98.1	10.2	16.4	13.9	100.9	10.6
TL100-2	1	14.1	10.6	98.8	8.5	15.4	12.6	98.7	9.7
	2	14.6	11.0	78.0	8.8	16.7	11.9	75.6	9.7
	3	13.5	10.6	99.4	8.4	15.3	11.5	100.8	9.2
TL100-3	1	13.8	12.5	98.9	9.3	12.5	11.5	102.0	8.5
	2	16.8	12.6	77.2	10.1	15.7	10.8	76.0	8.9
	3	13.7	13.0	99.3	9.4	14.0	10.3	101.9	8.3

* Refer to Figure 6 for the definition of these acronyms.

Table 3. TF Specimen Weld Sizes and Calculated Throat Size									
Specimen	Segment	Front				Back			
		Fillet Weld Leg Size		Segment Length (mm)	MTD* (mm)	Fillet Weld Leg Size		Segment Length (mm)	MTD* (mm)
		MPL* (mm)	LPL* (mm)			MPL* (mm)	LPL* (mm)		
TF-1	1	12.9	10.5	66.1	8.1	14.4	11.6	64.6	9.0
	2	14.2	11.6	62.8	9.0	13.7	12.3	60.9	9.1
	3	14.4	11.0	62.9	8.7	14.8	13.2	69.6	9.9
TF-2	1	12.4	13.6	66.2	9.2	12.5	12.6	60.8	8.9
	2	15.0	13.6	61.2	10.1	13.6	12.7	66.0	9.3
	3	13.2	13.7	63.2	9.5	13.5	12.5	62.7	9.2
TF-3	1	13.9	12.1	64.7	9.1	12.2	12.0	68.0	8.5
	2	13.5	11.8	65.0	8.9	13.1	11.6	62.1	8.7
	3	13.2	11.2	61.5	8.5	12.4	11.3	60.7	8.3
TF-4	1	14.3	11.7	63.6	9.0	14.8	12.5	62.0	9.5
	2	17.1	11.6	65.9	9.6	16.8	12.6	65.7	10.1
	3	13.7	10.8	58.2	8.5	15.4	12.5	60.9	9.7
TFa-1	1	9.4	8.7	56.8	6.4	8.4	7.5	66.8	5.6
	2	9.2	9.2	64.9	6.5	9.6	8.2	60.8	6.2
	3	9.0	8.8	68.2	6.3	9.1	8.4	64.2	6.2
TFa-2	1	9.4	8.2	61.4	6.2	8.4	7.5	60.6	5.6
	2	9.5	8.0	62.5	6.1	8.9	7.7	61.1	5.8
	3	9.6	8.8	64.0	6.5	9.0	7.1	67.1	5.6
TFa-3	1	9.0	8.3	57.9	6.1	8.9	8.1	65.5	6.0
	2	9.0	8.5	65.8	6.2	9.2	7.7	61.0	5.9
	3	8.8	8.1	67.4	6.0	9.1	8.2	65.9	6.1
TFa-4	1	9.3	9.6	62.4	6.7	8.5	9.4	61.5	6.3
	2	9.6	9.9	64.8	6.9	8.8	9.2	65.5	6.3
	3	8.5	9.3	61.3	6.3	8.4	7.4	60.0	5.5
* Refer to Figure 6 for the definition of these acronyms.									

$$d^* = d\left(\sin(\theta) + \cos(\theta)\right) \quad (1)$$

where θ is the angle of the fillet weld axis from the load direction, and d is the measured MPL fillet weld leg size. For transverse and 45° fillet welds the dimension d^* represents the weld leg size measured in the direction parallel to the applied load, and for longitudinal welds it represents the leg size, as shear deformation dominates. This dimension is introduced for reasons explained later.

The test results for the TL and TF specimens are shown in Table 7. The minimum throat areas are given for each specimen's transverse and nontransverse (i.e., longitudinal segments in the TL specimens and 45° segments in the TF specimens) weld segments. It should be noted that the throat areas given in Tables 6 and 7 are adjusted to account for which weld segments failed. For example, if all the welds on the front lap plate of the specimen failed, but none failed on the back lap plate, then the throat area reported is twice the front fillet weld throat area.

Table 4. Longitudinal Fillet Weld Specimen Weld Sizes and Calculated Throat Size					
Specimen	Segment No.	Fillet Weld Leg Size		Segment Length (mm)	MTD* (mm)
		MPL* (mm)	LPL* (mm)		
L100-1	1	12.9	12.2	98.2	8.9
	2	12.3	11.3	98.9	8.3
	3	12.3	11.6	100.8	8.4
	4	12.9	12.0	99.6	8.8
L100-2	1	14.7	12.6	99.3	9.6
	2	14.2	10.9	98.2	8.7
	3	13.1	11.7	99.6	8.7
	4	13.8	10.6	100.0	8.4
L100-3	1	13.4	12.8	101.6	9.2
	2	13.7	12.7	103.2	9.3
	3	12.3	13.0	102.0	8.9
	4	13.1	12.9	101.2	9.2
L150-1	1	12.6	11.2	150.0	8.4
	2	12.4	12.3	148.7	8.7
	3	14.0	11.6	150.6	8.9
	4	13.4	12.3	149.7	9.1
L150-2	1	13.5	11.4	150.8	8.7
	2	13.0	11.8	148.3	8.7
	3	13.0	11.3	151.6	8.5
	4	13.2	11.0	152.1	8.5
L150-3	1	12.6	10.5	151.7	8.1
	2	12.3	10.4	150.7	7.9
	3	12.9	10.8	147.3	8.3
	4	12.8	11.2	148.2	8.4

* Refer to Figure 6 for the definition of these acronyms.

Table 5. Transverse Fillet Weld Specimen Weld Sizes and Calculated Throat Size					
Specimen	Front/Back	Fillet Weld Leg Size		Segment Length (mm)	MTD* (mm)
		MPL* (mm)	LPL* (mm)		
T-1	Front	13.4	12.2	76.3	9.0
	Back	13.9	12.3	76.3	9.2
T-2	Front	13.9	12.0	76.2	9.1
	Back	14.0	12.1	76.3	9.1
T-3	Front	14.5	12.0	76.3	9.3
	Back	13.6	12.5	76.3	9.2

* Refer to Figure 6 for the definition of these acronyms.

Table 6. SOFW Connection Test Results from Current Research and Deng et al. (2006)							
Specimen	Fillet Weld Angle, θ (Degrees)	Ultimate Capacity (kN)	A_{throat} (mm^2)	Weld Metal UTS (MPa)	P/A_{throat} (MPa)	Normalized P/A_{throat}	Ultimate Δ/d^*
T-1	90°	1005	1373	569	732	1.29	0.0309
T-2		1026	1386	569	740	1.30	0.0285
T-3		1088	1406	569	774	1.36	0.0312
F1-1	45°	789	1169	631	675	1.07	0.0928
F1-2		763	973	631	783	1.24	0.0818
F1-3		745	987	631	755	1.20	0.1103
F2-1		813	995	605	816	1.35	0.1245
F2-2		840	1068	605	787	1.30	0.1003
F2-3		823	1003	605	820	1.36	0.1412
F3-1		755	1092	493	691	1.40	0.1427
F3-2		725	1062	493	683	1.38	0.1193
L1-1	0°	731	1447	631	505	0.80	0.1775
L1-2		762	1582	631	482	0.76	0.1529
L1-3		740	1476	631	502	0.80	0.1503
L2-1		830	1548	605	536	0.89	0.1491
L2-2		805	1461	605	551	0.91	0.1267
L2-3		802	1464	605	548	0.91	0.1544
L3-1		743	1451	493	512	1.04	0.2083
L3-2		700	1467	493	477	0.97	0.1477
L3-3		750	1467	493	511	1.04	0.1982
L100-1		1470	3383	569	434	0.76	0.0910
L100-2		1469	3422	569	429	0.75	0.0983
L100-3		1780	3746	569	475	0.83	0.1229
L150-1		2263	4997	569	453	0.80	0.1264
L150-2		2431	4864	569	500	0.88	0.1380
L150-3		2473	4766	569	519	0.91	0.1522

ANALYSIS AND DISCUSSION

Two methods of analyzing a MOFW connection are discussed herein. The first method, referred to as the strength summation approach, assumes that the capacity of a MOFW connection is the sum of the capacities of each of the individual weld segments that make up the connection. The primary assumption of this method is that all of the weld segments have sufficient deformation capacity to allow each segment to reach its individual capacity. The second method, referred to as the compatibility approach, examines how the differences in ductility of the various segments in a MOFW connection limit the contribution of the noncritical weld segment to the connection capacity. The critical segment in a MOFW connection is the segment that has an orientation closest to 90° to the applied load, and the noncritical segments are the remaining segments.

Using the measured properties of SOFW connection specimens from the current research and that of Deng et al. (2006), the strength summation approach is used to predict the TL and TF specimen capacities. Only properties from SOFW connection specimens that used the same electrode classification (E70T-7) as the TF and TL specimens were used, which includes all the specimens in Table 6 except the F1, F3, L1 and L3 series. Thus, the mean normalized P/A_{throat} values used for the analysis are 0.85, 1.34 and 1.31 for longitudinal, 45° and transverse weld segments, respectively. It should be noted that all of the specimens in Table 6 were fabricated with nominal 12.7 mm (½ in.) fillet welds made with three passes. However, as discussed by Ng et al. (2004)

Table 7. MOFW Connection Test Results						
Specimen	Ultimate Load (kN)	Throat Area, A_{throat} (mm^2)		Weld Metal UTS (MPa)	Test-to-Predicted Ratios	
		Transverse Weld Segment	Nontransverse Weld Segment		Prediction 1	Prediction 2
TF-1	2003	1121	2538	575	0.72	0.87
TF-2	2508	1229	2325	575	0.92	1.10
TF-3	2228	1118	2202	575	0.88	1.05
TF-4	2429	1325	2365	575	0.86	1.03
TFa-1	1544	801	1561	575	0.69	0.83
TFa-2	1734	738	1509	575	0.81	0.98
TFa-3	1840	769	1548	575	0.84	1.01
TFa-4	1704	861	1520	575	0.76	0.90
TL50-1	1484	1436	1804	575	0.76	0.83
TL50-2	1664	1406	1824	575	0.85	0.94
TL50-3	1573	1465	1735	575	0.81	0.88
TL50-4	1700	1437	1846	575	0.86	0.94
TL50a-1	1299	993	1222	575	0.78	0.85
TL50a-2	1186	1009	1280	575	0.69	0.76
TL50a-3	1213	1004	1239	575	0.72	0.79
TL50a-4	1472	1084	1373	575	0.80	0.87
TL100-1	2359	1602	4009	569	0.75	0.86
TL100-2	2218	1461	3779	569	0.76	0.87
TL100-3	1976	1552	3706	569	0.67	0.76

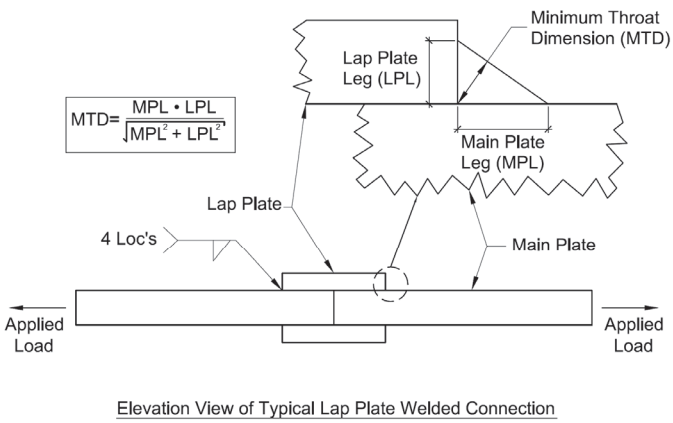

Fig. 6. Fillet weld leg size measurement definitions.

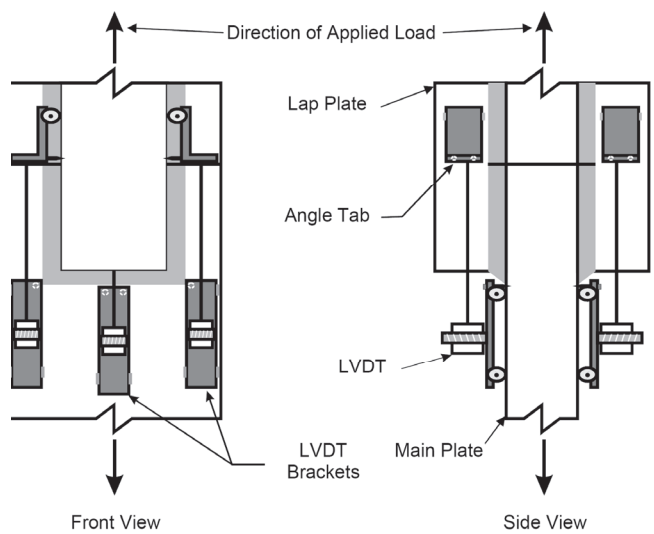

Fig. 7. Typical test specimen instrumentation and setup.

Table 8. Weld Size Effect for E70T-7 Electrodes (based on Ng et al., 2004)						
Specimen	Nominal Leg Size (mm)	P_m/A_{throat} (MPa)	Weld Metal UTS (MPa)	Normalized P_m/A_{throat}		Weld Size Effect
				Individual Assemblies	Mean	
T11	6.35	930	605	1.54	1.56	1.24
T12	6.35	1021	631	1.62		
T13	6.35	964	584	1.65		
T14	6.35	930	652	1.43		
T15	6.35	1015	652	1.56		
T25	12.7	783	605	1.30	1.26	
T26	12.7	822	631	1.30		
T27	12.7	710	584	1.22		
T28	12.7	788	652	1.21		

the unit strength of fillet welds is not independent of leg size. This can be seen in Table 8, where the average fillet weld unit strength of the specimens fabricated with 6.35-mm (¼-in.) welds is shown to be 1.24 times greater than the fillet weld unit strength of the specimens fabricated with 12.7-mm (½-in.) welds (three passes). To account for the greater unit strength expected of single-pass welds, the P/A_{throat} values in Table 6 are multiplied by the same ratio presented in Table 8, namely, 1.24, when predicting the TLa and TFa specimen capacities. However, it should be noted that the value of 1.24 is accounting for the variation in fillet weld unit strength as result of weld size and number of passes. Therefore, the 1.24 value is an upper bound for the TLa and TFa capacity predictions as the nominal fillet weld size in these specimens is 7.9 mm (5⁄16 in.), whereas the value was obtained from a comparison between 12.7-mm (½-in.) and 6.35-mm (¼-in.) nominal fillet weld sizes: thus, the true value may be somewhat lower.

Using the measured throat areas of the TL and TF specimens given in Table 7 and the P/A_{throat} values as described in the preceding paragraph, the capacity of each weld segment is calculated. The strength summation approach then predicts the TL or TF connection capacity by summing each weld segment's individual capacity. Using the strength summation approach, the test-to-predicted ratio for each of the TL and TF specimens is shown in Table 7 under Prediction 1. Figure 8 compares the test and predicted capacities using the strength summation approach and presents the associated mean test-to-predicted ratio and coefficient of variation. It is clear that the strength summation method provides a nonconservative prediction of MOFW connections.

The second method used to predict the capacity of a MOFW connection is the compatibility approach. Several research programs have verified that the deformation capacity of a fillet weld changes with a variation in loading angle: generally the closer the fillet weld orientation gets to 90° from the load direction, the smaller is its deformation capacity. The compatibility approach shows how this variation in fillet weld deformation capacity affects the capacity of MOFW connections. Figure 9 shows the fillet weld deformation of SOFW connections from this research, as well as that of Deng et al. (2006) and Miazga and Kennedy (1989). The figure reports the data in terms of Δ_{ult}/d^*, where Δ_{ult} is the deformation of the fillet weld at its ultimate capacity and d^* is as defined in Equation 1. The weld deformations reported by Miazga and Kennedy (1989) were normalized by dividing by the fillet weld leg size, d. The weld deformations given by Deng et al. (2006) were normalized by dividing by the leg size, d, only for orientations 0° and 90° and the deformations for welds with an orientation of 45° were normalized by dividing by $d\sqrt{2}$ (the weld dimension in the direction of loading). Since $d^* = d\sqrt{2}$ when $\theta = 45°$, using d^* allows a direct

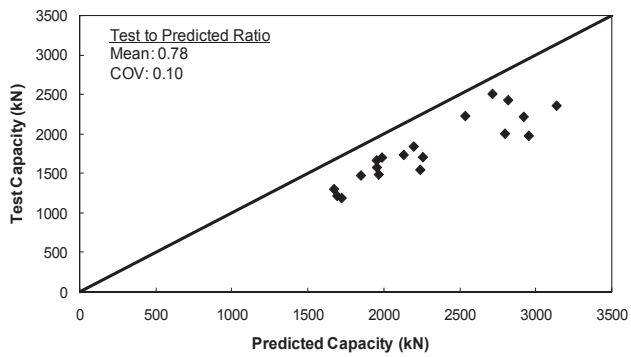

Fig. 8. Strength summation approach predictions.

comparison between the test data given by Miazga and Kennedy (1989) and that given by Deng et al. (2006). It should be noted that all the test data shown in Figure 9 were obtained using specimens whose plates remained elastic during the test, as the weld deformations with yielding base metal reported by Ng et al. (2004) were significantly larger.

There is significant scatter shown in the Δ_{ult}/d^* values in Figure 9 at weld orientations of 0° and 45°. The inconsistency in the two research programs at 45° suggests the need to look at two different predictions on the variation in weld deformation capacity with respect to the load angle, θ. A power relationship, similar to that presented in Lesik and Kennedy (1990), provides a good fit to the data when the 45° weld deformations from Deng et al. (2006) are not considered:

$$\frac{\Delta_{ult}}{d^*} = 0.20(\theta + 2)^{-0.36} \tag{2}$$

However, a linear relationship may be more appropriate when considering only the results of the current research and that of Deng et al. (2006):

$$\frac{\Delta_{ult}}{d^*} = 0.146 - 0.0013\theta \tag{3}$$

Other research projects, such as those of Butler et al. (1972) and Lesik and Kennedy (1990), have reported a nonlinear relationship between the load angle and fillet weld deformation capacity; however, the large scatter in test results at θ = 45° warrants considering both Equations 2 and 3.

A family of load–deformation response curves is a necessary component of the compatibility approach. Using the test results from the complementary test program and the test data from the tests of Deng et al. (2006), a general fillet weld response curve similar to the one given in Lesik and Kennedy (1990) was developed by Callele et al. (2005). The two curves—that of Callele et al. (2005) and that of Lesik and Kennedy (1990)—are shown in Figure 10. The difference between the two response curves is likely a result of the differences in fabrication technique of the test specimens from the two experimental programs. The load–deformation response curves developed by Callele et al. (2005) take the following mathematical form:

when ρ > 0.05,

$$\frac{P_\theta}{P_{U\theta}} = 1.47\rho - 95.42\,\rho^{1/2} + 887.57\rho^{1/3} - 2724.66\,\rho^{1/4} + 3286.37\rho^{1/5} - 1354.33\,\rho^{1/6} \tag{4}$$

when ρ ≤ 0.05,

$$\frac{P_\theta}{P_{U\theta}} = 8.476\rho \tag{5}$$

where

$$\rho = \frac{\Delta}{\Delta_{ult}} \tag{6}$$

The value $P_\theta/P_{U\theta}$, which is valid for an arbitrary θ, is the fraction of a weld segment's ultimate capacity mobilized by a particular normalized deformation, ρ.

Due to the complexity of Equation 4, a simpler form of the response curve has been developed as follows:

when ρ > 0.07,

$$\frac{P_\theta}{P_{U\theta}} = \left[\rho(2 - \rho)\right]^{.25} \tag{7}$$

when ρ ≤ 0.07,

$$\frac{P_\theta}{P_{U\theta}} = 8.7\rho \tag{8}$$

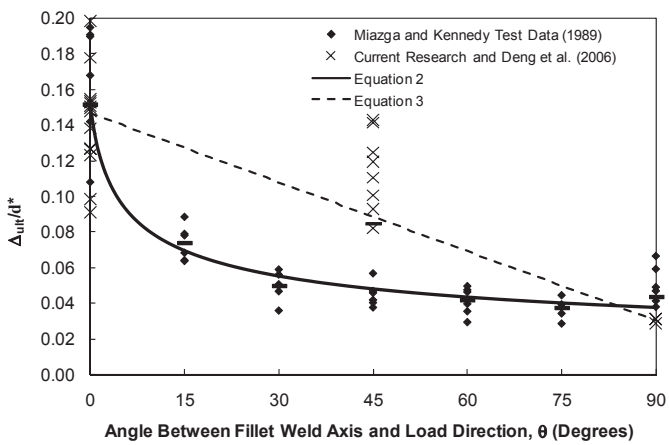

Fig. 9. Fillet weld ductility test data.

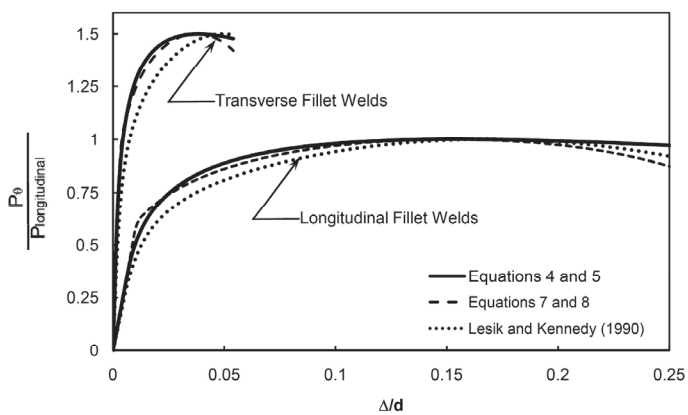

Fig. 10. Fillet weld load–response curves.

The form of Equation 7 is identical to that currently used by AISC—Equation J2.8 of the AISC *Specification* (AISC, 2005)—however, the coefficients in the equation have been modified to fit Equation 4. Though unnecessary for this analysis, Equation 8 has been provided to give an accurate description of the load–deformation response over the entire deformation range. Equations 7 and 8 are much simpler to use than Equations 4 and 5, yet as seen in Figure 10 the two sets of curves have good agreement, particularly up to the peak capacity. Thus, Equations 7 and 8 will be used in this analysis.

With estimates of both fillet weld deformation capacity and load–deformation response, the compatibility approach is now employed to estimate the TF and TL specimens' capacities. The maximum force that each weld segment could contribute to the connection capacity is calculated in the same manner as in the strength summation approach, except that in the compatibility approach the noncritical weld segment capacities are reduced by the calculated value of $P_\theta/P_{U\theta}$.

The value of $P_\theta/P_{U\theta}$ is determined by assuming that the capacity of a MOFW connection is reached when the Δ_{ult} deformation of the critical weld segment is reached. By assuming rigid body movement of the connection plates, the corresponding fillet weld deformation of a noncritical segment, (Δ/d^*), can be shown (Callele et al., 2005) to be a function of the weld deformation in the critical weld segment, (Δ_{ult}/d^*), and the filletweld orientations θ_1 and θ_2 of the noncritical and critical segments, respectively. Thus the deformation in the noncritical weld segment at the point where the critical weld segment reaches its deformation limit of (Δ/d^*) is:

$$\left(\frac{\Delta}{d^*}\right)_1 = \left(\frac{\Delta_{ult}}{d^*}\right)_2 \left(\frac{\sin(\theta_2)+\cos(\theta_2)}{\sin(\theta_1)+\cos(\theta_1)}\right) \quad (9)$$

Combining Equation 9 with a prediction of the weld segment's deformation, either by measured test results or Equations 2 or 3, the value of ρ for the noncritical segment is calculated. This value of ρ is then used with Equations 7 and 8 to calculate the fraction of the noncritical weld segment's maximum force that will contribute to the connection capacity. This fraction of the maximum force is referred to herein as the noncritical weld segment's strength reduction factor, M_w. The products of each noncritical segment's strength reduction factor and ultimate capacity are summed, along with the ultimate capacity of each critical weld segment, to predict the total MOFW connection capacity.

The compatibility approach procedure is used to predict the capacities of the TL and TF specimens using the measured strength and deformation values from specimens fabricated from E70T-7 wires from the current research and the test data from Deng et al. (2006). The test-to-predicted ratios for the TL and TF specimens are shown in Table 7 under Prediction 2. The comparison between the test and predicted values is shown in Figure 11. The mean test-to-predicted ratio of 0.90 represents a significant improvement over the strength summation approach. However, given that capacities of the TLa and TFa specimens were predicted using an upper-bound value to account for higher weld unit strengths in the 7.9-mm (5⁄16-in.) single-pass welds, the compatibility approach may give a better prediction of the MOFW connection capacities than the test-to-predicted ratio of 0.90 indicates.

The calculated values of M_w using measured values for weld strength and deformation capacity are 0.80 and 0.75 for the longitudinal fillet weld segments and 45° weld segments, respectively, when combined with a transverse weld. The smaller value of M_w for the 45° weld segments is the result of larger than expected measured Δ_{ult}/d^* values for the F2 specimens of Deng et al. (2006). The larger Δ_{ult}/d^* decreased the value of ρ, which therefore decreased the value of M_w for the 45° weld segments.

In spite of the fact that the compatibility approach does improve upon the prediction of the TL and TF specimen capacities as compared to the summation approach, it is still seen to overestimate the capacities. Therefore, to assess whether or not the compatibility approach is appropriate for design, it is necessary to perform a reliability analysis on the test data with an equation that takes into account the compatibility approach.

In order to use the compatibility approach in design, it is desirable to assess the variation in M_w for different noncritical weld segment orientations. This assessment is done for a transverse critical weld orientation in Figure 12 using the simplified response curve of Equations 7 and 8 along with the predicted weld deformations of both Equations 2 and 3. However, it would be too cumbersome to go through the compatibility approach for every weld connection design. Therefore, the following equation is proposed to simplify the evaluation of M_w, as it is a function only of the load angles

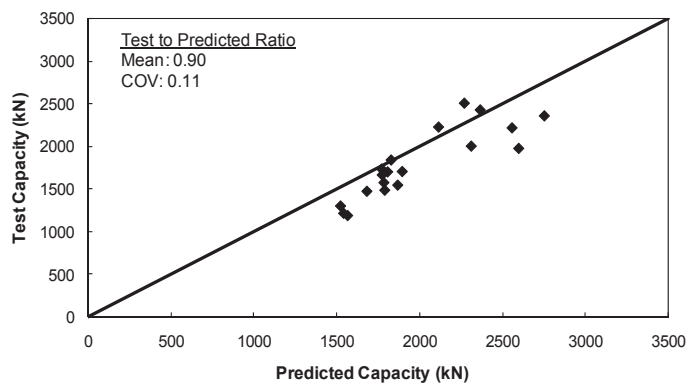

Fig. 11. Compatibility approach capacity predictions.

θ_1 and θ_2 of the weld under consideration (either critical or non-critical) and critical weld segments, respectively:

$$M_w = \frac{0.85 + \theta_1/600}{0.85 + \theta_2/600} \tag{10}$$

In addition to simplifying the design procedure greatly, Equation 10 tends to balance the significantly different curves for M_w obtained from Equations 2 and 3 shown in Figure 12. It is also consistent with the current Equation J2-9b in the AISC *Specification* (AISC, 2005) that is for the special case of combined transverse and longitudinal welds, but it eliminates the need for Equation J2-9a that acknowledges neither the higher strength of transverse welds nor the effect that the variation in deformation capacity with respect to weld orientation has on the strength of MOFW connections. Although the calculated value of M_w for a noncritical longitudinal weld segment is about 8% less than the value (0.85) from Equation 10, the equation is shown subsequently to provide an adequate margin of safety for design.

A reliability analysis was performed on the TL and TF test data to determine the reliability index obtained using the proposed design procedure and current resistance factors. The full details of this analysis can be found in Callele et al. (2005); however, a summary of the key parameters is provided in Table 9. For determining predicted values, both the Canadian design standard and the AISC *Specification* are considered, combined with the strength reduction factor, M_w, defined in Equation 10. The former design equation becomes:

$$V_r = 0.67\phi_w A_w X_u (1.00 + 0.50 \sin^{1.5}\theta) M_w \tag{11}$$

and the latter:

$$V_r = 0.67\phi A_w F_{EXX} (1.00 + 0.50 \sin^{1.5}\theta) M_w \tag{12}$$

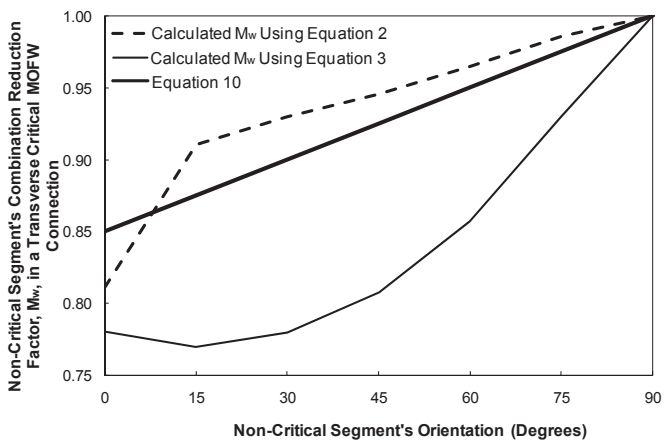

Fig. 12. Strength reduction factors for a MOFW connection with a transverse weld as the critical weld segment.

Table 9. Reliability Analysis Parameters

	Strength Summation Approach	Compatibility Approach
ρ_G	1.03	1.03
V_G	0.10	0.10
ρ_{M1}	1.15	1.15
V_{M1}	0.08	0.08
ρ_{M2}	1.23	1.23
V_{M2}	0.12	0.12
ρ_P	0.83	0.89
V_P	0.12	0.11
ρ_R	1.21	1.30
V_R	0.22	0.21
$\Phi(\beta)$	0.90	0.87
β	4.1	4.5

Because the product $0.67\phi_w = 0.60\phi$, where $\phi_w = 0.67$ and $\phi = 0.75$, predicted MOFW connection capacities—and, therefore, the resulting reliability index—are identical for the two equations. It should be noted that in the reliability analysis, only Equations 11 and 12 were used in the evaluation of the professional factor, ρ_P, and that the base metal strength at the fusion face, currently a required weld strength check in both design specifications, was not considered.

The reliability analysis of the strength summation approach simply uses $M_w = 1.0$ for all weld segments in a MOFW connection. Conversely, the compatibility approach predicts the capacity of a MOFW connection as the sum of each weld segment's capacity evaluated using Equation 11 or 12 with M_w as defined in Equation 10. The strength summation and compatibility methods result in reliability indices of 4.1 and 4.5, respectively. Considering that welded connections have small deformation capacities when compared with typical main structural elements, a reliability index of 4.0 to 4.5 is considered more suitable as a target (as compared with a reliability index of 3.0 for main members). Although both the strength summation and compatibility methods provide a reliability index within the target range, the use of Equation 10 is recommended for the following two reasons. The first is that the average test-to-predicted ratio of the strength summation method is very low, which indicates that this method does not accurately model MOFW connection behavior. The second reason to use Equation 10 is that the common MOFW connection of a welded joint that includes both transverse and longitudinal fillet welds is most susceptible to the differences in fillet weld deformation

capacity. The longitudinal weld capacity has been shown to be reduced by about 20% (see Figure 12), which points to a significant deficiency of the strength summation method. The use of Equation 10 with the accepted North American design provisions for fillet weld strength is therefore recommended for use in the design of MOFW connections. Although tests where the critical weld is not transverse to the load direction were not considered in the reliability analysis, an extension to these cases in order to generalize the procedure is reasonable since the concept of deformation compatibility is consistently applied.

As previously mentioned, the experimental research and derivation of Equation 10 have assumed that the fillet weld segments that comprise the MOFW connection have the same nominal size. However, for the case of MOFW connections with unequal leg sizes, the authors caution against the use of Equation 10 when the less ductile weld segment is smaller than the more ductile weld segment. When the less ductile weld segment is smaller, it is likely that the more ductile weld segment's capacity would be reduced more than Equation 10 predicts. In this case, Equation 9 could be modified as follows, where d_2 and d_1 are, respectively, the leg sizes of the less ductile and more ductile weld segments:

$$\left(\frac{\Delta}{d^*}\right)_1 = \left(\frac{\Delta_{ult}}{d^*}\right)_2 \left(\frac{\sin(\theta_2)+\cos(\theta_2)}{\sin(\theta_1)+\cos(\theta_1)}\right)\left(\frac{d_2}{d_1}\right) \qquad (13)$$

The deformation compatibility procedure described herein could then be applied using Equation 13 instead of Equation 9 and a different M_w value calculated. Muir (2008) gives additional considerations for cases where unequal weld sizes are used in the same joint.

It should also be noted that three recent reliability analyses have been carried out (Lesik and Kennedy, 1990; Deng et al., 2006; Callele et al., 2005) that have validated the use of Equations 11 and 12 for the prediction of fillet weld strength for any fillet weld orientation. However, current design procedures limit the use of these equations by requiring that the strength of the base material at the fusion face of the weld also be checked using virgin material properties that are not representative of the post-weld condition. This requirement effectively prevents the utilization of the full strength of fillet welds that approach 90° to the loading direction. Many test specimens used in the aforementioned reliability analyses exhibited a fracture surface that followed the fusion area between the fillet weld and base metal, yet Equations 11 and 12 were still shown to provide an adequate reliability index. It is, therefore, suggested that the check of the base metal strength along the fusion area is not required, provided matching electrodes are used. Removing this requirement would allow the designer to take advantage of the full 50% strength increase of transverse fillet welds over longitudinal fillet welds that has been observed in several research programs.

CONCLUSIONS AND RECOMMENDATIONS

By comparing test-to-predicted ratios and calculated reliability indices, the compatibility approach to the prediction of MOFW connection capacity has been shown to be superior to the predictions based on the strength summation approach. Therefore, Equations 10 and either 11 or 12 are recommended for design of concentrically loaded MOFW connections fabricated with equal-legged weld segments. The equations have been verified by comparison with 19 tests on MOFW connections fabricated with FCAW fillet welds. The design equations allow the evaluation of the capacity of any MOFW connection that is concentrically loaded.

Three recent research programs have verified the use of Equation 11 or 12 for the calculation of fillet weld design strength without the necessity for the designer to check the base metal strength on the fusion area. Therefore, it is also recommended that when matching electrodes are used for the fabrication of fillet welded connections, the base metal strength check be omitted and only Equation 11 or 12 be used.

ACKNOWLEDGMENT

This research was funded by the American Institute of Steel Construction and the Natural Sciences and Engineering Research Council of Canada. Their support is gratefully acknowledged.

REFERENCES

AISC (2005), *Specification for Structural Steel Buildings*, ANSI/AISC 360-05, American Institute of Steel Construction, Chicago, IL.

AWS (2005), *Specification for Carbon Steel Electrodes for Flux Cored Arc Welding*, ANSI/AWS A5.20/A5.20M:2005, American Welding Society, Miami, FL.

Butler, L.J., Pal, S. and Kulak, G.L. (1972), "Eccentrically Loaded Welded Connections," *Journal of the Structural Division*, ASCE, Vol. 98, No. ST5, May, pp. 989–1005.

Callele, L.J., Grondin, G.Y. and Driver, R.G. (2005), "Strength and Behaviour of Multi-orientation Fillet Weld Connections," Structural Engineering Report 255, Dept. of Civil and Environmental Engineering, University of Alberta, Edmonton, Alberta, Canada.

CSA (2001), "Limit States Design of Steel Structures," CSA S16-01, Canadian Standards Association, Toronto, Canada.

Deng, K., Grondin, G.Y. and Driver, R.G. (2006), "Effect of Loading Angle on the Behavior of Fillet Welds," *Engineering Journal*, AISC, Vol. 43, No. 1, pp. 9–23.

Lesik, D.F. and Kennedy, D.J.L. (1990), "Ultimate Strength of Fillet Welded Connections Loaded in Plane," *Canadian Journal of Civil Engineering*, Vol. 17, No. 1, pp. 55–67.

Manuel, T.J. and Kulak, G.L. (2000), "Strength of Joints that Combine Bolts and Welds," *Journal of Structural Engineering*, ASCE, Vol. 126, No. 3, March, pp. 279-287.

Miazga, G.S. and Kennedy, D.J.L. (1989), "Behavior of Fillet Welds as a Function of the Angle of Loading," *Canadian Journal of Civil Engineering*, Vol. 16, No. 4, pp. 583–599.

Muir, L.S. (2008) "Deformational Compatibility in Weld Groups," Proceedings, *Connections in Steel Structures VI*, June 23-25, Chicago, IL.

Ng, A.K.F., Deng, K., Grondin, G.Y. and Driver, R.G. (2004), "Behavior of Transverse Fillet Welds: Experimental Program," *Engineering Journal*, AISC, Vol. 41, No. 2, pp. 39–54.

Design Aspects of Single-Angle Members

PIERRE DUMONTEIL

Abstract

Used since the very beginning of steel construction, single-angle members are found in many different kinds of structures. Nearly all single-angle members are eccentrically loaded in some fashion, yet truss chords, tower legs and similar members not carrying transverse loads are usually designed as centrally loaded members. ANSI/AISC 360-05, *Specification for Structural Steel Buildings,* prescribes complex design calculations for eccentrically loaded single angles, but also provides simplified equations that adjust the *KL/r* ratio to account for eccentricities and end restraints. The purpose of this paper is to examine the possibility of simpler calculations and to explore the behavior of single-angle members.

Keywords: single angles, eccentric loads, lateral-torsional buckling, steel construction.

INTRODUCTION

Whether hot-rolled or cold-formed, angles are among the simplest steel shapes. Their shape affords simple connections with other angles or other shapes. Used since the very beginning of steel construction, single-angle members are found in many different kinds of structures: roof trusses, power transmission towers, conveyor trusses, etc.

Nearly all single-angle members are eccentrically loaded in some fashion or another. Even so, truss chords, tower legs, or similar members that do not carry transverse loads are traditionally designed as centrally loaded members. For eccentrically loaded single angles in general, the ANSI/AISC 360-05 specification (also referenced as the AISC *Specification* in this paper) prescribes design calculations that are undoubtedly complicated and tedious. Fortunately, AISC 360-05 follows the example of the ASCE Standard 10-90 and provides for most truss web members simple formulae that adjust the *KL/r* ratio to account for eccentricities and end restraints. The purpose of this paper is to examine whether simpler calculations are possible and to explore to some extent the behavior of single-angle members.

POINTS OF CONSIDERATION: FIVE OR THREE?

The first decision facing the designer is at which specific points in the section or "points of consideration" the combined stress should be computed. ANSI/AISC 360-05 is silent on this matter.

Pierre Dumonteil, retired licensed Professional Engneer, 6887 E. Long Ave, Englewood, CO, 80112. E-mail: pey.dumonteil@comcast.net

The elastic section moduli S_w and S_z relative to the principal axes are not listed in the AISC *Steel Construction Manual*, in which the section properties of structural steel angles are calculated on the simple assumption that the cross-section consists of two rectangles. If this model were geometrically exact, it would be theoretically necessary to consider the elastic section moduli at the five salient corners, numbered 1 to 5 on Figure 1a. This has been proposed by Yongcong Ding and M.K.S. Madugula (2004), who also included tables of moduli S_w and S_z for the steel angles listed in the AISC *Manual*. A different point of view is that of Lutz (1996) and Sakla (2001), who base their calculations on three points only, numbered 1 to 3 on Figure 1c. Why some experts use three points and others five is certainly a valid question, on which the following comments are offered.

1. The actual cross-section is that shown on Figure 1b. While there are no standards governing the fillet radii at the tips, it is a fact that the inside tips are always rounded. In practice, Points 3 and 4 of Figure 1a do not exist.

2. The stipulation of a nominal bending strength $M_n = 1.5M_y$ for compact angles implies a very substantial amount of plastic flow, essentially at the leg tips. The actual stress

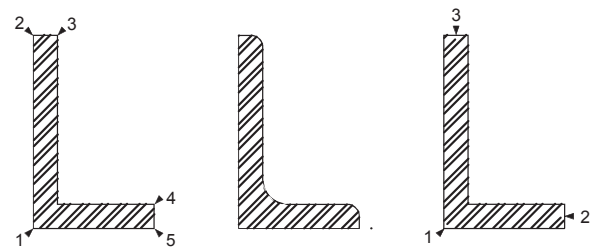

(a) Simplified Geometry, 5 Salient Corners (b) Actual Geometry with Fillets (c) Proposed Points of Consideration

Fig. 1. Geometry and points of consideration.

distribution is further complicated by residual stresses, which, at the tips, are compressive and may reach 0.25 times the yield stress (ECCS, 1976). As the angle reaches the limit state of yielding, the stress distribution in the vicinity of the toes is nearly uniform, and is probably better described by the stresses at Points 2 and 3 of Figure 1c.

3. For noncompact and slender angles, the limit state of local buckling is based on theories that assume a uniform stress across the thickness t of the leg. This is better expressed by the two tips of Figure 1c.

4. The limit state of lateral-torsional buckling applies to the whole cross-section and is not related to specific points in the section.

5. Considering only three points is, of course, simpler and reduces the amount of computation by at least one third. In this respect, the recommendation for equal-leg angles of ANSI/ASCE Standard 10-90 (1992) is noteworthy:

   The following section moduli based on centerline dimensions may be used in lieu of those based on overall dimensions:

$$S_u = \frac{b^2 t}{1.5\sqrt{2}} \qquad S_z = \frac{b^2 t}{3\sqrt{2}}$$

   In the ASCE document, the index u is used instead of the subscript w used in the AISC *Manual*; and the symbol b represents the leg width less half the thickness. Obviously, the ASCE standard wishes to avoid excessive accuracy.

For these reasons, it is strongly believed that the points of consideration should consist only of the three critical points, marked 1, 2 and 3 on Figure 1c. The corner (or heel) of the angle, Point 1, is seldom critical, but that possibility cannot be ruled out entirely.

Section properties could include fillets if their maximum and minimum radii were specified by an industry wide standard. Even so, more complicated calculations for section properties do not seem warranted, particularly in view of items 2 and 5 in the preceding paragraphs. Accordingly, the section moduli and other properties shown in Table 1 are based on the two-rectangle cross-section of Figure 1c.

LATERAL-TORSIONAL BUCKLING ABOUT GEOMETRIC AXES (EQUAL-LEG ANGLES)

Equal-leg angles may be treated either with the general method, based on the principal axes, or with a simpler approach that allows their design using properties about geometric axes. The axis of the applied bending moment must be parallel to one of the legs, as in Figure 2.

In the geometric axis approach, the worst case is that of maximum compression at the toes, in which the elastic lateral-torsional moment M_e is, according to Equation F10-4a:

$$M_e = 0.66\frac{Eb^4 t}{L^2}C_b\left(\sqrt{1+0.78\left(\frac{Lt}{b^2}\right)^2}-1\right) \qquad (1)$$

Letting $\varpi = \dfrac{Lt}{b^2}$, the lateral-torsional moment M_e is

$$M_e = 0.66EC_b t^3\frac{\sqrt{1+0.78\varpi^2}-1}{\varpi^2} = \frac{0.515EC_b t^3}{1+\sqrt{1+0.78\varpi^2}} \qquad (2)$$

This moment must be compared to the yield moment $M_y = 0.80S_xF_y$. For our purpose, a sufficient approximation to S_x is $S_x = \dfrac{b^2 t}{4}$. The nondimensional ratio M_y/M_e is then

$$\frac{M_y}{M_e} \approx 0.388\frac{F_y}{EC_b}\left(\frac{b}{t}\right)^2\left(1+\sqrt{1+0.78\varpi^2}\right) \qquad (3)$$

At this stage, it will be convenient to introduce the notation

$$\gamma = \frac{b}{t}\sqrt{\frac{F_y}{E}} \qquad (4)$$

Equation 3 becomes

$$\frac{M_y}{M_e} \approx 0.388\frac{\gamma^2}{C_b}\left(1+\sqrt{1+0.78\varpi^2}\right) \qquad (5)$$

In accordance with Equation F10-3 of the AISC *Specification*, the ratio of the nominal bending strength M_n to the yield moment M_y is:

$$\frac{M_n}{M_y} = 1.92 - 1.17\sqrt{\frac{M_y}{M_e}} \le 1.5 \qquad (6)$$

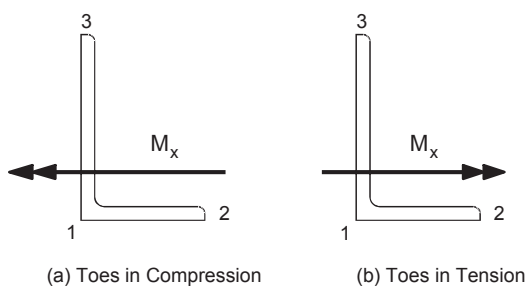

Fig. 2. Bending moment orientation.

Table 1. Section Moduli and Lateral-Torsional Constants of Angle Shapes*											
Angle Shape	I_w (in.^{4})	I_z (in.^{4})	α (deg.)	S_{w1} (in.^{3})	S_{w2} (in.^{3})	S_{w3} (in.^{3})	S_{z1} (in.^{3})	S_{z2} (in.^{3})	S_{z3} (in.^{3})	L_w (in.)	M_{w0} (kip-in.)
L8×8×1⅛	155	40.8	45	–	29.5	29.5	12.0	15.4	15.4	–	–
L8×8×1	141	36.7	45	–	26.6	26.6	11.0	13.8	13.8	–	–
L8×8×⅞	127	32.6	45	–	23.7	23.7	9.93	12.1	12.1	–	–
L8×8×¾	111	28.4	45	–	20.6	20.6	8.81	10.5	10.5	–	–
L8×8×⅝	94.8	24.1	45	–	17.4	17.4	7.62	8.84	8.84	–	–
L8×8×9⁄16	86.3	21.8	45	–	15.8	15.8	6.99	7.99	7.99	–	–
L8×8×½	77.7	19.6	45	–	14.2	14.2	6.34	7.14	7.14	–	–
L8×6×1	98.3	21.2	28.49	63.7	24.8	18.7	7.81	7.61	13.8	18.4	29600
L8×6×⅞	88.3	18.9	28.67	58.2	22	16.7	7.09	6.72	12.1	21.1	20000
L8×6×¾	77.7	16.5	28.84	52.1	19.1	14.6	6.32	5.82	10.4	24.8	12700
L8×6×⅝	66.4	14.0	29.01	45.3	16.2	12.3	5.50	4.92	8.73	30.0	7390
L8×6×9⁄16	60.6	12.7	29.09	41.7	14.7	11.2	5.06	4.45	7.89	33.4	5410
L8×6×½	54.5	11.5	29.16	37.8	13.2	10.1	4.60	3.99	7.04	37.8	3810
L8×6×7⁄16	48.3	10.1	29.24	33.8	11.6	8.88	4.12	3.52	6.19	43.3	2560
L8×4×1	73.4	7.87	13.89	27.1	23.1	14.9	4.51	3.49	11.9	20.0	15200
L8×4×⅞	66.0	7.00	14.18	24.8	20.5	13.2	4.11	3.07	10.3	23.1	10300
L8×4×¾	58.1	6.12	14.45	22.2	17.8	11.6	3.69	2.65	8.75	27.2	6500
L8×4×⅝	49.8	5.23	14.71	19.3	15.1	9.8	3.24	2.24	7.27	33.0	3790
L8×4×9⁄16	45.4	4.77	14.83	17.7	13.7	8.9	3.00	2.03	6.54	36.8	2770
L8×4×½	40.9	4.30	14.95	16.1	12.3	7.99	2.74	1.82	5.82	41.7	1950
L8×4×7⁄16	36.3	3.82	15.07	14.4	10.8	7.05	2.48	1.61	5.11	48.0	1310
L7×4×¾	41.2	5.68	17.94	19.8	13.9	9.22	3.28	2.60	7.28	21.8	7450
L7×4×⅝	35.4	4.85	18.23	17.4	11.8	7.84	2.88	2.19	6.05	26.4	4350
L7×4×½	29.2	3.99	18.50	14.6	9.62	6.40	2.44	1.78	4.85	33.4	2240
L7×4×7⁄16	25.9	3.54	18.63	13.1	8.50	5.66	2.20	1.58	4.26	38.4	1510
L7×4×⅜	22.6	3.09	18.75	11.5	7.35	4.90	1.95	1.36	3.66	45.2	954
L6×6×1	55.9	15.0	45	–	14.4	14.4	5.69	7.65	7.65	–	–
L6×6×⅞	50.5	13.3	45	–	12.8	12.8	5.18	6.73	6.73	–	–
L6×6×¾	44.7	11.6	45	–	11.2	11.2	4.63	5.82	5.82	–	–
L6×6×⅝	38.4	9.87	45	–	9.56	9.56	4.03	4.89	4.89	–	–
L6×6×9⁄16	35.2	8.98	45	–	8.69	8.69	3.72	4.43	4.43	–	–
L6×6×½	31.7	8.07	45	–	7.81	7.81	3.39	3.96	3.96	–	–
L6×6×7⁄16	28.2	7.15	45	–	6.9	6.90	3.04	3.49	3.49	–	–
L6×6×⅜	24.6	6.20	45	–	5.98	5.98	2.67	3.01	3.01	–	–
L6×6×5⁄16	20.8	5.23	45	–	5.03	5.03	2.29	2.53	2.53	–	–

* Refer to Figure 1c for applicable geometry

Table 1. Section Moduli and Lateral-Torsional Constants of Angle Shapes* (cont'd.)											
Angle Shape	I_w (in.^{4})	I_z (in.^{4})	α (deg.)	S_{w1} (in.^{3})	S_{w2} (in.^{3})	S_{w3} (in.^{3})	S_{z1} (in.^{3})	S_{z2} (in.^{3})	S_{z3} (in.^{3})	L_w (in.)	M_{w0} (kip-in.)
L6×4×⅞	31.6	5.87	22.85	20.8	11.8	8.23	3.16	2.94	6.71	13.3	14800
L6×4×¾	28.1	5.13	23.18	18.9	10.3	7.23	2.83	2.54	5.71	15.6	9390
L6×4×⅝	24.2	4.37	23.49	16.7	8.78	6.17	2.49	2.15	4.75	18.9	5480
L6×4×9⁄16	22.2	3.99	23.63	15.4	7.97	5.62	2.3	1.95	4.28	21.1	4020
L6×4×½	20.1	3.59	23.77	14.1	7.16	5.06	2.11	1.75	3.81	23.9	2840
L6×4×7⁄16	17.9	3.19	23.90	12.7	6.33	4.48	1.9	1.54	3.34	27.4	1910
L6×4×⅜	15.6	2.78	24.03	11.2	5.48	3.88	1.68	1.34	2.88	32.2	1210
L6×4×5⁄16	13.2	2.36	24.16	9.63	4.61	3.28	1.45	1.13	2.41	38.9	703
L6×3½×½	18.2	2.6	18.97	10.7	7.02	4.69	1.77	1.35	3.6	24.4	2290
L6×3½×⅜	14.2	2.01	19.27	8.53	5.37	3.6	1.42	1.03	2.71	33.0	975
L6×3½×5⁄16	12	1.71	19.42	7.32	4.52	3.04	1.23	0.871	2.27	40.0	567
L5×5×⅞	28	7.56	45	–	8.67	8.67	3.41	4.64	4.64	–	–
L5×5×¾	24.9	6.59	45	–	7.61	7.61	3.06	4	4	–	–
L5×5×⅝	21.6	5.6	45	–	6.5	6.5	2.68	3.37	3.37	–	–
L5×5×½	17.9	4.59	45	–	5.33	5.33	2.26	2.73	2.73	–	–
L5×5×7⁄16	16	4.07	45	–	4.72	4.72	2.04	2.4	2.4	–	–
L5×5×⅜	14	3.54	45	–	4.1	4.1	1.8	2.07	2.07	–	–
L5×5×5⁄16	11.9	2.99	45	–	3.46	3.46	1.55	1.74	1.74	–	–
L5×3½×¾	16.2	3.25	24.89	13.9	7.06	5.05	1.99	1.92	4.04	10.4	10300
L5×3½×⅝	14.1	2.77	25.26	12.4	6.01	4.33	1.75	1.62	3.34	12.6	6020
L5×3½×½	11.8	2.28	25.60	10.7	4.92	3.56	1.49	1.32	2.67	15.9	3120
L5×3½×⅜	9.19	1.77	25.90	8.57	3.78	2.75	1.2	1.01	2.02	21.4	1330
L5×3½×5⁄16	7.82	1.5	26.05	7.39	3.19	2.33	1.03	0.85	1.69	25.8	775
L5×3½×¼	6.39	1.22	26.18	6.12	2.58	1.89	0.861	0.689	1.36	32.6	399
L5×3×½	10.5	1.57	19.64	7.49	4.82	3.24	1.22	0.975	2.53	16.8	2360
L5×3×7⁄16	9.35	1.4	19.84	6.78	4.27	2.88	1.1	0.862	2.22	19.4	1590
L5×3×⅜	8.19	1.22	20.02	6.02	3.7	2.5	0.983	0.747	1.9	22.8	1010
L5×3×5⁄16	6.97	1.04	20.19	5.19	3.12	2.11	0.854	0.631	1.59	27.6	587
L5×3×¼	5.7	0.851	20.36	4.3	2.53	1.72	0.714	0.512	1.28	34.8	302
L4×4×¾	12	3.29	45	–	4.70	4.70	1.83	2.54	2.54	–	–
L4×4×⅝	10.5	2.80	45	–	4.04	4.04	1.61	2.13	2.13	–	–
L4×4×½	8.83	2.29	45	–	3.33	3.33	1.37	1.72	1.72	–	–
L4×4×7⁄16	7.91	2.04	45	–	2.96	2.96	1.24	1.52	1.52	–	–
L4×4×⅜	6.94	1.77	45	–	2.58	2.58	1.10	1.31	1.31	–	–
L4×4×5⁄16	5.93	1.50	45	–	2.18	2.18	0.953	1.10	1.10	–	–
L4×4×¼	4.85	1.22	45	–	1.77	1.77	0.793	0.893	0.893	–	–

* Refer to Figure 1c for applicable geometry

Table 1. Section Moduli and Lateral-Torsional Constants of Angle Shapes* (cont'd.)											
Angle Shape	I_w (in.^{4})	I_z (in.^{4})	α (deg.)	S_{w1} (in.^{3})	S_{w2} (in.^{3})	S_{w3} (in.^{3})	S_{z1} (in.^{3})	S_{z2} (in.^{3})	S_{z3} (in.^{3})	L_w (in.)	M_{w0} (kip-in.)
L4×3½×½	7.29	1.82	36.87	18.2	3.17	2.75	1.18	1.30	1.74	5.49	7530
L4×3½×⅜	5.75	1.41	37.05	14.9	2.45	2.14	0.948	0.995	1.32	7.38	3230
L4×3½×5⁄16	4.91	1.20	37.13	12.9	2.07	1.81	0.821	0.838	1.11	8.90	1880
L4×3½×¼	4.03	0.976	37.21	10.8	1.69	1.47	0.685	0.679	0.893	11.2	973
L4×3×⅝	7.29	1.62	28.09	9.12	3.77	2.82	1.14	1.17	2.17	7.31	7110
L4×3×½	6.14	1.33	28.49	7.96	3.1	2.34	0.976	0.951	1.73	9.20	3690
L4×3×⅜	4.85	1.03	28.84	6.51	2.39	1.82	0.79	0.728	1.3	12.4	1580
L4×3×5⁄16	4.15	0.876	29.01	5.66	2.02	1.54	0.687	0.614	1.09	15.0	923
L4×3×¼	3.41	0.716	29.16	4.73	1.64	1.26	0.575	0.499	0.88	18.9	477
L3½×3½×½	5.76	1.51	45	–	2.50	2.50	1.01	1.31	1.31	–	–
L3½×3½×7⁄16	5.17	1.35	45	–	2.23	2.23	0.919	1.15	1.15	–	–
L3½×3½×⅜	4.56	1.17	45	–	1.95	1.95	0.818	0.998	0.998	–	–
L3½×3½×5⁄16	3.9	0.995	45	–	1.65	1.65	0.71	0.84	0.84	–	–
L3½×3½×¼	3.21	0.812	45	–	1.34	1.34	0.593	0.679	0.679	–	–
L3½×3×½	4.62	1.16	35.54	11.4	2.38	2.01	0.847	0.947	1.33	4.70	6490
L3½×3×7⁄16	4.17	1.03	35.67	10.4	2.11	1.8	0.769	0.836	1.16	5.38	4390
L3½×3×⅜	3.68	0.896	35.79	9.4	1.84	1.57	0.686	0.724	1.00	6.31	2790
L3½×3×5⁄16	3.15	0.761	35.90	8.23	1.56	1.34	0.597	0.61	0.842	7.61	1630
L3½×3×¼	2.6	0.622	36.01	6.91	1.27	1.09	0.500	0.495	0.680	9.57	843
L3½×2½×½	3.82	0.784	25.92	4.93	2.32	1.69	0.676	0.655	1.32	7.50	3210
L3½×2½×⅜	3.04	0.609	26.40	4.08	1.80	1.32	0.55	0.501	0.986	10.1	1380
L3½×2½×5⁄16	2.61	0.519	26.62	3.57	1.53	1.12	0.481	0.423	0.825	12.2	803
L3½×2½×¼	2.15	0.425	26.83	3.00	1.24	0.916	0.405	0.344	0.664	15.4	415
L3×3×½	3.49	0.938	45	–	1.80	1.8	0.712	0.957	0.957	–	–
L3×3×7⁄16	3.16	0.833	45	–	1.61	1.61	0.647	0.842	0.842	–	–
L3×3×⅜	2.79	0.726	45	–	1.40	1.40	0.579	0.727	0.727	–	–
L3×3×5⁄16	2.40	0.617	45	–	1.19	1.19	0.504	0.612	0.612	–	–
L3×3×¼	1.98	0.504	45	–	0.976	0.976	0.423	0.495	0.495	–	–
L3×3×3⁄16	1.54	0.388	45	–	0.747	0.747	0.334	0.377	0.377	–	–
L3×2½×½	2.71	0.677	33.69	6.51	1.70	1.40	0.574	0.651	0.977	3.89	5470
L3×2½×7⁄16	2.45	0.601	33.88	6.04	1.52	1.25	0.523	0.574	0.854	4.46	3700
L3×2½×⅜	2.17	0.525	34.06	5.48	1.32	1.10	0.468	0.497	0.733	5.23	2360
L3×2½×5⁄16	1.87	0.446	34.22	4.84	1.13	0.935	0.409	0.419	0.614	6.31	1380
L3×2½×¼	1.55	0.366	34.37	4.1	0.919	0.765	0.345	0.34	0.496	7.94	714
L3×2½×3⁄16	1.20	0.281	34.52	3.25	0.704	0.587	0.274	0.26	0.376	10.7	305
L3×2×½	2.18	0.413	22.50	2.8	1.66	1.15	0.433	0.417	0.971	5.78	2730

* Refer to Figure 1c for applicable geometry

Table 1. Section Moduli and Lateral-Torsional Constants of Angle Shapes* (cont'd.)											
Angle Shape	I_w (in.^{4})	I_z (in.^{4})	α (deg.)	S_{w1} (in.^{3})	S_{w2} (in.^{3})	S_{w3} (in.^{3})	S_{z1} (in.^{3})	S_{z2} (in.^{3})	S_{z3} (in.^{3})	L_w (in.)	M_{w0} (kip-in.)
L3×2×3/8	1.75	0.32	23.18	2.36	1.29	0.904	0.354	0.318	0.713	7.80	1170
L3×2×5/16	1.51	0.273	23.49	2.08	1.10	0.771	0.311	0.268	0.593	9.44	685
L3×2×1/4	1.25	0.225	23.77	1.77	0.895	0.632	0.264	0.218	0.476	11.9	354
L3×2×3/16	0.975	0.174	24.03	1.40	0.685	0.486	0.211	0.167	0.36	16.1	151
L2½×2½×½	1.92	0.533	45	–	1.21	1.21	0.468	0.662	0.662	–	–
L2½×2½×3/8	1.56	0.412	45	–	0.952	0.952	0.382	0.5	0.5	–	–
L2½×2½×5/16	1.35	0.35	45	–	0.813	0.813	0.335	0.421	0.421	–	–
L2½×2½×1/4	1.12	0.287	45	–	0.667	0.667	0.283	0.341	0.341	–	–
L2½×2½×3/16	0.872	0.221	45	–	0.513	0.513	0.225	0.259	0.259	–	–
L2½×2×3/8	1.15	0.273	31.56	2.85	0.893	0.708	0.294	0.314	0.509	4.14	1930
L2½×2×5/16	1.00	0.233	31.81	2.55	0.762	0.607	0.258	0.264	0.424	4.99	1130
L2½×2×1/4	0.835	0.191	32.05	2.18	0.624	0.500	0.219	0.215	0.341	6.28	587
L2½×2×3/16	0.652	0.148	32.26	1.75	0.48	0.385	0.175	0.164	0.258	8.46	251
L2×2×3/8	0.752	0.206	45	–	0.587	0.587	0.229	0.318	0.318	–	–
L2×2×5/16	0.658	0.175	45	–	0.504	0.504	0.201	0.266	0.266	–	–
L2×2×1/4	0.552	0.143	45	–	0.416	0.416	0.171	0.215	0.215	–	–
L2×2×3/16	0.434	0.111	45	–	0.322	0.322	0.138	0.164	0.164	–	–
L2×2×1/8	0.303	0.0766	45	–	0.221	0.221	0.0991	0.112	0.112	–	-

* Refer to Figure 1c for applicable geometry

Substitution of Equation 5 into Equation 6 yields:

$$\frac{M_n}{M_y} = 1.92 - 0.729\frac{\gamma}{\sqrt{C_b}}\sqrt{1+\sqrt{1+0.78\varpi^2}} \le 1.5 \qquad (7)$$

For ϖ ranging of 0.2 to 7.0, the square root in Equation 7 is very close to a straight line, within ±2.0%:

$$\sqrt{1+\sqrt{1+0.78\varpi^2}} \cong 0.20\ \varpi + 1.35 \qquad (8)$$

Accordingly, the combination of Equations F10-3 and F10-4a of the AISC *Specification* may be expressed with the formula:

$$\frac{M_n}{M_y} \approx 1.92 - \left(1.0 + 0.15\varpi\right)\frac{\gamma}{\sqrt{C_b}} \le 1.5 \qquad (9)$$

For practical spans with the toes in compression, the results of Equation 9 compared to those of F10-3 and F10-4a are always within 2%.

In the case of maximum tension at the toes, Equation 5 becomes

$$\frac{M_y}{M_e} \approx 0.388\frac{\gamma^2}{C_b}\left(\sqrt{1+0.78\varpi^2}-1\right) = 0.303\ \frac{\gamma^2}{C_b}\ \frac{\varpi^2}{+\sqrt{+0.78\varpi^2}} \qquad (10)$$

This leads to

$$\frac{M_n}{M_y} \approx 1.92 - 0.644\frac{\gamma}{\sqrt{C_b}}\frac{\varpi}{\sqrt{1+\sqrt{1+0.78\varpi^2}}} \le 1.5 \qquad (11)$$

Making use of Equation 8 to replace the radical in Equation 11, the final result for tension at the toes is then, within 2% compared to F10-3 and F10-4a,

$$\frac{M_n}{M_y} \approx 1.92 - \frac{\varpi}{0.31\ \varpi + 2.1}\frac{\gamma}{\sqrt{C_b}} \le 1.5 \qquad (12)$$

Of all hot-rolled equal-leg angles, the most slender shape is the L6×6×5/16 with b/t = 19.2, or γ = 0.676 (F_y = 36 ksi). For M_e/M_y to reach the value of 1.0 with the toes in compression, ϖ must be at least 5, and the beam should have an unrealistic span of nearly 50 ft. The span would still be at least 30 ft for F_y = 50 ksi. As mentioned earlier, with hot-rolled equal-leg angles, Equation F10-2 never governs. The calculations are then fairly simple. If the tip of the outstanding leg is in compression, consider these factors corresponding to the three limit states:

Yielding $k_1 = 1.5$ (13a)

Lateral-torsional buckling $k_2 = 1.92 - \left(0.15\varpi + 1.0\right)\dfrac{\gamma}{\sqrt{C_b}}$ (13b)

Local buckling $k_3 = 2\,43 - 1\,72\gamma$ (13c)

Let k_m equal the smallest of the three; the design bending strength is then $\phi M_n = \phi k_m F_y(0.80S_x)$. To avoid having to look up the value of S_x, the following approximation will be found adequate

$$S_x \approx 0.276t\left(b - 0.43t\right)^2 \tag{14}$$

If the tip of the outstanding leg is in tension, local buckling does not occur, and the factor f_2 is equal to the right-hand side of Equation 12. Single-angle members are not very efficient beams, and, in many cases, the order of magnitude of the deflection should be checked. Without lateral support, the vertical deflection may be computed with an equivalent moment of inertia $I_{eq} \approx 0.65I_x \approx 0.075b^3t$; in most cases, this deflection should not exceed $L/300$.

LATERAL-TORSIONAL BUCKLING ABOUT PRINCIPAL AXES (EQUAL- AND UNEQUAL-LEG ANGLES)

The general method using the principal axes of the angle is based on Equation F10-6 of the AISC *Specification*

$$M_e = \frac{4.9EC_bI_z}{L^2}\left(\sqrt{\beta_w^2 + 0.052\left(\frac{Lt}{r_z}\right)^2} \pm \beta_w\right) \tag{15}$$

This formula is the specialized result of a bifurcation analysis of the elastic lateral-torsional stability of prismatic members (Timoshenko and Gere, 1961). Using the symbols of the AISC *Specification* and adding the moment modification factor C_b, the elastic buckling moment of an angle is

$$M_e = C_b\left(\sqrt{\left(\frac{P_{ez}\beta_w}{2}\right)^2 + GJP_z} \pm \frac{P_{ez}\beta_w}{2}\right) \tag{16}$$

P_{ez} is the Euler buckling load about the minor axis of inertia

$$P_{ez} = \frac{\pi^2 EI}{L^2} = \frac{\pi^2 EAr_z^2}{L^2} \tag{17}$$

GJ is the torsional rigidity of the angle

$$GJ = \frac{1}{3}GAt^2 = \frac{1}{3}Gt^3(d + b - t) \tag{18}$$

For unequal leg angles, β_w is not zero, and Equation 15 may be recast in the form

$$M_e = C_b\frac{P_z\beta_w}{2}\left(\sqrt{1 + \frac{4GJ}{P_z\beta_w^2}} \pm 1\right) \tag{19}$$

It is convenient to introduce a parameter u, such that

$$u^2 = \left(\frac{L}{\ell_w}\right)^2 = \frac{4GJ}{P_z\beta_w^2} = 0.0520\left(\frac{Lt}{\beta_w r_z}\right)^2 \tag{20}$$

The length ℓ_w is a characteristic of the section, listed in Table 1:

$$\ell_w = 4.385\frac{\beta_w r_z}{t} \tag{21}$$

From Equation 20, it is easily seen that

$$\frac{P_z\beta_w}{2} = \frac{2GJ}{\beta_w u^2} \tag{22}$$

Equation 19 may now be written

$$M_e = C_b\frac{2GJ}{\beta_w}\left[\frac{\left(\sqrt{1+u^2}\right) \pm 1}{u^2}\right] = \frac{C_bM_{w0}}{\left(\sqrt{1+u^2}\right) \pm 1} \tag{23}$$

Note that the quantity $M_{w0} = 2GJ/\beta_w$ has the dimensions of a moment and is a characteristic of the section, also listed in Table 1.

In the expression

$$M_e = C_b\,M_{w0}\Big/\left(\sqrt{1 + \left(\frac{L}{\ell_w}\right)^2} \pm 1\right) \tag{24}$$

the plus sign applies if the long leg is anywhere in compression, and the minus sign otherwise.

For practical spans with hot-rolled angles, the ratio M_y/M_e is smaller than 1.0, and buckling, if it occurs, occurs in the inelastic range. In other words, Equation F10-3 of the AISC *Specification* (given as Equation 6 previously) governs. Therefore, Equation F10-3 may be written

$$\frac{M_{nw(i)}}{M_{y(i)}} = 1.92 - 1.17\sqrt{\frac{F_y\,S_{w(i)}}{M_e}} \le 1.5 \tag{25}$$

Table 2. Geometric Axis Bending Strength ϕM_{nx} Using Principal and Geometric Axes					
Angle Shape	L (ft)	Design Bending Strength ϕM_{nx}			
		Principal Axes		Geometric Axes	
		C	T	C	T
L8×8×½	6	315	321	284	325
	8	309	315	281	325
	10	305	311	278	325
	12	300	305	275	325
	16	290	295	268	325
	20	280	285	260	325
L6×6×5/16	4	97.5	114	91.7	115
	6	97.5	110	90.7	115
	8	96.2	107	89.4	115
	10	93.4	104	87.9	115
	12	91.4	101	86.2	115
	16	86.8	95.5	82.8	113
L4×4×¼	4	38.8	39.6	35.3	40.8
	5	37.9	38.7	34.9	40.8
	6	37.6	38.2	34.5	40.8
	8	36.0	36.7	33.6	40.8
	10	34.8	35.5	32.6	40.8
	12	33.8	34.2	31.7	39.6
Horizontal moments M_x are in kip-in., with C_b =1.0 and F_y = 36 ksi. "C" denotes toe (Point 3) in compression, "T" toe in tension.					

Because the parameter u varies over a much larger range than ϖ, a linear approximation similar to Equation 8 is not possible. The nominal bending strength M_{nw} must be computed at the three points of consideration i = 1, 2, 3. For equal-leg angles, the length β_w is nil, and the elastic buckling moment is

$$M_e = \sqrt{GJP_z} \approx 0.46 C_b E \frac{b^2 t^2}{L} \qquad (26)$$

This approximation is the formula included in the AISC *Specification*. Which is preferable, the geometric or the principal axis method. Comparative results are listed in Table 2, which shows the design horizontal moment, ϕM_{nx}, computed with both methods. In that comparison, the three limit states are included in accordance with the AISC *Specification*. The principal axis method appears more conservative for the toe in tension, the geometric axis method for the toe in compression.

COMBINED FORCES AND DUE REGARD TO SIGNS

Lutz (1996) and Sakla (2001) have shown the importance of attaching the proper signs to the several terms of the interaction equations. However, a substantial change from the previous specification for single angles—which allowed the use of Equations H1-1a and H1-1b—is that the current AISC *Specification* (AISC, 2005) restricts their use to "…singly symmetric members…that are constrained to bend about a *geometric axis* (*x* and/or *y*)…". A strict interpretation of the AISC *Specification* is that the governing clause is Section H2, and the applicable interaction equation is H2-1, reproduced here:

$$\left| \frac{f_a}{F_a} + \frac{f_{bw}}{F_{bw}} + \frac{f_{bz}}{F_{bz}} \right| \le 1.0$$

The AISC *Specification* also states that

$$F_a = \phi F_{cr} \qquad F_{b_w} = \phi M_{nw} / S_w \qquad F_{bz} = \phi M_{nz} / S_z \qquad (27)$$

Section H2 adds: "Use the section modulus for the specific location in the cross-section and consider the sign of the stress." Accordingly, H2-1 may be written

$$\left| \frac{P_r}{\phi P_n} \pm \frac{M_{rw}}{\phi M_{nw}} \pm \frac{M_{rz}}{\phi M_{nz}} \right| \le 1.0 \qquad (28)$$

It is always permissible, but often overly conservative, to replace the absolute value in Equation 28 with the sum of the absolute values of its terms. It is usually advantageous to take the sense of the stress into account. The systematic use of a sign convention is helpful; the author uses that of Figure 3 (although it is not the only valid one by any means).

If the toe of the short leg is always taken as Point 2, positive moments M_w and M_z cause Point 2 to be in compression. A positive moment M_x gives $M_w > 0$ and $M_z < 0$ as shown on Figure 4. A positive moment M_y gives both $M_w > 0$ and $M_z > 0$. The combinations for the points of consideration 1, 2 and 3 are then

$$\begin{aligned} \left| \frac{P_r}{\phi P_n} + \frac{M_{rw}}{\phi M_{nw}[1]} - \frac{M_{rz}}{\phi M_{nz}[1]} \right| &\le 1.0 \\ \left| \frac{P_r}{\phi P_n} + \frac{M_{rw}}{\phi M_{nw}[2]} + \frac{M_{rz}}{\phi M_{nz}[2]} \right| &\le 1.0 \\ \left| \frac{P_r}{\phi P_n} - \frac{M_{rw}}{\phi M_{nw}[3]} + \frac{M_{rz}}{\phi M_{nz}[3]} \right| &\le 1.0 \end{aligned} \qquad (29)$$

SINGLE-ANGLE COMPRESSION MEMBERS

Section E5 of the AISC *Specification*, entitled "Single Angle Compression Members" introduces the notion of an effective slenderness ratio *KL/r* to account for the effects of eccentricity and end restraints inherent to single angles used as web members. Lutz (2006) provides the background for this approach, which has been common practice in steel transmission tower design (ASCE, 1988, 1992; ECCS, 1976).

The Appendix recasts Equations E5-1 to E5-4 in what is believed to be a slightly clearer form. Note that the validity of Section E5 is restricted to angles with a leg length ratio $\rho = b_l/b_s < 1.7$, thereby excluding the sizes L8×4, L7×4 and L6×3½, which must be handled as eccentrically loaded columns.

Normally, connecting through the long leg is less efficient than through the short leg. Except for $L/r_y < 20$, the long-leg connection has a larger *KL/r* ratio, hence less strength. The reverse situation for $L/r_y < 20$ is due to the length-independent terms $4(\rho^2 - 1)$ or $6(\rho^2 - 1)$. However, as this occurs in the inelastic range of the column curve, the difference in design strengths is insignificant. For instance, a 10-in. long L3×2×¼ strut (an unusually stocky web member) has a ratio $L/r_y = 17.4$. Attached through the long leg, $KL/r = 73.9$ and $\phi P_n = 28.9$ kips; connected through the short leg, $KL/r = 75.9$ and $\phi P_n = 28.4$ kips, a very small difference indeed. For members of usual proportions and barring other considerations, web members connected to the chord or gusset through the short leg are more efficient.

To help the designer find the minimum-weight equal-leg angle, Tables 3 and 4 may be useful. They are limited to equal-leg shapes; the former applies to box trusses, the latter to planar trusses. The tables list the least-weight sections for member lengths ranging from 5 to 16 ft and required axial strengths from 10 to 50 kips. Also listed are the unit weight and the design axial strength $P_c = \phi P_n$. The shaded cells in the tables cover combinations of lengths and axial forces that are, in the writer's experience, unlikely to occur in practice.

The tables do not address the question of whether equal-leg web members are more efficient than unequal-leg angles connected through the short leg, a question without a clear answer. In general, an equal-leg angle will be stronger than the unequal-leg angle of the same weight, but not always. In most cases, the differences are small enough to make it reasonable to standardize on only a few equal-leg sizes for a given job.

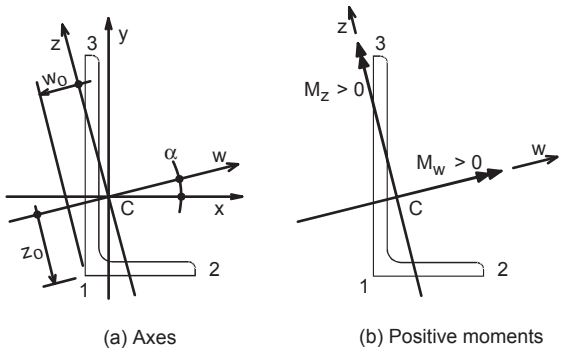

Fig. 3. System of principal axes.

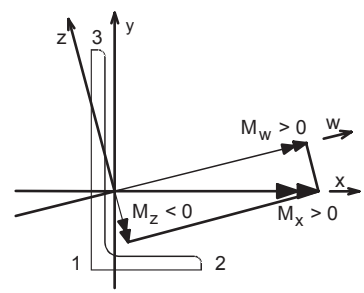

Fig. 4. Bending about geometric axis x-x.

Table 3. Single Equal-Leg Angles as Web Members of Box or Space Trusses: Least-Weight Sections								
Length L, ft		Required Axial Strength P_r, kips (LRFD)						
		10	15	20	25	30	40	50
5	Size	L2½×2½×3/16	L3×3×3/16	L3×3×¼	L3½×3½×¼	L3½×3½×¼	L4×4×5/16	L4×4×⅜
	lb/ft	3.07	3.71	4.89	5.74	5.74	8.17	9.72
	P_c	13.3	17.8	24.2	30.5	30.5	46.6	55.4
6	Size	L2½×2½×3/16	L3×3×3/16	L3×3×¼	L3½×3½×¼	L4×4×¼	L4×4×5/16	L4×4×⅜
	lb/ft	3.07	3.71	4.89	5.74	6.59	8.17	9.72
	P_c	10.8	15.8	21.2	27.7	33.4	42.9	50.9
7	Size	L3×3×3/16	L3×3×¼	L3½×3½×¼	L4×4×¼	L4×4×¼	L4×4×⅜	L5×5×5/16
	lb/ft	3.71	4.89	5.74	6.59	6.59	9.72	10.3
	P_c	13.5	17.7	24.8	30.8	30.8	46.5	53.8
8	Size	L3×3×3/16	L3½×3½×¼	L3½×3½×¼	L4×4×¼	L4×4×5/16	L4×4×⅜	L5×5×5/16
	lb/ft	3.71	5.74	5.74	6.59	8.17	9.72	10.3
	P_c	11.4	21.5	21.5	28.1	35.4	41.9	50.5
10	Size	L3×3×¼	L3½×3½×¼	L4×4×¼	L4×4×5/16	L4×4×⅜	L5×5×5/16	L5×5×⅜
	lb/ft	4.89	5.74	6.59	8.17	9.72	10.3	12.3
	P_c	10.7	15.9	22.1	27.1	31.9	44.0	53.1
12	Size	L3½×3½×¼	L4×4×¼	L4×4×5/16	L5×5×5/16	L5×5×5/16	L5×5×⅜	L6×6×5/16
	lb/ft	5.74	6.59	8.17	10.3	10.3	12.3	12.4
	P_c	12.2	17.1	21.0	36.3	36.3	43.1	51.6
14	Size	L4×4×¼	L4×4×5/16	L5×5×5/16	L5×5×5/16	L5×5×⅜	L6×6×5/16	L6×6×⅜
	lb/ft	6.59	8.17	10.3	10.3	12.3	12.4	14.8
	P_c	13.6	16.7	29.5	29.5	34.9	44.8	54.1
16	Size	L4×4×¼	L5×5×5/16	L5×5×5/16	L5×5×⅜	L6×6×5/16	L6×6×⅜	L6×6×7/16
	lb/ft	6.59	10.3	10.3	12.3	12.4	14.8	17.2
	P_c	11.1	24.3	24.3	28.8	38.3	45.5	52.4

Notes: 1. $P_c = \phi P_n$ is the design compressive axial strength (LRFD), kips, using ASTM A36 steel (F_y = 36 ksi).
2. Web members must be welded or bolted (two bolts minimum) on same side of chord or gusset.

The AISC *Specification* is silent on the subject of single-angle truss chords or legs. Both the ASCE Manual (1988) and the ASCE Standard ANSI/ASCE 10-90 specify that single-angle tower leg members (i.e., chords braced in both directions) may be designed using $KL/r = L/r_z$, where L is the system length and r_z the minor radius of inertia. In addition, both documents limit the ratio L/r_z to a maximum value of 150. This recommendation is followed in Table 5, which lists least-weight equal-leg angles for chord members.

BEHAVIOR OF AXIALLY LOADED SINGLE ANGLES

The behavior predicted by Chapter H for unsymmetrical angles is in contradiction with what Section E5 leads one to expect. According to Section E5, angles with practical slenderness ratios are substantially stronger if they are connected through the short leg. The beam-column approach of Chapter H leads to the opposite conclusion (Sakla, 2001): from a maximum if the load is applied at the centroid, the axial strength would fall off rapidly away from the centroid. Dr. Lutz's comments (2006) show how difficult it is to reconcile the experimental evidence embodied in Section E5 with the beam-column approach of Chapter H. Section E5 is based on an experimental program intended to validate a simpler approach, similar to that in the ASCE Standard (Mengelkoch and Yura, 2002). More recently, finite element models have been used to further support Section E5 (Earls and Keelor, 2007).

To gain some insight into the behavior of an axially loaded single angle, consider such an angle hinged at both ends.

Table 4. Single Equal-Leg Angles as Web Members of Planar Trusses: Least-Weight Sections								
Length L, ft		Required Axial Strength P_r, kips (LRFD)						
		10	15	20	25	30	40	50
5	Size	L2½×2½×3⁄16	L3×3×3⁄16	L3×3×¼	L3½×3½×¼	L4×4×¼	L4×4×5⁄16	L5×5×5⁄16
	lb/ft	3.07	3.71	4.89	5.74	6.59	8.17	10.3
	P_c	12.0	16.1	21.7	27.5	32.7	42.0	55.0
6	Size	L3×3×3⁄16	L3×3×¼	L3½×3½×¼	L4×4×¼	L4×4×¼	L4×4×3⁄8	L5×5×5⁄16
	lb/ft	3.71	4.89	5.74	6.59	6.59	9.72	10.3
	P_c	14.4	19.1	24.9	30.3	30.3	45.8	51.9
7	Size	L3×3×3⁄16	L3×3×¼	L3½×3½×¼	L4×4×¼	L4×4×5⁄16	L4×4×3⁄8	L5×5×3⁄8
	lb/ft	3.71	4.89	5.74	6.59	8.17	9.72	12.3
	P_c	11.9	15.5	22.4	27.9	35.2	41.8	59.7
8	Size	L3×3×¼	L3½×3½×¼	L4×4×¼	L4×4×¼	L4×4×5⁄16	L5×5×5⁄16	L5×5×3⁄8
	lb/ft	4.89	5.74	6.59	6.59	8.17	10.3	12.3
	P_c	12.5	18.9	25.6	25.6	32.0	45.8	55.7
10	Size	L3½×3½×¼	L4×4×¼	L4×4×5⁄16	L4×4×3⁄8	L5×5×5⁄16	L5×5×5⁄16	L6×6×5⁄16
	lb/ft	5.74	6.59	8.17	9.72	10.3	10.3	12.4
	P_c	13.3	19.0	23.3	27.4	40.0	40.0	52.4
12	Size	L4×4×¼	L4×4×5⁄16	L4×4×3⁄8	L5×5×5⁄16	L5×5×5⁄16	L6×6×5⁄16	L6×6×3⁄8
	lb/ft	6.59	8.17	9.72	10.3	10.3	12.4	14.8
	P_c	14.2	17.4	20.4	31.7	31.7	47.3	57.6
14	Size	L5×5×5⁄16	L5×5×5⁄16	L5×5×5⁄16	L5×5×3⁄8	L6×6×5⁄16	L6×6×5⁄16	L6×6×7⁄16
	lb/ft	10.3	10.3	10.3	12.3	12.4	12.4	17.2
	P_c	24.8	24.8	24.8	29.3	40.1	40.1	54.9
16	Size	L5×5×5⁄16	L5×5×5⁄16	L5×5×3⁄8	L6×6×5⁄16	L6×6×5⁄16	L6×6×7⁄16	L6×6×½
	lb/ft	10.3	10.3	12.3	12.4	12.4	17.2	19.6
	P_c	19.9	19.9	23.5	32.6	32.6	44.4	50.1

Notes: 1. $P_c = \phi P_n$ is the design compressive axial strength (LRFD), kips, using ASTM A36 steel (F_y = 36 ksi).
2. Web members must be welded or bolted (two bolts minimum) on same side of chord or gusset.

The elastic bifurcation buckling load P may be found from a general equation developed in Timoshenko and Gere (1961), specialized for axially loaded angles by dropping the bending moments M_1 and M_2 and setting $C_w = 0$:

$$f(P) = \begin{vmatrix} P_{ez} - P & 0 & P(e_z - z_0) \\ 0 & P_{ew} - P & -P(e_w - w_0) \\ P(e_z - z_0) & -P(e_w - w_0) & GJ \quad -Ps_1 \end{vmatrix} = 0 \quad (30)$$

In this equation, w_0 and z_0 are the coordinates of the shear center, and e_w and e_z are the eccentricities of the point of application, relative to the centroid. The other symbols are:

$$P_{ew} = \frac{\pi^2 EI_w}{L^2} \qquad P_{ez} = \frac{\pi^2 EI_z}{L^2}$$
$$s_1 = \beta_w e_z + \beta_z e_w + r_w^2 + r_z^2 + w_0^2 + z_0^2$$
$$\beta_w = \frac{1}{I_w}\int_A z(w^2 + z^2)\,dA - 2z_0 \qquad (31)$$
$$\beta_z = \frac{1}{I_z}\int_A w(w^2 + z^2)\,dA - 2w_0$$

Care must be taken to apply the proper signs to the torsional parameters β_w and β_z and to the coordinates w_0 and z_0 of the shear center. For instance with the sign conventions of Figure 3, β_w and β_z are positive, w_0 and z_0 negative. Equation 30

Table 5. Single Equal-Leg Angles as Chord Members of Box Trusses: Least-Weight Sections								
Length L, ft		Required Axial Strength P_r, kips (LRFD)						
		20	25	30	40	50	65	80
4	Size	L3×3×3/16	L3×3×¼	L3×3×¼	L3½×3/½×¼	L3½×3/½×5/16	L4×4×⅜	L3½×3/½×½
	lb/ft	3.71	4.89	4.89	5.74	7.11	9.72	11.0
	P_c	23.6	33.0	33.0	41.4	52.5	76.2	81.2
5	Size	L3×3×¼	L3×3×¼	L3½×3½×¼	L4×4×¼	L4×4×5/16	L4×4×⅜	L5×5×⅜
	lb/ft	4.89	4.89	5.74	6.59	8.17	9.72	12.3
	P_c	27.1	27.1	36.1	43.5	57.4	68.3	95.0
6	Size	L3×3×¼	L3½×3½×¼	L3½×3½×¼	L4×4×5/16	L4×4×5/16	L5×5×5/16	L5×5×⅜
	lb/ft	4.89	5.74	5.74	8.17	8.17	10.3	12.3
	P_c	21.4	30.5	30.5	50.2	50.2	69.5	87.4
7	Size	L3½×3½×¼	L3½×3½×¼	L4×4×¼	L4×4×5/16	L4×4×⅜	L5×5×⅜	L5×5×7/16
	lb/ft	5.74	5.74	6.59 lb/ft	8.17	9.72	12.3	14.2
	P_c	25.0	25.0	33.5	42.9	50.9	79.2	92.5
8	Size	L4×4×¼	L4×4×¼	L4×4×5/16	L4×4×⅜	L5×5×5/16	L5×5×⅜	L5×5×7/16
	lb/ft	6.59	6.59	8.17	9.72	10.3	12.3	14.2
	P_c	28.4	28.4	35.8	42.4	57.1	70.6	82.3
10	Size	L5×5×5/16	L5×5×5/16	L5×5×5/16	L5×5×5/16	L5×5×⅜	L6×6×⅜	L6×6×7/16
	lb/ft	10.3	10.3	10.3	10.3	12.3	14.8	17.2
	P_c	44.4	44.4	44.4	44.4	53.7	79.2	94.6
12	Size	L5×5×5/16	L5×5×5/16	L5×5×5/16	L6×6×5/16	L6×6×5/16	L6×6×7/16	L6×6×½
	lb/ft	10.3	10.3	10.3	12.4	12.4	17.2	19.6
	P_c	32.6	32.6	32.6	52.1	52.1	75.2	85.6
14	Size	L6×6×5/16	L6×6×5/16	L6×6×5/16	L6×6×5/16	L6×6×7/16	L6×6×9/16	L8×8×½
	lb/ft	12.4	12.4	12.4	12.4	17.2	21.9	26.4
	P_c	41.5	41.5	41.5	41.5	57.2	71.9	134

Notes: 1. $P_c = \phi P_n$ is the design compressive axial strength (LRFD), kips, using A36 steel (F_y = 36 ksi).
2. KL/rz is limited to 150.

is a cubic equation in P, whose smallest positive root is the critical or elastic buckling load P. Knowing that $0 < P \le P_{ez}$, the equation may be solved by a numerical method such as the Birge-Vieta iteration (Hildebrand, 1987).

If the ends of the angle are fully restrained, Equation 30 still applies, except that P_{ew} and P_{ez} are multiplied by 4. Yu (1985) lists similar equations that include certain factors reflecting different end restraints. All these equations have the same form, which shows that while the quantitative results will be somewhere between the two extremes of full restrained or hinged ends, the qualitative behavior will remain the same. Therefore, Equation 30 provides a good behavioral model for an axially loaded single-angle member.

If $e_z = z_0$, Equation 30 breaks down into two equations

$$P = P_{ez} \tag{32a}$$

$$(P_{ew} - P)(GJ - Ps_1) - P^2(e_w - w_0)^2 = 0 \tag{32b}$$

The condition $e_z = z_0$ means that the load is applied on a line $S - w'$ issued from the shear center S parallel to w-w as shown on Figure 5. Furthermore, if the coordinate e_w is not larger that a certain value e_{w1}, the critical load is constant and equal to P_{ez}. If the load is applied to the right of point M, then Equation 32b has a root smaller than P_{ez}, and that root is the critical load. Since an equal-leg angle is singly symmetric, line $S - w'$ is of course the principal axis w-w. Note, however,

that the sign of the coordinate e_{w1} depends on several parameters, in particular the length L of the member. For instance, for a L5×5×5/16 angle, e_{w1} = –0.54 in. for L = 60 in., +0.03 in. for L = 84 in., and +0.39 in. for L = 96 in. For shorter spans and thinner angles, the critical load at the centroid may be considerably less than that at the shear center.

The general case of an axially loaded unequal-leg angle (or of an unsymmetrical open shape in general) does not seem to have been investigated to any extent. Usually, the discussion is limited to the fact that if the load is applied at the shear center, Equations 32 replace Equation 30, and the buckling modes are uncoupled (Timoshenko and Gere, 1961). Since the centroid of a unequal-leg angle is not on line *S-w'*, applying the axial thrust at the centroid results in a critical load always less than at the shear center, P_{ez}. For instance, a 96-in.-long L6×4×3/8 has an elastic buckling load $P = P_{ez}$ = 86.3 kips if the thrust is applied at the shear center, and $P = 0.90P_{ez}$ = 77.1 kips if it is applied at the centroid.

The behavior of eccentrically loaded angles predicted by Section E5 is qualitatively confirmed by the results of Equation 30. Examining these results is easier if we use the distances δ_x and δ_y shown on Figure 6. Consider again the 96-in.-long L6×4×3/8. If it is attached through its long leg to a chord or gusset ½ in. thick, it could be assumed that the load is applied in the plane of contact ($\delta_x = 0$) at the middle of the long leg (δ_y = 3 in.). This assumption leads to P = 63.5 kips. If applying the load in the plane of contact might be judged too optimistic, move the axial force to the centerline of the gusset, or δ_x = –0.25 in. away; the critical load becomes P = 63.3 kips, a negligible decrease. On the other hand, if the angle is connected through its short leg so that δ_x = 2 in. and δ_y = 0, the critical load is P = 83.9 kips for δ_y = 0, decreasing to P = 82.9 kips for δ_y = –0.25 in. Since there is no apparent reason why the axial force should be acting at mid-thickness of the chord rather than at mid-thickness of the web member, it seems reasonable to assume that the transfer of force takes place in the plane of contact. In any case, theory confirms that connecting an angle through its short leg is more efficient than attaching it through its long leg.

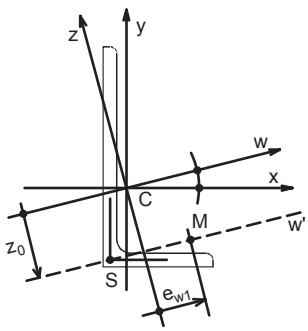

Fig. 5. Shear center S *and line* S-w'.

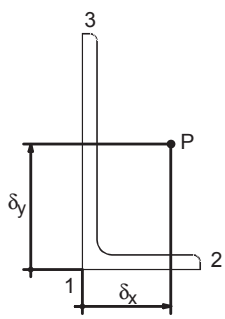

Fig. 6. Point of application of axial load.

Figure 7 presents results obtained by moving the axial load in the plane of contact, that is, along the outside perimeter of the angle. The curve for an L5×5×3/8 is not shown, as it is practically identical to that for an L6×4×3/8 attached through the long leg, shown on the figure. The elastic buckling load for either short- or long-leg connection does not vary much in the vicinity of the shear center, but falls off rather rapidly for equal-leg angles or unequal-leg angles attached through the long leg. From a stability standpoint, a single-angle member, web or chord, is more efficiently loaded at or near its shear center. Flexural yielding considerations may modify this conclusion.

The elastic critical load depends on the thickness t of the angle. In the determinant of Equation 30, the parameter s_1 is nearly independent of t, the Euler loads are roughly proportional to t, while the torsional rigidity GJ increases with the cube of t. Increasing the thickness reduces the twisting tendency of the member, which is translated by flatter curves than those shown on Figure 7. In other words, thicker angles are less sensitive to axial load location; the L5×5×3/8, whose curve is the same as that of the L6×4×3/8 attached through the long leg, has a smaller fall-off than the thinner L5×5×5/16.

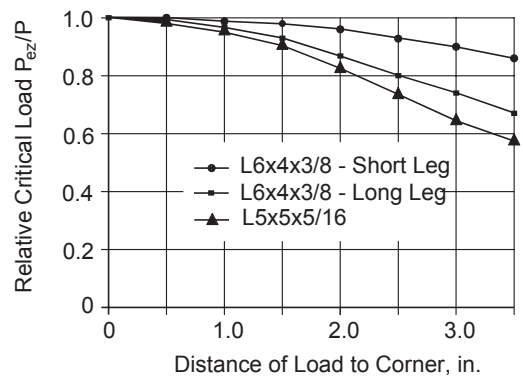

Fig. 7. Relative critical load of 8-ft-long single-angle loaded in plane of contact.

The complete differential equations derived by Timoshenko and Gere (1961) include not only the thrust, P, which may be eccentric, but also two end moments about the principal axes, M_1 and M_2 (M_1 is the buckling moment listed in Equation 15). It is obvious from the very form of these equations that there is a strong interaction between axial force and moments. If there is an axial thrust P, the presence of constant moments has for only effect to increase or decrease the eccentricities e_w and e_z. While it may lead to a safe design, simply adding the effects of the two types of loads as in a beam-column does not seem consistent with the behavior of a single angle.

CONCLUSIONS

Several arguments, not the least being simplicity, are presented to limit the number of critical points or "points of consideration" in the cross- section of a steel angle to three. Table 1 lists the corresponding section moduli.

The several clauses in the AISC *Specification* governing lateral-torsional buckling are examined, and some simplifications are proposed. Calculations summarized in Table 2 show that the geometric and principal axis approaches lead to somewhat different results, but not exceedingly so. Suggestions are made regarding due regard to stress signs recommended by the AISC *Specification*.

Section E5 of the AISC *Specification* is a very welcome simplification for the design of single-angle web members. Tables 3, 4 and 5 are presented to aid the designer in the selection of economical sizes in accordance with the requirements of that Section.

Not only has Section E5 introduced a new approach in to the design of eccentrically loaded single-angle web members, it also shows that connecting such members through the short leg is a more efficient use of material. This, however, is in contradiction with the results of beam-column calculations specified in Sections E3 or E7, according to which connecting an angle through its long leg would indicate a stronger member. A theoretical equation presented by Timoshenko and Gere (1961)is used to examine the qualitative behavior of eccentrically loaded single angles. According to it, the shear center plays a key role in the behavior of a steel angle, and the load transfer from chord to web may be assumed to take place in the plane of contact. The elastic critical load is not too sensitive to the position of the load along the connected leg. Finally, it confirms the experimental evidence that an angle is stronger if it is connected through its short leg.

REFERENCES

AISC (2000), *Load and Resistance Factor Design Specification for Single-Angle Members,* American Institute of Steel Construction, Chicago, IL.

AISC (2005), *Specification for Steel Buildings—ANSI/AISC 360-05,* American Institute of Steel Construction, Chicago, IL.

ASCE (1988), *Manual of Standard Practice No. 52, Guide for Design of Steel Transmission Towers,* 2nd edition, American Society of Civil Engineers, Reston, VA.

ASCE (1992), *Design of Latticed Steel Transmission Structures—ANSI/ASCE 10-90,* American Society of Civil Engineers, Reston, VA.

ECCS (1976), Introductory Report, Sub-Chapter 3.1.5, "Angles" and Sub-Chapter 9.2, "Angles in Lattice Transmission Towers," *Proceedings from the Second International Colloquium on Stability.*

Earls, C.J. and Keelor, D. Christian (2007), "Toward the Simplified Design of Single-Angle Beam-Columns," *Engineering Journal*, Vol. 44, No. 1.

Hildebrand, Francis B. (1987), *Introduction to Numerical Analysis*, rev. 2nd edition, Dover Publications, New York.

Lutz, LeRoy A. (1996), "A Closer Examination of the Axial Capacity of Eccentrically Loaded Single Angle Struts," *Engineering Journal*, Vol. 33, No. 2.

Lutz, LeRoy A. (2006), "Evaluating Single-Angle Compression Struts Using an Effective Slenderness Approach," *Engineering Journal*, Vol. 43, No. 4.

Mengelkoch, N.S. and Yura, J.A. (2002), "Single-Angle Compression Members Loaded Through One Leg," *Proceedings of the Structural Stability Research Council,* Annual Technical Session.

Sakla, Sherif S. S. (2001), "Tables for the Design of Eccentrically Loaded Single Angle Struts," *Engineering Journal*, Vol. 38, No. 3.

Timoshenko, Stephen P. and Gere, James M. (1961), *Theory of Elastic Stability,* 2nd edition, McGraw-Hill, New York.

Yongcong, Ding and Madugula, Murty K. S. (2004), "Elastic and Plastic Section Moduli of Steel Angles About Principal Axes," *Engineering Journal*, Vol. 41, No. 1.

Yu, Wei-Wen (1985), *Cold-Formed Steel Design,* John Wiley and Sons, New York.

APPENDIX

EFFECTIVE SLENDERNESS RATIO OF SINGLE-ANGLE WEB MEMBERS

In this Appendix, the symbols r_x, r_y and r_z are the radii of gyration listed in the tables of dimensions of the AISC manuals.

1. Planar Trusses

For web members of planar trusses, the relevant equations are E5-1 and E5-2. For equal-leg angles ($r_u = r_x = r_y$) or unequal-leg angles connected through the long leg ($r_u = r_y$):

a. When $L/r_u \le 80$

$$\frac{KL}{r} = 72 + 0.75\frac{L}{r_u} \tag{A2-1}$$

b. When $L/r_u > 80$

$$\frac{KL}{r} = 32 + 1.25\frac{L}{r_u} \le 200 \tag{A2-2}$$

For unequal-leg angles connected through the short leg, with $\rho = b_l/b_s < 1.7$:

a. When $L/r_x \le 80$

$$\frac{KL}{r} = 72 + 0.75\frac{L}{r_x} + 4(\rho^2 - 1) \ge 0.95\frac{L}{r_z} \tag{A2-3}$$

b. When $L/r_x > 80$

$$\frac{KL}{r} = 32 + 1.25\frac{L}{r_x} + 4(\rho^2 - 1) \ge 0.95\frac{L}{r_z} \le 200 \tag{A2-4}$$

2. Box or Space Trusses

For web members of box trusses, the relevant equations are E5-3 and E5-4. For equal-leg angles ($r_u = r_x = r_y$) or unequal-leg angles connected through the long leg ($r_u = r_y$):

a. When $L/r_u \le 75$

$$\frac{KL}{r} = 60 + 0.8\frac{L}{r_u} \tag{A2-5}$$

b. When $L/r_u > 75$

$$\frac{KL}{r} = 45 + \frac{L}{r_u} \le 200 \tag{A2-6}$$

For unequal-leg angles connected through the short leg, with $\rho = b_l/b_s < 1.7$:

a. When $L/r_x \le 75$

$$\frac{KL}{r} = 60 + 0.8\frac{L}{r_x} + 6(\rho^2 - 1) \ge 0.82\frac{L}{r_z} \tag{A2-7}$$

b. When $L/r_x > 75$

$$\frac{KL}{r} = 45 + \frac{L}{r_x} + 6(\rho^2 - 1) \ge 0.82\frac{L}{r_z} \le 200 \tag{A2-8}$$

Current Steel Structures Research

REIDAR BJORHOVDE

The ultimate use of the results of structural engineering research work should be their incorporation in some form, in design standards or building codes. This is often regarded as the highest level of peer recognition, since the groups that decide what goes into such essential documents are composed of outstanding researchers and practicing engineers. Since strength and performance of structures should not be expected to vary from one locale to another throughout the world, it might also be anticipated that design codes could be very similar. Unfortunately this is rarely so, for a number of reasons. Basic philosophies may vary, and fundamental attitudes toward risk and safety have profound effects on contemporary thinking and the evolution of what is perceived as practical and desirable. Recent developments may reflect state-of-the-art approaches, but to gain access and incorporation into what the profession regards as the preferred solutions takes a great deal of time and extensive evaluations. This is as it should be, because the codes and standards have to be beyond the vagaries of professional politics. As such, the design requirements reflect proven records of safety and performance and economy.

The issues mentioned in the previous paragraph are particularly thorny for the engineers who venture into the international arena because their designs have to satisfy local requirements and preferences. Familiarity with one country's codes and regulations is difficult enough, and aiming to practice in vastly different locales demands skills that go far beyond common engineering prowess. Yet there are numerous companies, some of which occupy substantial staffs and capabilities, that practice in many areas of the world. Successful projects bring novel techniques to the firms and their home offices, which positions them uniquely for preferential treatment in many regions. This has made for a changing business climate in all respects, and the global perspective is essential for such assignments. Familiarity with international codes is critical, and at the same time it must be recognized that the bottom line is really that numerical results of designs will almost always be similar, regardless of the standard that has been used. Thus, designs based on the American or the European codes, to mention two of the most prominent sets of design criteria that adhere to similar philosophies, will usually turn out to be close. This is in spite of the significant differences in their approaches to tolerances and mathematical apparatus (Bjorhovde, 2006).

The strength and behavior of connections under monotonic and cyclic loads are addressed in one of the projects presented in this paper. One of the interesting features of this study is the hybrid nature of the connections, whereby elements of different steel grades are used in the connections, to achieve improved performance as well as economy. Such thinking has also gone into examinations of the behavior of tubular (HSS) members in structures, for which two major projects have recently been initiated in Europe. Structural stability and the assessment of first- and second-order effects are examined in a project that aims at improving how these parameters are treated, using an energy-based solution. Last, but not least, a major research effort has focused on how to extend service life and performance for a range of different types of welded joints and structures.

References are provided throughout the paper, whenever such are available in the public domain. However, much of the work is still in progress, and in many cases reports or publications have not yet been prepared for public dissemination.

MEMBERS AND CONNECTIONS

Performance of Dual-Steel Connections of High Strength Components under Monotonic and Cyclic Loading: This study has been conducted at the Polytechnic University of Timisoara in Timisoara, Romania, with Professor Dan Dubina as the director.

As defined by the researchers, a dual-steel structure is for all practical purposes a hybrid assembly, where mild- to medium-strength steel is used for the elements that are intended to provide energy dissipation through ductility, stiffness and strength. Higher-strength steel is used for the elements that are to provide stability and strength following the force redistribution that will take place along with the formation of plastic hinges in the structure. In this context the grades of steel that will provide for the energy dissipation through ductility are typically 36 and 50 ksi (235 and 350 MPa) yield stress materials; the grades of steel to be used for the post-plastic hinge structural elements are required to have a yield stress of 65 to 100 ksi (460 to 700 MPa) (Dubina et al., 2007). The very high strength of these components is chosen to ensure that they will remain elastic during the

Reidar Bjorhovde, Research Editor for *Engineering Journal,* 5880 E. Territory Ave., Suite 202, Tucson, AZ, 85750-1803. E-mail: rbj@bjorhovde.com

entire structural response. The dual-steel principles have also been extended to connections, considering ductile and brittle detailing (Dubina et al., 2008).

Reflecting design and fabrication preferences in Romania, a substantial testing program for welded built-up T-stub connections was developed. As will be seen, the end-plate thicknesses in particular are much smaller than what is commonly used in the United States for moment connections; end-plate shear connections are almost never used in American practice. Using test specimens modeling end-plate moment connections with a ⅝-in. (15-mm) beam web in 36-ksi steel and end-plates thicknesses of 5⁄16, ⅜, ½, ⅝ and ¾ in. (8, 10, 12, 16 and 20 mm) in 65- and 100-ksi steel, a total of 18 different connections were developed. The end plates were bolted to the test frame, using ¾-in. Grade 8.8 bolts (same as ASTM A325 bolts). Six of the specimen types had two-sided web stiffeners (Type A), another six had one-sided stiffeners only (Type B), and the final six had no web stiffeners (Type C). Three test specimens of each type were made, one to be tested monotonically and two to be tested cyclically. The project thus included a total of 54 specimens.

Part of the aim of the testing program was to verify the design models of Eurocode 3 (CEN, 2005a) and Eurocode 8 (CEN, 2005b), including the detailed connection design requirements as well as the fatigue criteria. Fatigue was considered in combination with the high cyclic tests that were performed.

Figure 1 shows the appearance of two of the Type C (with 65-ksi end plates) [parts a (⅜-in. end plate) and b (⅝-in. end-plate)] and one of the Type A (with a ¾-in., 36-ksi end plate) connections, along with the monotonic and cyclic load-deformation diagrams. The monotonic curves mirror the hysteresis curves of the cyclic tests. It is also noted that full reversal of the load from tension to compression was not feasible for the unstiffened (Type C) and the one-sided-stiffener (Type B) configurations, due to local buckling considerations.

In general, the specimens exhibited adequate ductility, and the limit states predicted by the component model of Eurocode 3, Part 1-8, were observed for all of the tests, including the cyclic ones. It is interesting to note that the specimens with the thickest end plates (¾-in.) did not display as high ductility as the other specimens, even for the tests that had 36-ksi end plates. Finally, the fatigue performance of all of the connections was in agreement with requirements of Eurocode 3, Part 1-9.

Performance-Based Approaches for High Strength Tubular Columns and Connections Subjected to Seismic and Fire Loads: This project is a three-year (2008–2011) joint effort among the University of Liège in Belgium, the University of Trento in Italy and the University of Thessaly in Greece. The industrial partners are Centro Sviluppo Materiall and Stahlbau Pichler from Italy. Funding is provided

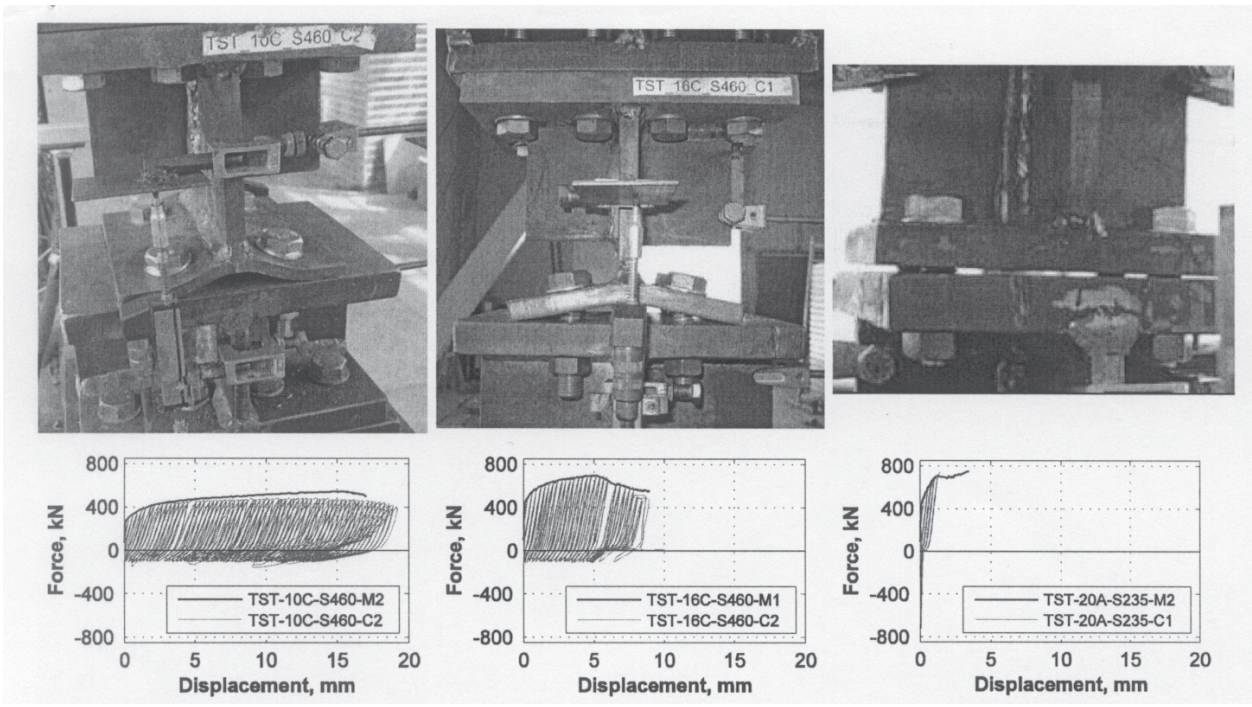

(a) (b) (c)

Fig. 1. Dual-steel end-plate connection tests (courtesy of Professor Dan Dubina).

by the Research Fund for Coal and Steel of the European Commission. Professor Jean-Pierre Jaspart of the University of Liège is the project coordinator.

The project aims at developing capacity design criteria for HSS members and structures as is commonly done in Europe for other types of cross-sections for seismic design. The work will also extend to performance under fire conditions. Full-scale fire tests will be conducted for circular tubes (CHS), along with column tests, column base tests and wide-flange beam-to-tubular column connection tests. Since the project got under way in late summer 2008, no results are available at this time. However, the researchers and their industrial partners feel that the construction industry will benefit significantly once complete data and coherent methods of analysis have been developed.

Design and Integrity Assessment of High Strength Tubular Structures for Extreme Loads: This project is another three-year (2008–2011) joint effort among the University of Liège in Belgium, the University of Trento in Italy and the University of Thessaly in Greece. The industrial partners are Centro Sviluppo Materiall, Stahlbau Pichler and Instituto de Soldarua e Qualidade (Institute for Welding and Quality) from Italy; Fundacion ITMA from Spain; and Korrosions och Metallforskningsinstitutet (Institute for Corrosion and Metal Research) from Sweden. Funding is provided by the Research Fund for Coal and Steel of the European Commission. Professor Jean-Pierre Jaspart of the University of Liège is the project coordinator.

The project is obviously tied very closely to the other HSS study, just discussed. Some specific tests to be conducted are tension-loaded circular bolted flange connections for CHS. Simple design rules for such joints will be developed, along with suitable software.

ANALYSIS OF STEEL STRUCTURES

Imperfections for Global Analysis of Frames: EC3 Drawbacks and Energy-Based Procedure: This is a collaborative research project involving the University of Navarra in Pamplona and the University of Cantabria in Santander, both in Spain. Professor Eduardo Bayo of the University of Navarra is the project director and lead researcher.

Just like the 2005 AISC *Specification* (AISC, 2005) and soon to appear 2010 AISC *Specification,* through the use of the direct analysis method, Eurocode 3 (EC3) (CEN, 2005) promotes the use of direct global analysis of steel frames for stability and strength in addition to the various traditional approaches. Although the 2005 AISC *Specification* gives the advanced procedure in Appendix 7, it is anticipated that this approach will be the preferred solution for future applications (to be given in Chapter C of the 2010 edition). In EC3, the advanced method requires that local as well as global imperfections be defined to allow for stability checks without going to individual member evaluations. EC3 provides for two such methods, as follows:

Method 1: The local and global imperfections are uncoupled, and the global (frame) imperfection is defined as an amount of initial sway and the local imperfection is defined as an initial bow.

Method 2: The local and global imperfections are derived on the basis of the shape of the elastic buckling mode of the structure, using a scaling technique that takes into account the relative stiffness of the frame.

The researchers have examined the magnitudes of the sway and bow that result from using the two methods for typical plane frames, and the findings are very different—"shockingly diverse," as observed by the authors (Serna et al., 2009). As an illustration, Figure 2 shows an elementary

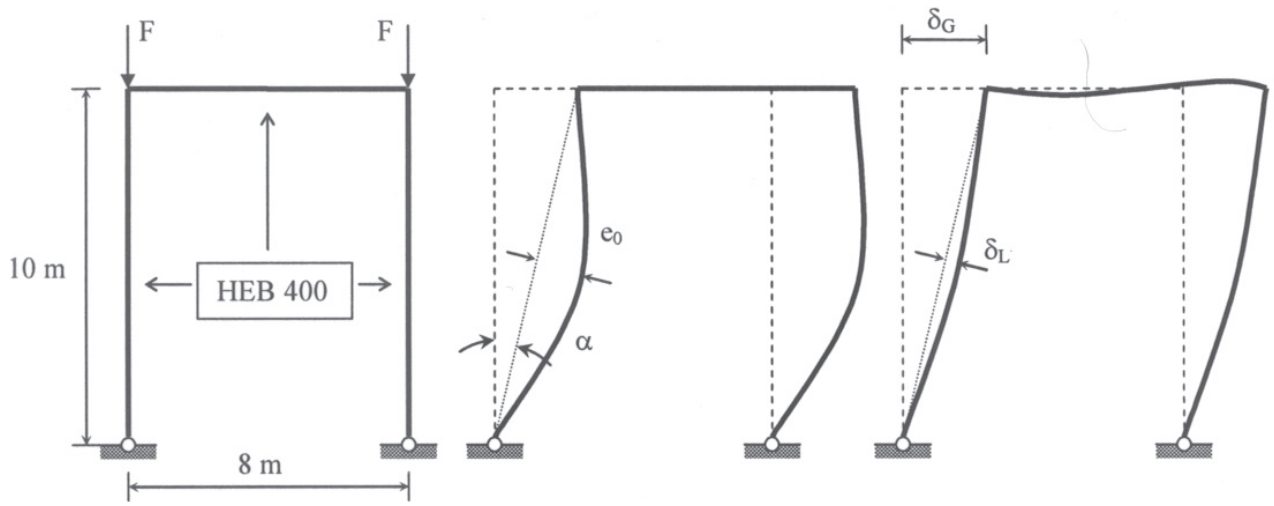

Fig. 2. Frame imperfections for Eurocode 3 Methods 1 and 2 (courtesy of Professor Eduardo Bayo).

one-bay, one-story rigid frame subjected to equal gravity loads at the top of the columns. Part b of the figure shows the imperfections that have been determined by Method 1, with an initial sway imperfection of $h/300$, corresponding to a displacement at the top of the column of 10/300 = 0.033. EC3 requires that the initial bow must be taken as $L/300$, where L is the column length, which corresponds to column buckling curve "a" in Figure 3 and an elastic analysis. (Note that Eurocode 3 uses five column curves ["multiple column curves"], designated as curves a_0, a, b, c and d. Figure 3 shows these column curves, along with the AISC column curve (the heavy line curve in the figure) as it was developed for the Specification (Bjorhovde, 2006). Resistance factors are not incorporated with the column curves shown in Figure 3.)

Consequently, for Method 1 the ratio between the maximum value of the bow and the displacement at the top of the column is 1.0. For the results of the analysis using Method 2 (i.e., the buckled frame shape shown in part c of Figure 2), the ratio between the two imperfections is 0.15, and this is independent of the absolute values of the imperfections. In addition to these discrepancies between the two methods, the researchers also note that it is very difficult to apply either of the two methods to three-dimensional frames. For Method 1, for example, EC3 does not indicate the appropriate direction of the imperfections that is necessary to arrive at the governing solution.

A new, energy-based procedure has been developed by the researchers; it is currently undergoing additional evaluations and testing (Serna et al., 2009). The procedure uncouples the imperfections. The global (frame) imperfection is defined on the basis of the sway buckling mode of the frame, using a scaling factor that is related to the relative global slenderness. This allows for the definition of the locations of the joints of the frame, and the local (member) imperfections then follow the non-sway buckling mode of the frame with a scaling factor that is related to this mode. The energy-based procedure will be further tested and evaluated for use with the design code.

FATIGUE-PERFORMANCE OF WELDED STRUCTURES

Extension of Service Life of Existing and New Welded Steel Structures: Known as the REFRESH project, this is a very large, 3½-year study focusing on the development of criteria and methods to increase the service life of fatigue-loaded welded structures. Emphasizing high-frequency post-weld improvement techniques for existing structures *in situ* as well as structures being designed and fabricated, the overall aim is to arrive at methods that are amenable to a dependable quality control system that can be interfaced with the design codes. Funded by the Federal Ministry of Education and Research in Germany, a number of universities and research organizations have been involved in the recently (June 2009) completed study. Overall management and direction of the project has been provided by the Production and Manufacturing Technologies Division of the Research Center of the University of Karlsruhe.

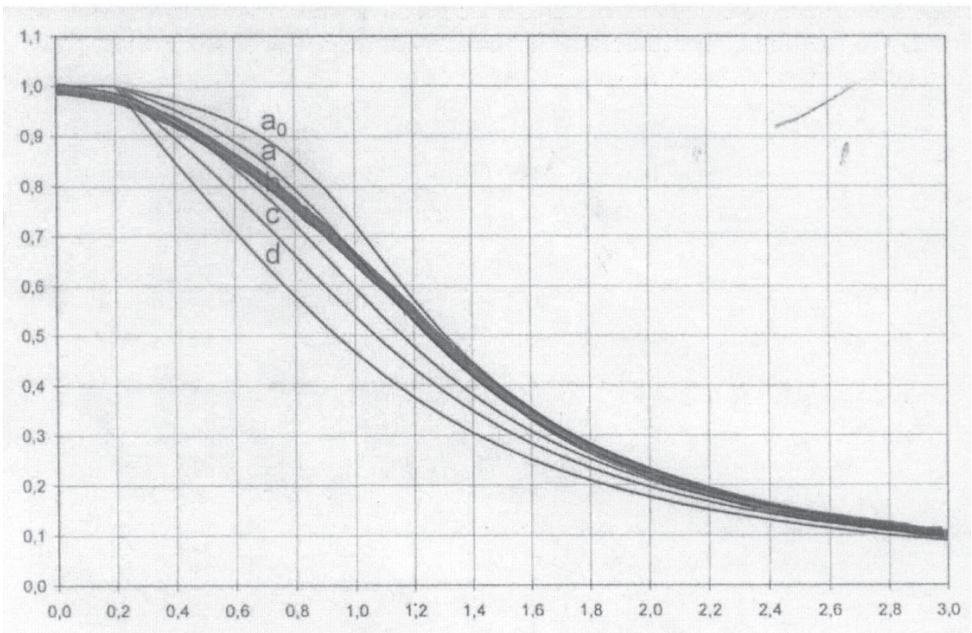

Fig. 3. Eurocode 3 column curves and the AISC column curve (courtesy of Reidar Bjorhovde [2006]).

The primary focus of the project is to examine the efficiency of high-frequency peening methods for the improvement of the fatigue resistance of welds and welded structures. Specifically, the two methods that have been evaluated in detail are high-frequency impact treatment (HiFIT) and ultrasonic impact treatment (UIT). Both methods focus on the use of hardened steel pins that hammer the weld toe with a frequency of 150 to 200 Hz, deforming the material plastically. This reduces or eliminates the notch effect, hence increasing the fatigue resistance of the weld, in spite of the increased surface hardness of the weld due to the peening.

The HiFIT-tool uses a single pin with a diameter of 3 to 4 mm (approximately 0.1 to 0.15 in.); the choice of diameter depends on the weld local geometry and the hardness of the toe. The UIT-tool uses an ultrasonic converter to develop the hammering effect, with three or four pins hammering the weld toe simultaneously. The pin diameter is 3 to 5 mm (0.1 to 0.2 in.), depending on the application. Figures 4 and 5 show close-ups of the equipment and the appearance of the weld toes after the peening has been completed.

Quality control methods are a major part of the project, pre- and post-peening, to assess weld hardness and residual stress levels. Hardness is measured by usual techniques; residual stresses are determined by hole-drilling or X-ray diffraction methods.

A broad range of fatigue tests have been conducted to verify the efficiency of the peening methods. The test parameters include steel material properties, plate thickness, specimen scale and notch details (butt welds and fillet welds), as well as transverse and longitudinal stiffeners. Fatigue crack location and behavior after initiation are monitored very carefully. The fatigue test results are currently being evaluated, but the initial findings show that the fatigue strength for butt welds and longitudinal stiffeners with S690 steel (for all practical purposes, the same as ASTM A514) can be doubled. The results are similar for both types of treatment. The cracks that developed following the HiFIT peening primarily took place in the base metal; these results are being further examined. For fillet-welded stiffeners in S690 steel the crack initiation moved from the weld toe to the root; for such cases the fatigue could also be doubled.

Since the REFRESH project was completed very recently (June 2009), detailed research reports and technical papers are currently not available.

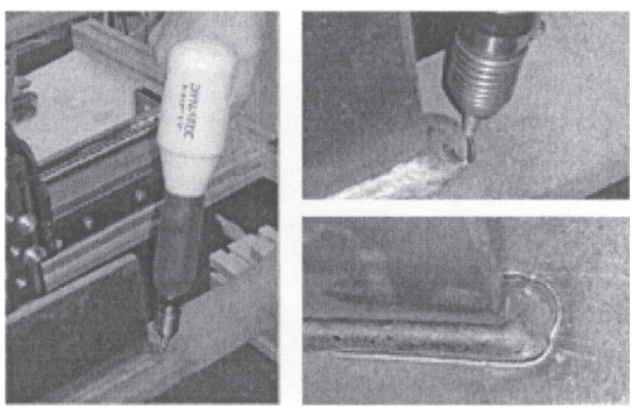

Fig. 4. Peening by high-frequency impact treatment (courtesy of Professor Alain Nussbaumer).

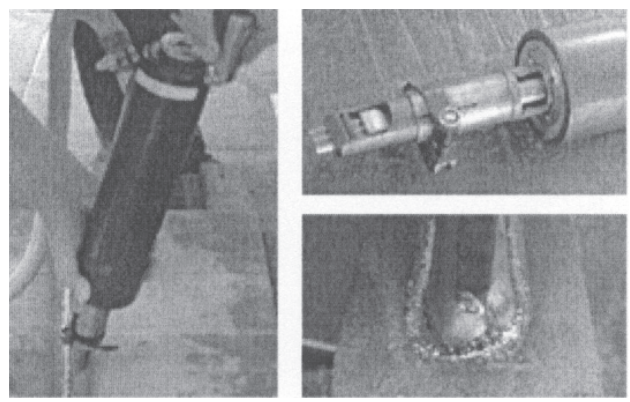

Fig. 5. Peening by ultrasonic impact treatment (courtesy of Professor Alain Nussbaumer).

REFERENCES

American Institute of Steel Construction (AISC) (2005), *Specification for Structural Steel Buildings*, AISC, Chicago, IL.

Bjorhovde, Reidar (2006), "International Steel Design Codes: Commonalities and Differences," in *Steel—A New and Traditional Material for Building*, Dan Dubina and Viorel Ungureanu, Eds., Taylor & Francis Group, London, U.K., pp. 3–13.

CEN (Comité Européen de Normalisation) (2005a), *Eurocode 3—Design of Steel Structures—EN 1993-1*, CEN, Brussels, Belgium.

CEN (Comité Européen de Normalisation) (2005b), *Eurocode 8—Design Provisions for Earthquake Resistance of Structures—EN 1998-1*, CEN, Brussels, Belgium.

Dubina, D. and Dinu, F. (2007), "High Strength Steel for Seismic Resistant Building Frames," *Proceedings, Sixth International Conference on Steel and Aluminium Structures* (Ed. R. G. Beale), Oxford Brooks University, Oxford, U.K., pp. 133–140.

Dubina, D., Stratan, A., Muntean, N. and Grecea, D. (2008), "Dual-Steel T-Stub Behavior under Monotonic and Cyclic Loading," in *Connections in Steel Structures VI*, R. Bjorhovde, F. S. K. Bijlaard and L. F. Geschwindner, Eds., AISC, Chicago, IL, pp. 185–196.

Serna, M. A., Bayo, E. and Ibañez, J. R. (2009), "Imperfections for Global Analysis of Frames: EC3 Drawbacks and Energy Based Procedure," 7th EUROMECH Solid Mechanics Conference, Lisbon, Portugal, September 7–11.

ACKNOWLEDGMENTS

Special thanks are due the following members of the International Structural Steel Research Advisors (ISSRA) who provided input to this paper:

Eduardo Bayo, University of Navarra, Pamplona, Spain

Dan Dubina, Technical University of Timisoara, Timisoara, Romania

Jean-Pierre Jaspart, University of Liège, Liège, Belgium

Alain Nussbaumer, Swiss Federal Institute of Technology, Lausanne, Switzerland

Additional assistance has been provided by Jean-François Demonceau, University of Liège, Liège, Belgium.

ERRATA

Reduced Beam Section Spring Constants

Paper by BART MORTENSEN, JANICE J. CHAMBERS and TONY C. BARTLEY
(2nd Quarter, 2008)

In the left column of page 109, the definition of γ should be changed to

$$\gamma = \sin^{-1}\left(\frac{b}{2R}\right)$$

GUIDE FOR AUTHORS

SCOPE: The ENGINEERING JOURNAL is dedicated to the improvement and advancement of steel construction. Its pages are open to all who wish to report on new developments or techniques in steel design, research, the design and/or construction of new projects, steel fabrication methods, or new products of significance to the uses of steel in construction. Only original papers should be submitted.

GENERAL: Papers intended for publication may be submitted by mail to the Editor, Keith Grubb, ENGINEERING JOURNAL, AMERICAN INSTITUTE OF STEEL CONSTRUCTION, One East Wacker Drive, Suite 700, Chicago, IL, 60601, or by email to grubb@aisc.org.

The articles published in the *Engineering Journal* undergo peer review before publication for (1) originality of contribution; (2) technical value to the steel construction community; (3) proper credit to others working in the same area; (4) prior publication of the material; and (5) justification of the conclusion based on the report.

All papers within the scope outlined above will be reviewed by engineers selected from among AISC, industry, design firms, and universities. The standard review process includes outside review by an average of three reviewers, who are experts in their respective technical area, and volunteers in the program. Papers not accepted will not be returned to the author. Published papers become the property of the American Institute of Steel Construction and are protected by appropriate copyrights. No proofs will be sent to authors. Each author receives three copies of the issue in which his contribution appears.

MANUSCRIPT PREPARATION: Manuscripts must be provided in Microsoft Word 2003 format. A laser-quality proof or high quality PDF must accompany your submittal. Download our complete author guidelines at **www.aisc.org/ej**.

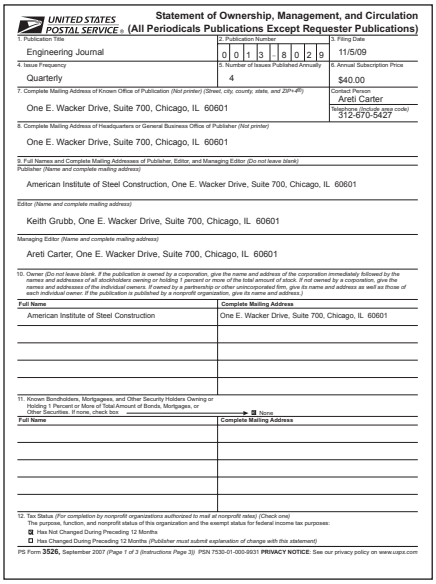

UNITED STATES POSTAL SERVICE ® **Statement of Ownership, Management, and Circulation (All Periodicals Publications Except Requester Publications)**

1. Publication Title	2. Publication Number	3. Filing Date
Engineering Journal	0 0 1 3 - 8 0 2 9	11/5/09
4. Issue Frequency	5. Number of Issues Published Annually	6. Annual Subscription Price
Quarterly	4	$40.00

7. Complete Mailing Address of Known Office of Publication *(Not printer) (Street, city, county, state, and ZIP+4®)*: One E. Wacker Drive, Suite 700, Chicago, IL 60601 — Contact Person: Areti Carter; Telephone (Include area code): 312-670-5427

8. Complete Mailing Address of Headquarters or General Business Office of Publisher *(Not printer)*: One E. Wacker Drive, Suite 700, Chicago, IL 60601

9. Full Names and Complete Mailing Addresses of Publisher, Editor, and Managing Editor *(Do not leave blank)*

Publisher *(Name and complete mailing address)*: American Institute of Steel Construction, One E. Wacker Drive, Suite 700, Chicago, IL 60601

Editor *(Name and complete mailing address)*: Keith Grubb, One E. Wacker Drive, Suite 700, Chicago, IL 60601

Managing Editor *(Name and complete mailing address)*: Areti Carter, One E. Wacker Drive, Suite 700, Chicago, IL 60601

10. Owner *(Do not leave blank. If the publication is owned by a corporation, give the name and address of the corporation immediately followed by the names and addresses of all stockholders owning or holding 1 percent or more of the total amount of stock. If not owned by a corporation, give the names and addresses of the individual owners. If owned by a partnership or other unincorporated firm, give its name and address as well as those of each individual owner. If the publication is published by a nonprofit organization, give its name and address.)*

Full Name	Complete Mailing Address
American Institute of Steel Construction	One E. Wacker Drive, Suite 700, Chicago, IL 60601

11. Known Bondholders, Mortgagees, and Other Security Holders Owning or Holding 1 Percent or More of Total Amount of Bonds, Mortgages, or Other Securities. If none, check box → ☒ None

Full Name	Complete Mailing Address

12. Tax Status *(For completion by nonprofit organizations authorized to mail at nonprofit rates) (Check one)*
The purpose, function, and nonprofit status of this organization and the exempt status for federal income tax purposes:
☒ Has Not Changed During Preceding 12 Months
☐ Has Changed During Preceding 12 Months *(Publisher must submit explanation of change with this statement)*

PS Form **3526,** September 2007 *(Page 1 of 3 (Instructions Page 3))* PSN 7530-01-000-9931 **PRIVACY NOTICE**: See our privacy policy on www.usps.com

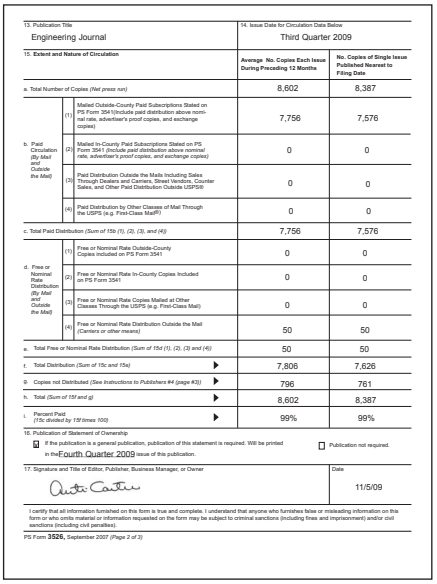

13. Publication Title	14. Issue Date for Circulation Data Below
Engineering Journal	Third Quarter 2009

15. Extent and Nature of Circulation			Average No. Copies Each Issue During Preceding 12 Months	No. Copies of Single Issue Published Nearest to Filing Date
a. Total Number of Copies *(Net press run)*			8,602	8,387
b. Paid Circulation *(By Mail and Outside the Mail)*	(1)	Mailed Outside-County Paid Subscriptions Stated on PS Form 3541(Include paid distribution above nominal rate, advertiser's proof copies, and exchange copies)	7,756	7,576
	(2)	Mailed In-County Paid Subscriptions Stated on PS Form 3541 (Include paid distribution above nominal rate, advertiser's proof copies, and exchange copies)	0	0
	(3)	Paid Distribution Outside the Mails Including Sales Through Dealers and Carriers, Street Vendors, Counter Sales, and Other Paid Distribution Outside USPS®	0	0
	(4)	Paid Distribution by Other Classes of Mail Through the USPS (e.g. First-Class Mail®)	0	0
c. Total Paid Distribution *(Sum of 15b (1), (2), (3), and (4))*			7,756	7,576
d. Free or Nominal Rate Distribution *(By Mail and Outside the Mail)*	(1)	Free or Nominal Rate Outside-County Copies included on PS Form 3541	0	0
	(2)	Free or Nominal Rate In-County Copies Included on PS Form 3541	0	0
	(3)	Free or Nominal Rate Copies Mailed at Other Classes Through the USPS (e.g. First-Class Mail)	0	0
	(4)	Free or Nominal Rate Distribution Outside the Mail *(Carriers or other means)*	50	50
e. Total Free or Nominal Rate Distribution *(Sum of 15d (1), (2), (3) and (4))*			50	50
f. Total Distribution *(Sum of 15c and 15e)* ▶			7,806	7,626
g. Copies not Distributed *(See Instructions to Publishers #4 (page #3))* ▶			796	761
h. Total *(Sum of 15f and g)* ▶			8,602	8,387
i. Percent Paid *(15c divided by 15f times 100)* ▶			99%	99%

16. Publication of Statement of Ownership
☒ If the publication is a general publication, publication of this statement is required. Will be printed in the Fourth Quarter 2009 issue of this publication. ☐ Publication not required.

17. Signature and Title of Editor, Publisher, Business Manager, or Owner — Areti Carter — Date: 11/5/09

I certify that all information furnished on this form is true and complete. I understand that anyone who furnishes false or misleading information on this form or who omits material or information requested on the form may be subject to criminal sanctions (including fines and imprisonment) and/or civil sanctions (including civil penalties).

PS Form **3526,** September 2007 *(Page 2 of 3)*

There's always a solution in steel.

ENGINEERING JOURNAL
American Institute of Steel Construction
One East Wacker Drive, Suite 700
Chicago, IL 60601